Axonal transport in motor neuron diseases

The role of KIF5A

Markella Baklou

University of Naples Federico II

School of Medicine

Ph.D program in Neuroscience, 34th cycle

Supervisor

Professor Giuseppe Pignataro

PhD co-ordinator

Professor Maurizio Taglialatela

Thesis submitted for the degree of Ph.D in Neuroscience

June 2022

Abstract

A growing number of studies are currently focusing on axonal transport defects as a common nominator in neurodegeneration. KIF5A, a major component of the axonal transport machinery, has been associated with MNDs, including Amyotrophic Lateral Sclerosis and Hereditary Spastic Paraplegia. The role of KIF5A in SMA and specifically in mitochondrial transport via the KIF5A/TRAKs/Miro1 complex, to our knowledge, has not been studied yet. Our study aims to investigate the potential implication of Kif5a and Miro1 in a SMA mouse model and identify a therapeutic intervention. Also, we attempt to identify a potential interaction of KIF5A with SMN and to better characterise two C-terminal mutations in KIF5A causing ALS and HSP.

Our results show a differential expression of *Kif5a* and *Miro1* in different brain regions and consistently lower Kif5a and Miro1 levels in the spinal cord of SMNΔ7 mice during the course of the disease. We report significantly upregulated levels of mir-140-3p in the spinal cord of SMA mice and identify miR-140-3p as a regulator of Kif5a expression. Finally, we provide preliminary data suggesting a KIF5A-SMN interaction in motor neurons and a loss of TRAK1 binding with KIF5A in the case of the HSP mutation.

The results are suggestive of the implication of Kif5a and Miro1 in the anterograde transport defects observed in SMA mice, consistent with previous studies in ALS. MiR-140-3p could potentially restore Kif5a levels and the axonal transport deficits in SMA. Future in-vivo studies are required to assess the effects of mir-140-3p in SMA and to confirm SMN as a novel KIF5A cargo. Also, we suggest that the HSP mutation potentially has a different pathogenic mechanism, in regards to TRAK1 binding, to the ALS mutations. Overall, with this thesis we report the first association of Kif5a and Miro1 in SMA pathogenesis and we suggest that KIF5A-elevating strategies could be beneficial to SMA and potentially other MNDs.

Acknowledgements

Firstly, I would like to thank my supervisor, Prof. Pignataro for trusting me with this project and always having my best interest in mind. I always felt encouraged to think independently and speak freely and this has given me confidence in my work. His support in all aspects of my PhD journey in Naples is something I will always be grateful. This project would have not been possible without his advice and guidance throughout the past 3 years.

A special thanks to my lab supervisor Valeria, whose help for this project has been invaluable, from experimental planning to data analysis, for all our discussions these years and, despite not always seeing eye to eye, for being reliable and supportive especially in difficult periods; to Giusy for learning so much from her and for sharing the bench and also her time, protocols and knowledge with me, which I appreciate; to my group and especially Paola for her help with immunohistochemistry; to Prof. Van Den Bosch for giving me the amazing opportunity to join his lab in Leuven and Adria from whom I learned a lot about cell cultures and live-imaging and helped me with the imaging experiments. I also have to thank Prof. Taglialatela for trusting me for this position despite my seemingly different background and everyone who welcomed me to the department.

A big thank you to all my friends and colleagues at the lab who helped me carry out this project, especially Brenda, Gabriella, Lidia and Yi-Shin for their friendship and our long hours commiserating about our difficulties and who I feel lucky to have met. Also, a big thank you to my friends, Katerina, Aggeliki, Nadine, Chrysi, Elsa, Georgia and Nikoletta for their encouragement and support.

Lastly, I would like to thank my family and especially my mother for always believing in me and my nephews, Michalis and Nikolas who I might have neglected at times but I really missed during these years.

Table of contents

Abbreviations

AD autosomal dominant

ALS amyotrophic lateral sclerosis

AR autosomal recessive

ASO antisense oligonucleotide

C9orf72 Chromosome 9 open reading frame 72

CMT Charcot-Marie-Tooth

CNS central nervous system

FTD frontotemporal dementia

FUS fused in sarcoma

GABARAP GABA type A receptor-associated protein

GOF gain of function

GWAS genome wide association study

HDAC6 histone deacetylase 6

HSP hereditary spastic paraplegia

ICC immunocytochemistry

IHC immunohistochemistry

iPSC induced pluripotent stem cell

KHC kinesin heavy chain

KIF kinesin family member

KLC kinesin light chain

LMN lower motor neurons

LOF loss of function

MAP microtubule associated protein

Miro1 mitochondrial Rho GTPase

MN motor neuron

MND motor neuron disease

NEIMY neonatal intractable myoclonus

NMD nonsense-mediated decay

NMJ neuromuscular junction

PLA proximity ligation assay

RBP RNA-binding proteins

RNP ribonucleoprotein

SC spinal cord

SMA spinal muscular atrophy

SMN survival motor neuron (protein)

snRNP small nuclear ribonucleoprotein

SOD1 superoxide dismutase 1

SPG spastic paraplegia gene

TDP-43 TAR DNA binding protein 43

TRAK1 trafficking kinesin protein 1

UMN upper motor neurons

UTR untranslated region

WB western blot

1. INTRODUCTION

Normal neuronal function is heavily dependent on the efficient transport of essential proteins and organelles along the axons via the kinesin/dynein system. Disruption of the axonal transport can cause neurodegeneration and is a common feature of motor neuron diseases (MNDs). With the kinesins being a core component of the transport machinery, their role in neurodegenerative diseases is of significant interest (Guo *et al*, 2019). The contribution of axonal transport impairment in the pathology of the two most common MNDs in adults and children, ALS and SMA but also MNDs in general, will be discussed below.

1.1 Axonal transport

As the genetic material and most of the proteins synthetised localise in the cell soma, intracellular transport is a prerequisite for proper cell function and survival (Morfini *et al*, 2012). This is especially true for neurons due to their unique morphology with dendrites and long axons, that may extend up to 1m, in order to maintain communication between the cell soma and the axon terminals but also direct the cargo in specific compartments (Guo *et al*, 2020). Early real-time imaging of axons has provided with significant insight on this movement of the various organelles, vesicles and proteins along the axons, termed axonal transport (Brady *et al*, 1982). Bidirectional axonal transport is essential for both the transport of proteins and cytoskeletal filaments, organelles and RNAs to the specific axonal compartment where they are required but also for the clearance of damaged organelles and protein aggregates from the axon. In addition, it allows for the neuron to respond to signals and stress insults (Millecamps & Julien, 2013). Axonal transport can be classified as slow or fast according to the speed that cargo is transported (Table 1.1).

Major rate components & cargo structure of axonal transport		
Rate component	Average rate (mm/day)	Moving cargo
FAST TRANSPORT		
Anterograde	200-400	Small vesicles, neurotransmitters, membrane proteins
Retrograde	50-100	Mitochondria
	200-300	Lysosomal vesicles & enzymes
SLOW TRANSPORT		
Slow component a	0.2-1	Neurofilaments, microtubules
Slow component b	2-8	Actin filaments, cytosolic protein complexes

Table 1.1: *The transport speed of some major cargo in fast and slow transport. Both the average rates and cargo differ between fast and slow transport [Compiled with information from Brown, 2014; Morfini et al, 2012].*

Fast axonal transport is bidirectional, so cargo is transported from the cell soma to the axon terminals (anterograde transport) and from the axons towards the cell soma (retrograde transport). Proteins transported by the slow axonal transport have only been observed in the anterograde direction (Morfini *et al*, 2012). The transport machinery, however, is the same in both cases and it is mainly comprised of microtubules, molecular motors and the various cargoes (Fig. 1.1) (De Vos *et al*, 2008).

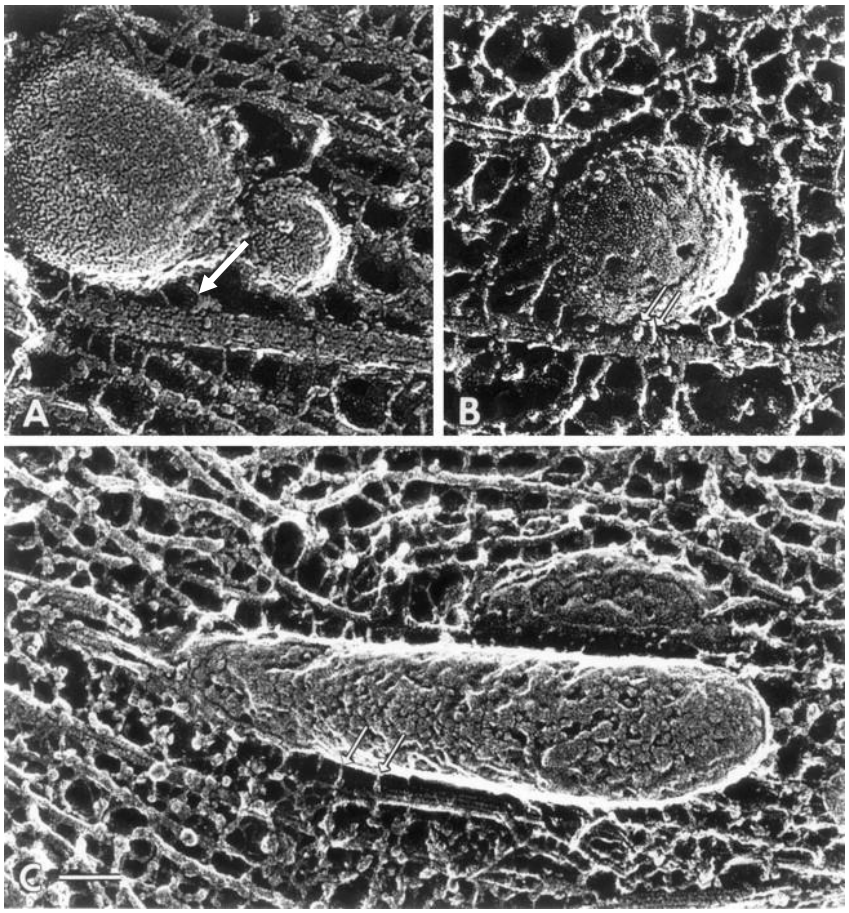

Figure 1.1: A-C: *Early electron microscopic images of axons have revealed the presence of "cross-bridges" between the various organelles (cargoes) and the microtubules, now known as molecular motors, indicated here as white arrows. As shown, more than one motor can be transporting one cargo [Image from: Hirokawa 1996].*

1.2 Components of transport machinery

Microtubules

The microtubules are tubular structures of 25nm diameter that act as the rails on which the cargo is being transported by the molecular motors. They are heterodimers of α- and β-tubulins, stabilised by microtubule-associated proteins (MAPs) such as tau and they are polarised with plus and minus ends. Microtubules polymerise faster at the plus end than at the minus end and their direction differs in different cell types. In neuronal axons the plus end is always towards the periphery (unipolar) and

mixed in dendrites. As a result, the direction of anterograde axonal transport (and anterograde motors) is always towards the plus end and for the retrograde transport towards the minus end (Hirokawa & Noda, 2008). The exact mechanism of the polarisation of the axons is not yet clarified, however the axon initial segment (AIS) seems to play a role serving as a template for the polarity of the whole axon and also separates the dendritic and axonal compartments (Guedes-Dias & Holzbaur, 2019).

The molecular motors involved in microtubule-based axonal transport neurons are the kinesin superfamily and dynein powering the anterograde and retrograde axonal transport respectively (Fig. 1.2) (Hirokawa *et al*, 2009). The anterograde transport motors are analysed below.

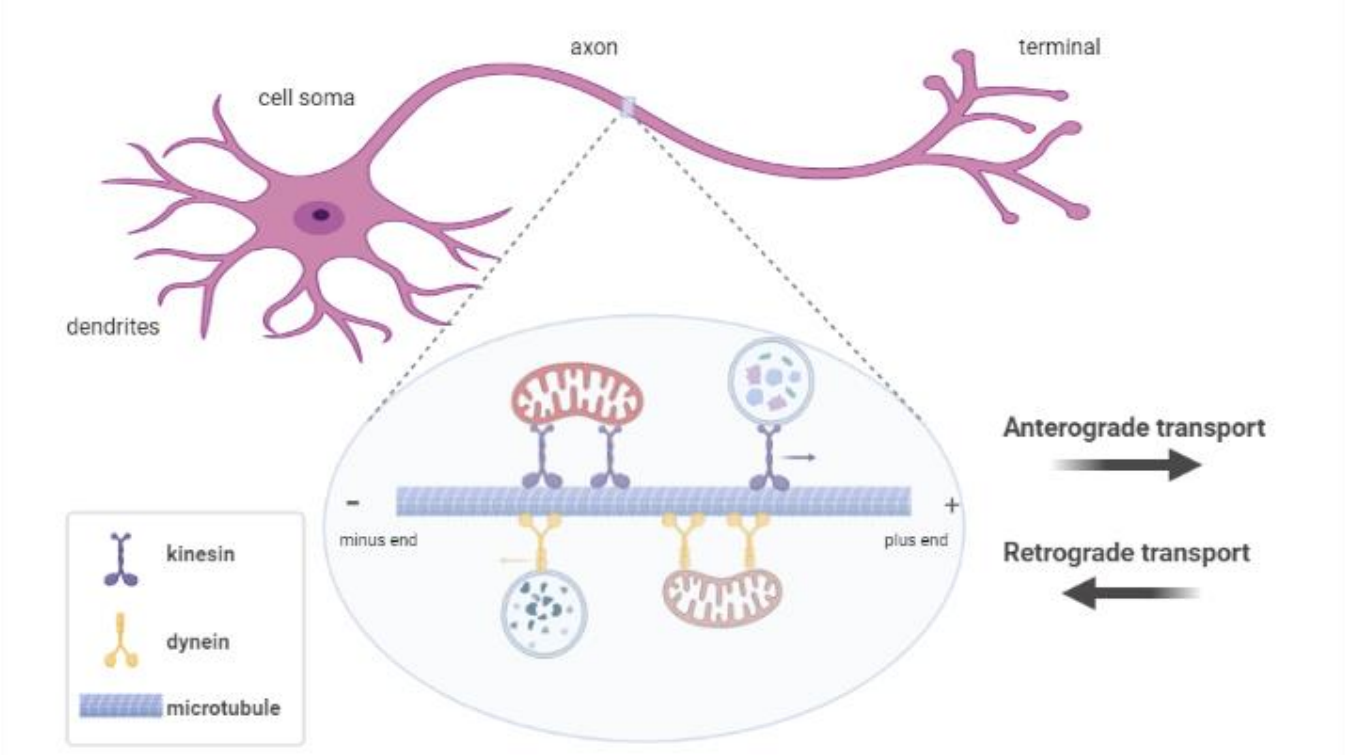

Figure 1.2: Schematic representation of major components of the fast axonal transport machinery. *Kinesins move towards the plus end of the microtubules and therefore transport cargoes from the cell soma to the axon terminals. Dynein transports cargoes towards the cell soma. The two major membrane-bound organelles, mitochondria and vesicles are shown. Membrane-less RNP granules (not shown) can also be transported by motor proteins either directly or by associating with the membrane-bound cargoes (Pushpalatha & Besse, 2019) [Image created in BioRender.com].*

Molecular motors

Kinesins are the molecular motors that are responsible mainly for the anterograde axonal transport of cargo, although they also play a role in cell division during meiosis - mitosis (Mann & Wadsworth 2019). The mammalian kinesin superfamily (KIFs) is comprised of around 45 genes, most of which are expressed in the brain. They can be classified into 15 KIF families, in recent nomenclature termed kinesin 1 to kinesin 14b and encode for at least the double number of KIF proteins (Hirokawa *et al*, 2009). Each KIF has a characteristic velocity that ranges from 0.2 μm/sec to 1.5 μm/sec and as mentioned above, corresponds to fast axonal transport (Hirokawa & Takemura, 2005). All KIFs, however, have a conserved globular motor domain. Depending on the position of the motor domain KIFs can be either N-, M- or C-KIFs when the motor domain is at the N-terminal, middle or C-terminal domain, respectively. C- and N-KIFs have a stalk and a cargo binding domain. N-KIFs move towards the plus ends (cell soma) and C- and M-KIFs towards the minus ends (neuronal terminals) while M-KIFs can also depolymerise the microtubules. KIFs share a 30-60% homology of their motor domain while the other two domains vary (Hirokawa *et al*, 2010; Hirokawa & Takemura, 2005).

The motor domain (head) contains a microtubule-binding region and an ATP-binding sequence which hydrolyses ATP in order to produce the chemical energy required for the motor protein to move along the microtubule (Hirokawa & Noda, 2008). The stalk domain is mainly responsible for the dimerization of kinesin and the unique cargo binding domain is involved in recognition and binding of the cargo (Hirokawa *et al*, 2009). Most KIFs form homodimers however heterodimers or monomers have also been identified (Hirokawa & Takemura, 2005). As most KIFs form dimers, they have two motor domains and the movement on the microtubule is achieved by cycles of out-of-phase ATP hydrolysis which results to one head being bound to the microtubule and one being unattached and able to take a step forward, searching for the next binding site on the microtubule (Hancock, 2016).

While for the anterograde cargo transport there are many different kinesins available, only one dynein, cytosolic dynein 1 is responsible for the retrograde transport (Olenick & Holzbaur, 2019). The dynein complex is comprised of two heavy chains, with N- terminal and C- motor domain, which are associated with intermediate, light intermediate and light chains (De Vos *et al*, 2008). The heavy chains are involved in the ATP hydrolysis and microtubule binding while the cargo binding is achieved via the other chains which also bind to a co-factor named dynactin (Olenick & Holzbaur, 2019).

Axonal cargo

Axonal cargo, as mentioned above, can be transported either in the anterograde or retrograde direction or bi-directionally. Certain adaptor proteins can recruit kinesin or dynein to specific cargo. Kinesins can bind to different cargo either by directly binding to the cargo binding domain or via kinesin light chain (KLC) or adaptor proteins. The various cargoes that have been identified in anterograde axonal transport are membranous organelles including synaptic vesicle components, ion channels, adhesion molecules as well as organelles such as mitochondria and lysosomes (Guillaud *et al*, 2020).

1.3 Kinesin 1 superfamily

The first kinesin identified is the kinesin 1 (previously called conventional kinesin or KIF5) superfamily. It is the most abundant motor and it is an N-kinesin thus the motor domain is located at the N-terminus, powering the anterograde transport towards the plus end of the microtubules and the axon terminal. Unlike some other kinesins it is found in dimers and in some cases, tetramers composed by two kinesin heavy chains (KHCs) and two KLCs. In mammals, after gene duplication, there are three KHCs identified, KIF5A, KIF5B and KIF5C (Hirokawa & Noda, 2008).

Structure

As already mentioned, kinesin 1 contains three main domains, the motor (also called head), stalk and the cargo binding domain (tail). The motor domain contains the nucleotide (ATP) and the microtubule binding sites and it is highly conserved among the kinesin 1 subtypes, however they have different cargo binding domains. These two domains are linked via the stalk domain, which in the dimer state they form a coiled-coil stalk (Qin *et al*, 2020). The motor domain is linked to the stalk by a 14AA sequence which is called neck linker and it is important for the conformational changes required for the movement of kinesin 1 on the microtubules (Hancock, 2016) (Fig. 1.3).

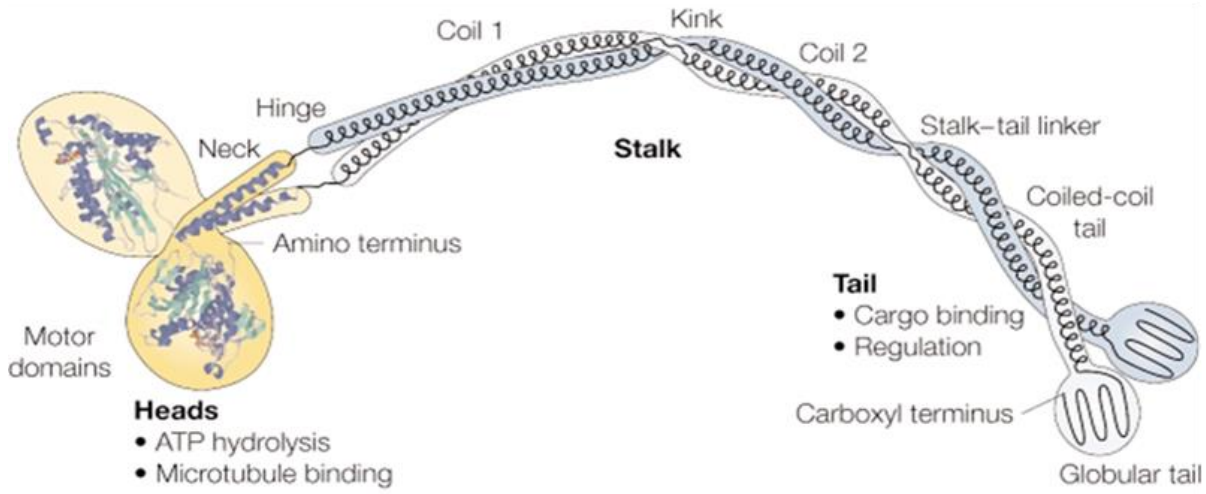

Figure 1.3: The different domains of kinesin 1 dimers and their role. *The catalytic motor domain contains the binding sites for microtubules and ATP and is relatively small in kinesins (in relation to dynein), the stalk domain, involved in dimerisation and the tail which is involved in cargo binding but also in regulation of the transport and the specificity of the cargo. The neck linker which has a key role in the walking process is also depicted [Image from Woehlke & Schliwa, 2000].*

Motor movement

More specifically, the movement is initiated by the docking of the neck linker to the motor domain upon sensing of the binding of ATP to the highly conserved motifs of the motor domain ATP pocket. This is achieved by conformational changes of the motifs which are interacting directly with ATP and enter a closed state, enclosing the ATP molecule. Each kinesin head hydrolyses one molecule of ATP which generates the energy required for the movement. The product of the hydrolysis, Pi leaves the pocket and the motor domain is in an ADP state. This in turn induces other conformational changes in the binding pocket which returns in its initial open state conformation (Qin *et al*, 2020). While the heads are in the open or closed conformation (with ATP or without ATP) but not the ADP state, they are strongly bound to the microtubules. The movement of the two heads of kinesin 1 can be explained by the hand-over-hand movement of the two heads (leading and trailing), that allows for kinesin to walk on the microtubules for several micrometres (Adio *et al*, 2006). After releasing of the Pi, the trailing head detaches from the microtubule (so only the leading head is attached) and passes the leading head by making a 16nm step and attaching on the next binding site of the microtubule. Studies have shown that the ATP is hydrolysed only when one head is bound on the microtubules so the movement is coordinated through these cycles of alternating ATP hydrolysis of the two heads (Isojima *et al*, 2016). Kinesin 1 can also pause when the microtubule path is blocked or crowded and it then either detaches or takes a side-step (Hancock *et al*, 2016).

Cargo binding & motor regulation

While the motor domain is responsible for the movement of kinesin on the microtubules, the adjacent stalk domain connects the head with the tail, dimerises the KHCs and allows for the motor protein to obtain the inactive-folded conformation, when not is not bound to a cargo, via a flexible structure, called kink (see Fig. 1.3). Upon cargo binding, kinesin remains in the active, non-folded conformation. The C-terminal domain or tail is a globular domain responsible for cargo binding but also for kinesin 1 regulation (Jeppesen & Hoerber, 2012). Cargo can bind either directly to the tail, via various adapter proteins or the KLCs, as already mentioned (Fig. 1.4).

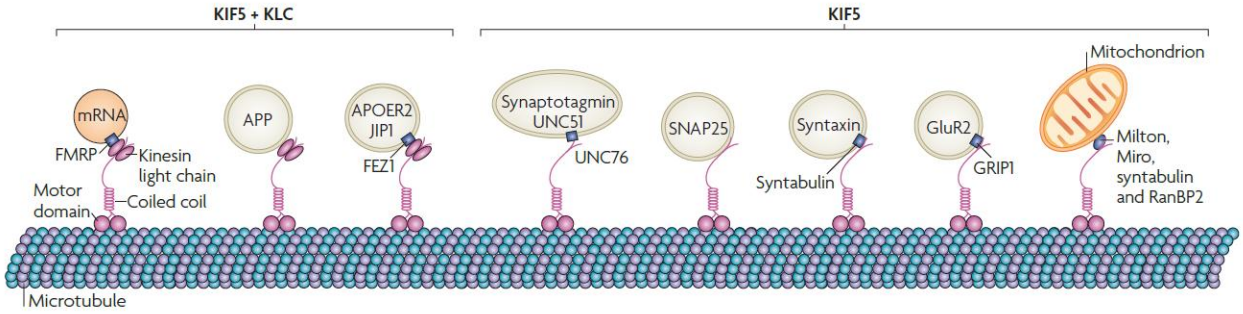

Figure 1.4: Kinesin 1 and cargo binding. *Kinesin 1 can bind cargo either through the kinesin light chain (KLC), their cargo binding domain or via adaptor proteins or protein complexes. Transported cargo include: the fragile X mental retardation protein (FMRP), β-amyloid precursor protein (APP), apolipoprotein E receptor 2 (APOER2), transported indirectly via KLC and synaptotagmin, soluble N-ethylmaleimide-sensitive factor attachment protein 25 (SNAP25), syntaxin, GluR and organelles such as mitochondria directly without KLC. Neurofilaments (not shown) are also a KIF5 cargo although the mechanism is not yet known [Image from Hirokawa et al, 2009].*

Kinesin regulation is important to prevent unnecessary ATP hydrolysis by the motor domain when cargo is not transported. Early studies have shown that motors have evolved auto-inhibitory mechanisms though an interaction of the tail with the motor domain (Coy *et al,* 1999) and inhibition of ADP release (Hackney & Stock, 2008) but also a direct binding of the tail with the microtubules has been detected (Dietrich *et al*, 2008). The region that plays an important role in auto-inhibition is a highly conserved nucleotide sequence QIAKPIRP in the cargo-binding domain (Figure 1.5B), also called IAK at position 919-926 of the human protein. Although the exact mechanism of IAK inhibition is not yet clarified, it is suggested that when kinesin is folded in half at the inactive, cargo-free state, the IAK motif could either directly prevent the interaction of the head with the microtubules or induce a conformational change that achieves this inhibition (Hackney & Stock, 2020). A coiled-coil region of the stalk domain has also been shown to contribute to the inactive-state inhibiting the ADP release, suggesting a double lockdown mechanism (Kaan *et al,* 2011). Finally, microtubule post-translational modifications have also been shown to alter the affinity of the motor domain to tubulin thus regulating

the motor movement (Verhey & Hammond, 2009) such as histone deacetylase 6 (HDAC6) which deacetylates α-tubulin and inhibits transport (Rossaert & Van Den Bosch, 2020).

Activation of kinesin 1 is suggested to be the result of cargo binding to the tail which interrupts the interaction of the tail with the motor domain and also the KLCs or the adaptor proteins. KLCs have been shown to inhibit the microtubule tail binding, thus alleviating the inhibition of transport (Wong & Rice, 2010) as well as adaptor proteins have been recently shown to activate kinesin 1 (Fenton *et al*, 2021; Henrichs *et al*, 2020).

1.4 Kinesin 1 subtypes

KIF5A is the longest of the three kinesin 1 subtypes however they all have a high homology especially in the motor and stalk domain (Fig. 1.5). KIF5A and KIF5C are exclusively expressed in the brain and spinal cord. KIF5A shows a pan-neuronal expression, with similar levels in various neuron types and higher expression in the motor and sensory cortex (Kuzma *et al*, 2013). In neurons, KIF5C is expressed only in some subpopulations but at higher levels than KIF5A and is significantly enriched in motor neurons, whereas KIF5B is ubiquitously expressed, including neurons and glial cells. KIF5B, the most abundantly expressed of the three, showed high expression in the olfactory sensory neurons and is upregulated in the neurons during the axonal elongation stage (Kanai *et al*, 2000). So, while KIF5B shows a predominantly glial expression and KIF5C is expressed in a subset of neuronal types, KIF5A expression is pan-neuronal and is localised in the cell soma, dendrites and axons (Reid *et al*, 2002).

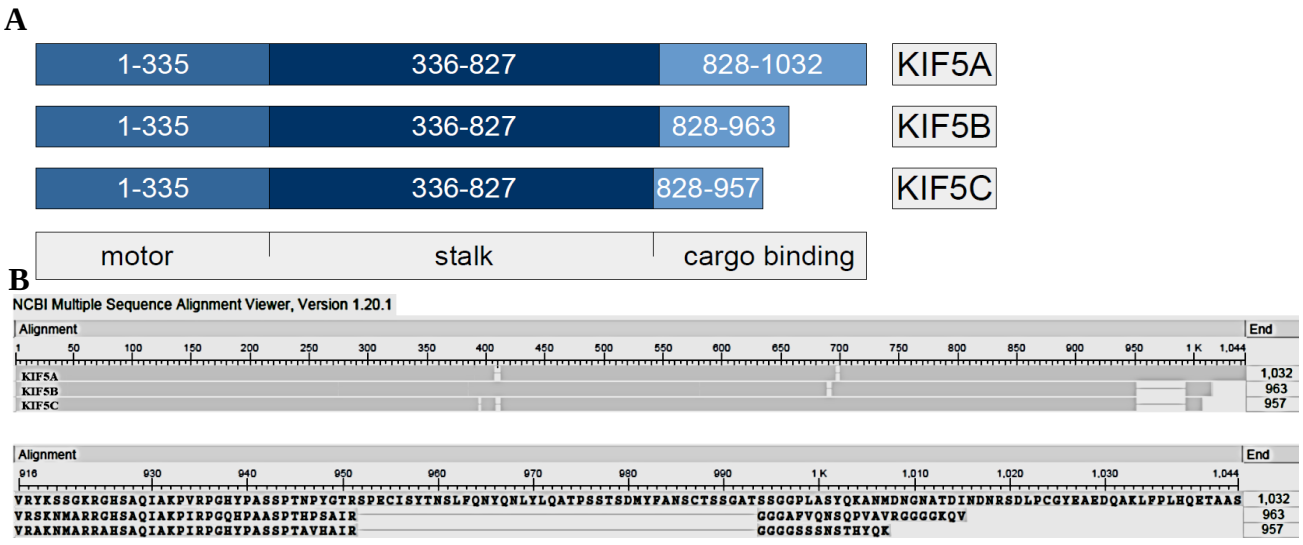

Figure 1.5: A. *The three subtypes of human kinesin 1 protein, KIF5A, B and C and their basic domains.* ***B.*** *Full protein and cargo binding domain alignment of the 3 KIF5s. The motor and stalk domains are highly conserved among all three KIF5s. The KIF5A cargo binding domain is longer, however they all share some regions, for example the highly conserved IAK motif at 919-926aa.*

Although there seems to be a functional redundancy between the three kinesins 1, the differential distribution and expression in various cells types and in different developmental stages as well as the different cargo binding domains have been suggested to play a role in their unique functions (Campbell *et al,* 2014; Kanai *et al,* 2000).

KIF5A is the only kinesin 1 associated with neurodegenerative diseases. Kif5B-/- mice are embryonical lethal and in-vitro studies showed a perinuclear accumulation of mitochondria in null cells (Tanaka *et al,* 1998), however neurodegenerative disease-causing *KIF5B* mutations have not been reported to date (Kalantari & Filges, 2020). *KIF5C* missense mutations in the motor domain are associated with neurodevelopmental abnormalities and structural congenital anomalies (Poirier *et al,* 2013), consistent with the increased Kif5C expression observed in MNs during development (Kanai *et al,* 2004).

1.5 Axonal transport defects and disease

As axonal transport is critical for the survival and maintenance of neurons early observations have linked the inhibition of fast transport with neurodegeneration. In many cases this follows a dying-back pattern where the axons start to degenerate from the distal part and the synapse and progressively affect the rest of the axon towards the cell soma (Morfini *et al,* 2012). Indirect evidence of defective axonal transport is the accumulation of various organelles and proteins, a hallmark in many neurodegenerative diseases (De Vos *et al,* 2008). For example, Tau accumulations in Alzheimer's disease (AD) and α-synuclein in Parkinson's disease (PD) and also, early indirect evidence in ALS have shown an abnormal accumulation of hyperphosphorylated neurofilaments and organelles such as mitochondria in the proximal axon of motor neurons. Axonal transport defects are found to precede neurodegeneration (Bisland *et al,* 2010) and thus it has been suggested that axonal transport defects could be the cause and not the consequence of neurodegeneration (Morfini *et al,* 2012).

This hypothesis is further supported by genetic evidence. An increasing number of mutations have been detected in various components of the transport machinery and are shown to be associated with neurodegeneration (Table 1.2).

Mutations in axonal transport machinery in motor neuron diseases				
Gene	Protein	Axonal transport defect	Cell type affected	Disease
KIF5A (SPG10)	Kinesin heavy chain isoform 5A	Anterograde transport-ATP production	UMNs (motor cortex) & LMNs (brainstem/spinal cord)	HSP, CMT, ALS
DYNC1H1 (CMT20)	Cytoplasmic dynein 1 heavy chain 1	Dynein binding-unknown mechanism	Motor & sensory neurons	CMT
SPG11 (ALS5)	Spatacsin	Reduced tubulin acetylation/ microtubule instability	Motor neurons	HSP, ALS
SOD1	Superoxide dismutase 1	Neurofilament phosphorylation- impaired binding of motor proteins	UMNs (motor cortex) & LMNs (brainstem/spinal cord)	ALS
FUS	Fused in sarcoma	Axonal transport of vesicles & mitochondria	UMNs (motor cortex) & LMNs (brainstem/spinal cord)	ALS
TARDBP	TAR DNA binding protein 43 (TDP-43)	Axonal transport of mRNP granules	UMNs (motor cortex) LMNs (brainstem/spinal cord)	ALS, FTD
C9orf72	Chromosome 9 open reading frame 72	Axonal transport of vesicles & mitochondria	UMNs (motor cortex) LMNs (brainstem/spinal cord)	ALS

Table 1.2: *Selected genes whose mutations have been associated with MNDs [Compiled with information from Guo et al, 2019].*

1.6 Motor neuron diseases (MNDs)

Axonal transport defects have been better characterised in MNDs since these affect the motor neurons which are heavily dependent on axonal transport. These disorders include amyotrophic lateral sclerosis (ALS), spinal muscular atrophy (SMA), primary lateral sclerosis (PLS) and hereditary spastic paraplegia (HSP) (De Vos *et al*, 2012). Although there are clinically and genetically distinct, they do share some important features such as axonal transport and RNA processing defects that result in the characteristic motor neuron vulnerability (Fig. 1.6) (James & Talbot, 2006).

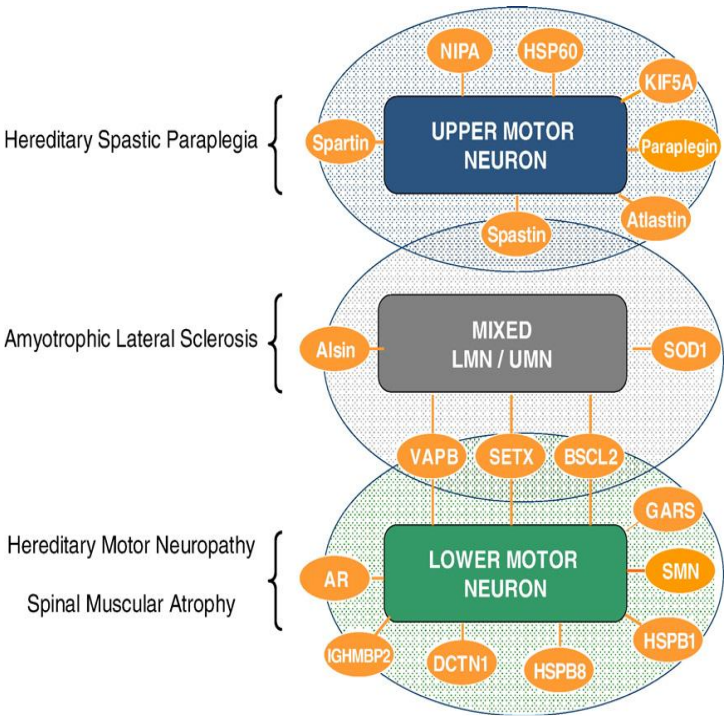

Figure 1.6: *Genetic and phenotypic overlap in MNDs. LMN: lower motor neuron, UMN: upper motor neuron [Image from James & Talbot, 2006].*

1.7 SMA

Spinal muscular atrophy is the most common fatal MND in children, affecting 1 in 5,000-10,000 infants in Europe and has a carrier frequency of 1 in 50. It is inherited in an autosomal recessive pattern and is caused by loss of the survival motor neuron (SMN) protein (Prior *et al,* 2000). SMA is characterised by the progressive degeneration of the lower motor neurons of the anterior horn of the spinal cord resulting in muscle weakness and atrophy, mainly affecting the lower extremities (Wirth *et al,* 2020).

Clinical presentation

Due to the vast clinical heterogeneity of the disease, there has been an attempt to categorise SMA into different subtypes, according to the presenting phenotype and age of onset (Table 1.3). However, after the genetic characterisation of the disease it is apparent that the phenotypic spectrum is more of a continuum rather than distinct subtypes (Prior *et al*, 2000).

	SMA 0	SMA I	SMAII	SMA III	SMA IV
Age of onset	prenatal	<6 months	6-18 months	>18 months	adult
Lifespan	<< 6 months	8-10 months	~ 25 years	normal	normal
Major clinical features	Reduced in utero movement Severe hypotonia/ weakness Respiratory distress/ failure	Muscle weakness Lack of motor development Severe respiratory muscle weakness Bradycardia	Poor muscle tone Slow decline in motor function Scoliosis Progressive respiratory muscle weakness	Proximal muscle weakness Loss of motor skills Fatigue	Fatigue Proximal muscle weakness

Table 1.3: *Clinical classification of SMA phenotype and major phenotypes [Compiled with information from Prior et al, 2000].*

SMA genotype-phenotype correlation

The SMN region, located on 5q13.2, has a very complex organisation with repetitive sequences, deletions/duplications and pseudogenes and contains two *SMN* genes in tandem, *SMN1* (telomeric) and *SMN2* (centromeric copy) (Biros & Forrest, 1999; Lefebvre *et al,* 1995). Most humans have one or more copies of the *SMN2* gene, which is absent in other species. Both genes share 99.9% of their sequence and can encode for a 294aa full length protein. However, while *SMN1* encodes for a full-length 294aa protein (SMN1) only a small percentage of *SMN2* produces the full-length, functional protein and due to alternative splicing, it encodes for a shorter protein lacking exon 7 (SMN2) (Fig. 1.7) (Prior *et al,* 2000). SMN2 is unstable and not fully functional and thus prone to get degraded (Wirth *et al,* 2020).

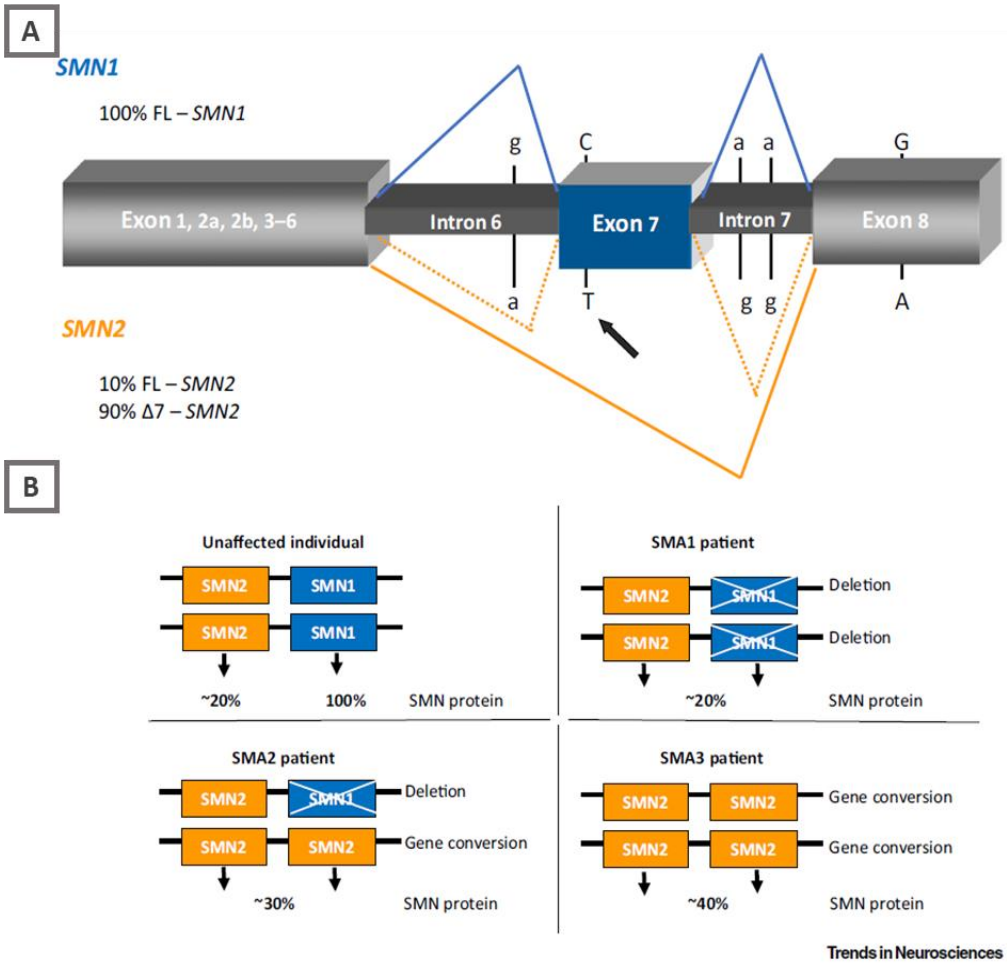

Figure 1.7: SMN genes and splicing in SMA types. A. *The SMN1 gene and the splicing events that produce the normal full-length SMN1 protein (blue) and SMN2 gene that produces the Δ7 SMN2 protein by alternative splicing (orange). The two genes differ by 5 nucleotides. The c.840C>T variant at position +6, indicated by an arrow, destroys an exonic splicing enhancer and instead creates an exonic splicing silencer in SMN2. This allele also produces a small amount (~10%) of FL SMN protein.* ***B.*** *Healthy individuals have two copies of SMN1 and two copies of SMN2 genes. Deletion or gene conversion mechanisms lead to different amounts of SMN protein and different types of SMA and disease severity [Image from: Wirth et al, 2020].*

An homozygous deletion of the *SMN1* gene accounts for the 95% of SMA cases and the rest is due to a small deletion, splicing or missense mutation (Burghes & Beattie, 2009). Genetic diagnosis can be sought, usually following a positive newborn screening on died blood spots, which detects the most common deletion in *SMN1*. Genetic diagnosis is reached by *SMN1* dosage analysis of exon 7 and additional sequencing for point mutations if required. Also, as SMN2 can significantly ameliorate the phenotype, (Table 1.4) prognostic tests to measure SMN2 levels can also be conducted (Mercuri *et al*, 2018).

SMN2 genotype phenotype correlation			
SMN2 copy number	**SMA I**	**SMAII**	**SMA III/IV**
1	96%	4%	0%
2	79%	16%	5%
3	15%	54%	31%
4	1%	11%	88%

Table 1.4: *SMN2 as a genetic modifier of disease severity in SMA patients [Compiled with information from Prior et al, 2000].*

SMN protein & tissue specificity

SMN, which is as already mentioned ubiquitously expressed, is essential for all cells and its complete loss is embryonically lethal (Thelen & Kye, 2020). A recent post-mortem study revealed that the highest SMN levels in the spinal cord are observed during embryogenesis and significantly decrease postnatally. This demonstrates the significance of SMN in early motor neuron development (Ramos *et al,* 2019).

The reduced levels of SMN1 (~20-40%) observed in SMA patients have been associated with selective defects in lower motor neurons and dying-back axonopathy at the neuromuscular junction (NMJ) and also degeneration and loss of motor neurons in the spinal cord and the brainstem nuclei (Donlin-Asp *et al,* 2017). Whether NMJ defects precede MN loss is still controversial, nevertheless there are significant NMJ defects observed such as in synaptic vesicles transport and acetylcholine clustering (Wirth *et al,* 2020).

The reason for the selective degeneration of motor neurons still remains unclear but also why some motor neurons are more susceptible than others to cell death in SMA. It has been suggested that this could be due to different tissue- or cell-specific splicing pattern (Wirth *et al,* 2020). Also, it has been observed that SMA is characterised by an acute phase when there is an extensive loss of MNs with notably low SMN levels and a chronic stage with some MNs with higher SMN levels being able to survive, adding to the observed heterogeneity of SMN and SMA (Rodrigues-Muela *et al,* 2017). Another hypothesis for the selective degeneration is that SMN, which is found to be actively transported along the axons (Zhang *et al,* 2003), is mislocalised and thus defects in axonal transport could contribute to the pathogenesis (Bricceno *et al,* 2012).

Although the lower motor neurons are primarily affected in SMA, non-neuronal populations have also been found to be associated with the disease. These include cells of the CNS (astrocytes, microglia and sensory neurons) but also non-CNS cells (heart, Schwann and muscle cells) (Simone *et al,* 2016).

SMN protein & function

SMN is a small, 38kd RNA binding protein highly conserved protein among higher vertebrates (Singh *et al,* 2017). It has four main domains, the lysine-rich domain, the Tudor domain, a proline-rich and the YG-box domain (Figure). The lysine-rich domain is responsible for self-association and binding to Gemin2 and forming the SMN-Gemin2 complex, an important SMN functional complex. The Tudor domain which has homology with other Tudor domains and is usually found in proteins involved in

RNA metabolism, binds to Sm proteins as well as other proteins. The Pro-rich sequence is involved in actin dynamics and the YG-box as well as part of exon 7 is responsible for self-oligomerisation of SMN, crucial for its localisation in the different cellular compartments (Burghes & Beattie, 2009).

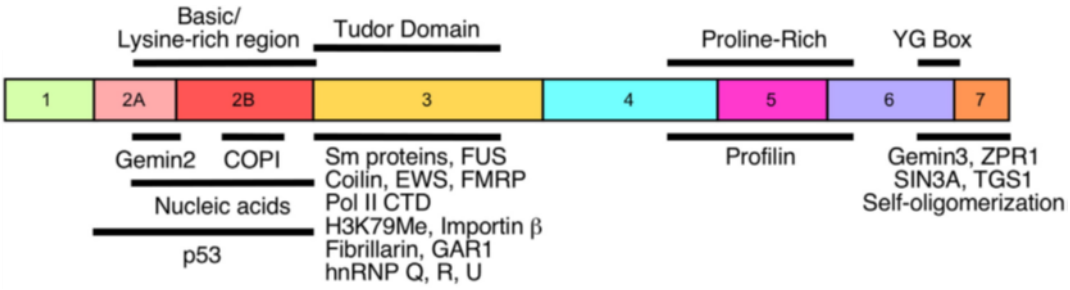

Figure 1.8: SMN protein domains. *The different SMN domains are shown above and the corresponding proteins that are associated with these domains are shown below the boxes. Numbers indicate exons. Of note are the N-terminal Gemin-2 and nucleic acids-binding domains, the central Tudor domain and C-terminal proline-rich and the YG box. Mutations in all domains have been associated with SMA [Image from Singh et al, 2017].*

SMN localises in the cytoplasm and the nucleus of all cells and is found to interact with a large number of proteins and involved in several different pathways (Burghes & Beattie, 2009). In the nucleus it is localised in the Cajal bodies or gems (gemini of Cajal bodies) (Fallini *et al*, 2012). Specifically in the motor neurons, as shown in Figure 1.9, SMN is localised in the cell soma, the axon and axon terminals at the NMJ with distinct roles in small nuclear ribonucleoprotein (snRNP) biogenesis and assembly, axonal transport and local translation respectively (Jablonka & Sendtner, 2017).

snRNP biogenesis & assembly

The most well studied function of the SMN protein is its involvement in the snRNP assembly by the SMN-Gemin-Unrip complex (Burghes & Beattie, 2009). Spliceosomal snRNPs are part of the splicing machinery responsible for mRNA splicing. Each snRNP is a complex of one or two uridine-rich small nuclear RNA (snRNA) (U1, U2, U4, U5, U6, U11, U12, U4atac, U6atac), seven Sm proteins and several other proteins specific for each snRNP. An SMN complex with gemins 2-8 and UNR interacting protein (Unrip) chaperons the snRNAs as they are exported from the nucleus into the cytoplasm where each of them binds to the set of the 7 Sm proteins and form the snRNPs. The snRNPs recognise splicing sites and catalyse the intron removal of the pre-mRNA (Chaytow *et al*, 2018; Battle *et al*, 2006). More specifically, studies in mice have shown that in absence of SMN the snRNP assembly is reduced and this reduction is correlated with disease severity. SMN is also shown to play a role in the assembly of other RNPs although these mechanisms are not thoroughly studied (Chaytow *et al*, 2018). Lack of SMN is shown to result in an accumulation of mis-spliced transcripts, including proteins that bind to Ca^{+2} and consequently disturb calcium homeostasis, especially in the NMJ, a major hallmark in SMA (Wirth *et al*, 2020).

Despite the contribution of the effects of mis-splicing in SMA phenotype, the housekeeping role of SMN in splicing alone cannot explain the observed selectivity of the motor neuron impairment in SMA. One explanation could be that mis-splicing of some proteins could have a more detrimental effect on MNs than other types of cells. Expression and splicing studies have tried to establish the effect of SMN levels on the expression of several genes, although this correlation is still controversial. It has also been shown that general mis-splicing events mostly occur during the late stages of the disease. Therefore, an additional role of SMN in MN specific pathways is more likely (Chaytow *et al*, 2018). These roles include an SMN involvement in local translation, translation defects and axonal RNA transport with recent studies focusing on the axonal localisation and role of SMN (Wirth, 2020).

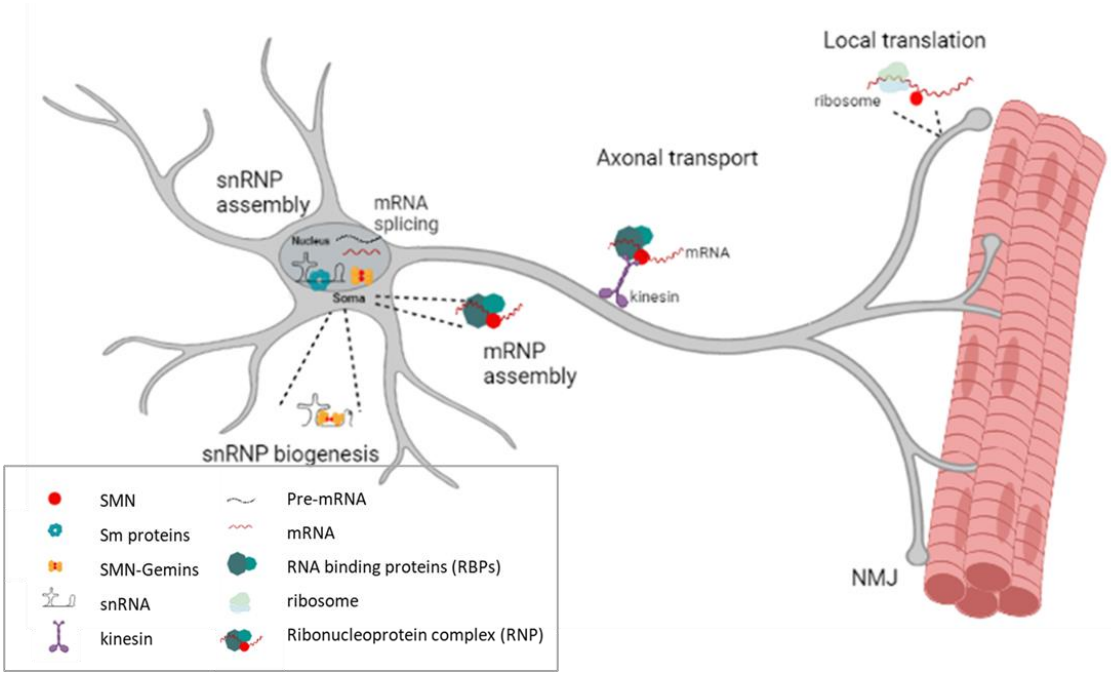

Figure 1.9: The main SMN protein functions. *SMN is physiologically mostly found as a part of a complex. Its main nuclear roles involve the snRNP biogenesis and mRNA splicing however it is also involved in the mRNP granule assembly and transport along the axons via kinesin in order for mRNA to be locally translated in the axonal compartment [Image created in BioRender.com].*

Axonal transport & local translation

We now know that there is ribosome-bound mRNA in axons, constituting the axonal transcriptome, whose local translation plays an important role in synapse transmission and survival and is associated with neurodegenerative diseases (Khalil *et al,* 2018). Indeed, studies have shown that axons and dendrites have a different transcriptome than the soma and this is suggestive of local translation, independent of the cell soma, of different sets of mRNAs that are supplied in different cellular compartments. Therefore, transport and localisation of the mRNA seems to play an important role in axonal homeostasis and this is achieved by the binding affinity of RBPs for kinesin and facilitated by adapter proteins and molecular chaperons (Khalil *et al*, 2018).

Moreover, apart from the well-established role of SMN in the nucleus and the cell soma, more recent studies placed SMN also at the axonal and dendritic compartment, suggesting that SMN is actively transported in axons (Pagliardini *et al,* 2000). Indeed, in vitro and in vivo studies have confirmed not only that SMN is localised in the axons and axon terminals (Dombert *et al,* 2014), but it is actively transported along the axons (Zhang *et al,* 2003) acting as a molecular chaperon for messenger RNPs (mRNPs) (Donlin-Asp *et al,* 2017).

Studies on induced pluripotent stem cell (iPSC) derived motor neurons from SMA patients have reported reduced axonal elongation and smaller growth cones at late stages of differentiation (Boza-Morán *et al,* 2015). More specifically, it has been suggested that SMN localisation gradually shifts during neurodevelopment from primarily nuclear to cytoplasmic/axonal (Giavazzi *et al,* 2006) with exon-7 playing a crucial role in the cytoplasmic localisation in neurons (Zhang *et al,* 2003). In axons, SMN also colocalises with Gem2, however the SMN complex seems to be different in composition than the nuclear one (Fallini *et al,* 2011). Live imaging experiments showed that the SMN/Gem2 complex is actively transported as well as SMN granules at a rate consistent with fast, microtubule-based axonal transport (>1micron/sec) (Donlin-Asp *et al,* 2016). SMN can bind directly to mRNAs or indirectly, via RNA-binding proteins (RBPs) and transports the mRNAs along the axons in order to be locally translated (Thelen & Kye, 2020).

Further colocalization experiments have identified a number of different RBPs and mRNAs that interact with SMN (Thelen & Kye, 2020). Several poly-A tailed mRNAs have been found to be transported by SMN, such as β-actin and growth-associated and protein 43 (Gap43) (Donlin-Asp *et al,* 2017; Fallini *et al,* 2014; Zhang *et al,* 2003). In addition, β-actin mRNA (but not protein) is downregulated in growth cones of SMA mice and in general there is a 50% reduction in the mRNA transcripts localised along the axons with SMN knockdown (Chaytow *et al,* 2018).

A similar reduction in mRNA-binding proteins HuD, Igf2-mRNA binding protein 1 (IMP1) and also plastin3 (PLS3) with a role in neuronal development is also detected in axons (Donlin-Asp *et al,* 2016; Boza-Morán *et al,* 2015). HuD, a neuron specific mRNA-binding protein with a role in neuronal development, is shown to interact and be co-transported with SMN (Fallini *et al,* 2011) and IMP1, important for mRNA localisation is also interacting with SMN (Donlin-Asp *et al,* 2017). The SMN/HuD/IMP1 complex has been implicated in β-actin and Gap43 mRNA trafficking and translation as well as another SMN interactor, hnRNP-R and -Q, also implicated in mRNA processing and transport in neurons have been identified (Dombert *et al,* 2014; Rossoll *et al,* 2002). Finally, there are many other proteins interacting with SMN such as FMRP, FUS and TDP-43 and this interaction has linked SMN to ALS (Thelen & Kye, 2020).

To summarise, there are accumulating evidence of SMN localisation in axons where it interacts with RNA granules that are actively transported along the axons. Although the exact mechanisms of SMA transport defects are not yet fully characterised, it seems that SMN is required for correct mRNP assembly and transport (Khalil *et al*, 2018).

SMA treatments

During the past decade there have been significant advances in treatment but also therapeutical interventions for SMA patients (Fig. 1.10). The main strategies focus on targeting SMN either with splicing correction with antisense oligonucleotides and small molecules or gene replacement (Wirth 2020).

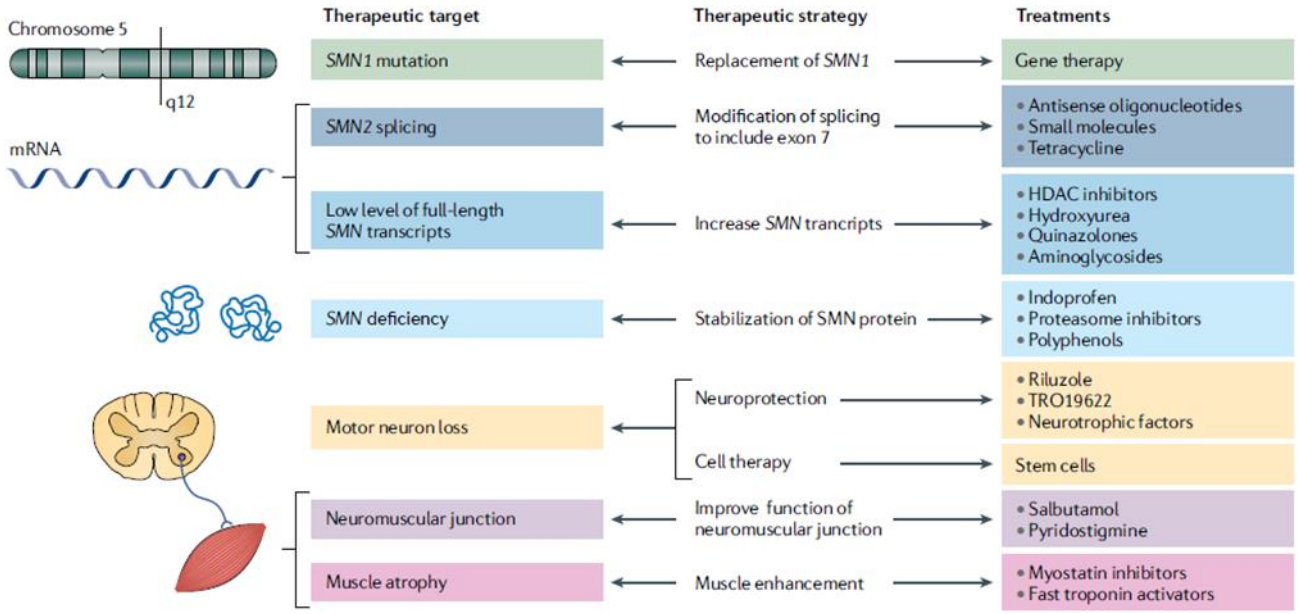

Figure 1.10: Current therapeutic targets, strategies and treatments. *SMN enhancing strategies either by viral gene therapy or by correcting SMN2 splicing with antisense oligonucleotides or small molecules are the most successful approaches. Other strategies targeting the neuronal and muscular symptoms of SMN loss are also tested in combination with SMN enhancing therapies [Image from Mercuri et al, 2020].*

Currently there are 3 FDA approved drugs for SMA: nusinersen (Spinraza), Adeno-associated virus serotype 9 (AVXS-101) (Zolgensma) and risdiplam (Evrysdi) which are all SMN enhancing therapies. Nusinersen is an antisense oligonucleotide targeting the intronic splicing silencer N1 (ISS-N1) which promotes the inclusion of exon7 of *SMN2* thus enhancing the production of the full length, functional SMN protein. AVXS-101 is a gene therapy treatment which delivers one or more copies of SMN1 via the adeno-associated viral vector, AAV9 and risdiplam is a small molecule that specifically promotes the inclusion of exon7 of *SMN2*. Nusinersen, the first drug approved in 2016, showed a favourable effect in all ages and types of SMA and it is the only one currently administered regardless of age and disease severity. In general, these treatments are age and severity dependent with most favourable

results in presymptomatic and less severely affected patients. Clinical trials with both SMN and non-SMN targeting treatments in various SMA types and ages are ongoing and results are expected regarding also combination treatments (Mercuri *et al*, 2020).

1.8 ALS

ALS is the most common adult-onset MND with a prevalence between 4.1-8.4 in 100,000 (Longinetti & Fang, 2019). It is characterised by a selective degeneration of upper and lower motor neurons and progressive atrophy of skeletal muscles resulting in paralysis and death within an average of 2-5 years after diagnosis. ALS shares genetic and clinical features with frontotemporal dementia (FTD) and there is evidence of other non-motor neuronal groups affected in some patients (Kim *et al*, 2020). Almost 10% of the ALS patients show a familial, mostly autosomal dominant pattern (familial ALS) while the sporadic type without a clear genetic component, accounts for the remaining 90% of ALS cases (Smith *et al*, 2019). The most common genetic cause of ALS is a hexanucleotide repeat expansion in Chromosome 9 open reading frame 72 (*C9orf72*), accounting for 40% of fALS, as well as mutations in superoxide dismutase 1 (SOD1), TAR DNA binding protein (TARDBP, TDP-43) and Fused in sarcoma (FUS) (Volk *et al*, 2018) (Table 1.5).

ALS genes					
Gene	**% of fALS**	**Inheritance**	**Onset/penetrance**	**Other associated phenotypes**	**Potential effect on axonal transport**
C9orf72	39-45%	AD	50% by 58 yrs 100% by 80 yrs	FTD, PLS, Parkinsonism, chorea, psychiatric features	Mitochondrial transport defects
SOD1	15-20%	AD, AR	50% by 46 yrs 90% by 70 yrs	-	Defects in mitochondrial transport, microtubule stability, modulation of motor proteins
FUS	4-8%	AD	50-70% by 51 yrs >90% by 71 yrs	FTD, Parkinsonism	Defects in mitochondrial transport & microtubule acetylation
TDP-43	1-4%	AD	53.5 ±12 yrs	FTD	Defects in mitochondrial & mRNP granule transport, microtubule stability/ acetylation dynactin 1 downregulation

Table 1.5: The most common disease-causing genes in ALS and their major characteristics. *Axonal transport defects and specifically mitochondrial is a common feature in all ALS types. AD: autosomal dominant, AR: autosomal recessive [Compiled with information from: Volk et al, 2018; de Vos & Hafezparast, 2017; Siddique & Siddique, 2001 (last revision 2021)].*

To date variants in more than 25 genes have been associated with ALS, most presenting with a dominant inheritance pattern and a gain-of-function mechanism. Although fALS is monogenic, recent observations of co-occurrence of ALS/MND associated mutations/variants and incomplete penetrance in ALS patients, have led to the suggestion that there could be a more complex, digenic or oligogenic mode of inheritance (Brenner *et al,* 2018; van Blitterswijk *et al,* 2012). The affected pathways are various, including RNA toxicity, disruption of proteostasis, mitochondrial defects and axonal transport impairment (Kim *et al,* 2020; Smith *et al,* 2019).

Current treatment options for ALS are not curative. Antisense oligonucleotides (ASOs) and viral-directed gene delivery strategies hold promising results for monogenic diseases and can be beneficial as personalised treatment in fALS types as well as drugs targeting common pathways in sporadic cases. It has been recently pointed out that although GOF mechanisms are driving ALS, LOF also contributes to disease and thus future therapies need to take into consideration the mutation mechanism. Therefore, next-generation therapies are combination therapies that aim to target both GOF and LOF (Kim *et al,* 2020).

ALS and axonal transport defects

Early indirect evidence of axonal transport impairment in ALS have shown an abnormal accumulation of hyperphosphorylated neurofilaments and organelles such as mitochondria in the proximal axon of motor neurons and after the development of the SOD1G93A mouse model there are direct evidence of axonal transport impairment and the implication of kinesins in the pathology (Burk & Pasterkamp, 2019). Live imaging experiments have shown a reduction of the anterograde transport of mitochondria in vitro in several SOD1 mutations but also in vivo in ALS mouse and rat models (Magrané *et al,* 2014; Bilsland *et al,* 2010). Moreover, recent studies have shown that KIF5A, but not KIF5C, expression is significantly decreased in the spinal cord of SOD1 mice (Maniatis *et al,* 2019).

ALS causing mutations in FUS and TDP-43 have also been shown to result in axonal transport defects and reduced mitochondrial motility. Transport of FUS RNA granules is dependent on kinesin and other RNA transport-related proteins such as TDP-43 and SMN and it has been shown that SMN and kinesin 1 mRNA and protein are found in FUS-inclusions leading to decreased axonal localisation of SMN (Groen *et al,* 2013) and misdistribution of mRNA (Yasuda *et al,* 2017). Finally, *C9orf72* repeat expansions lead to defects in mitochondrial transport and there is also evidence of RNP axonal mislocalisation (Khalil *et al,* 2018; De Vos & Hafezparast, 2017).

1.9 KIF5A & MNDs

KIF5A mutations in ALS

The latest genome wide association study (GWAS) in ALS in Caucasian population identified *KIF5A* as a causative gene (Nicolas *et al*, 2018) with an independent study replicating the results (Brenner *et al*, 2018). The two studies revealed a mutational hotspot in the C-terminal domain of the gene (Table 1.6). These mutations affect the C-terminal exons 26 and 27 and specifically four different mutations were shown or predicted to affect the splicing of introns 26 or 27 resulting in exon 27 skipping, frameshift and thus a longer aberrant protein p.(Asn999Valfs*39).

KIF5A variants	Position	Predicted consequence	RT-PCR validation
c.2987delA	exon 26	p.Asp996fs	-
c.2989delA	exon 26	p.Asn997fs	-
c.2993-3C>T	intron 26	5' splice junction	-
c.2993-1G>A	intron 26	-	mRNA not detected
c.2996delA	exon 27	p.Asn999fs	-
c.3019A>G	exon 27	p.(Arg1007Gly)	p.Asn999Valfs*39 mRNA
c.3020G>A	exon 27	p.Arg1007Lys	-
c.3020+1G>A	intron 27	**p.(Asn999Valfs*39)**	p.Asn999Valfs*39 mRNA
c.3020+2T>C	intron 27		mRNA not detected
c.3020+2T>A	intron 27	3' splice junction	p.Asn999Valfs*39 mRNA
c.3020+3A>G	intron 27		-

Table 1.6: *Variants in KIF5A in familial & sporadic ALS patients, reported by Brenner et al, 2018; Nicolas et al, 2018. RT-PCR of patients peripheral blood or lymphoblasts for 3 mutations confirmed the presence of the p.Asn999Valfs*39.*

KIF5A mutations in the Asian population were also reported to account for 0.16%-0.41% of sporadic ALS in China (Zhang *et al*, 2019). An additional Japanese study of sporadic ALS patients has also recently confirmed the presence of the c.2993-3 C>A splice variant resulting in the same aberrant protein p.Asn999Valfs*39 (Nakamura *et al*, 2021). In all three populations more than 10 *KIF5A* mutations were reported (Fig. 1.11), all in a 36bp region in the cargo binding domain and resulting in the loss of the normal C-terminal sequence and a longer, aberrant protein. Many KIF5A patients presented with a typical (for each population) ALS phenotype however Nicolas *et al* reported an earlier age of onset and a longer survival and therefore the genotype-phenotype correlation is not clear at this stage (Zhang *et al*, 2019).

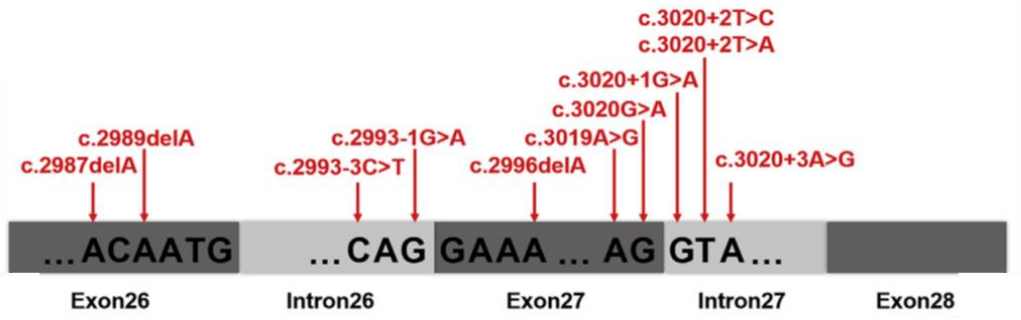

Figure 1.11: *The mutational hotspot in the KIF5A C-terminal domain associated with ALS [Image from Zhang et al, 2019].*

The two initial studies by Brenner and Nicolas *et al* also identified a benign KIF5A variant, the rs113247976 as the most frequent genetic factor contributing to ALS (3.40% in fALS). It has a reported allele frequency of 1.13% in gnomAD dataset (in healthy individuals) and has been detected mainly in combination with other monoallelic mutations in ALS genes (38% of fALS). Therefore it could be a risk factor for ALS hypothesised to lower the threshold for phenoconversion in carriers of additional ALS gene mutations and incomplete penentrance mutations (Brenner *et al*, 2018). This hypothesis is consistent with an oligogenic mode of inheritance that has been suggested for ALS (van Blitterswijk *et al*, 2012). The molecular mechanism, however, of these novel ALS *KIF5A* mutations is unclear.

1.10 Genotype-phenotype correlation in *KIF5A* mutations

Different types of *KIF5A* mutations (missense, non-sense, splicing, frameshift) have been reported in all three domains of the gene and the site of mutation seems to dictate the phenotype (Fig. 1.12A). Motor and stalk domain mutations have been previously associated with HSP type 10 (SPG10) (Reid *et al*, 2002) and CMT type 2 (Crimella *et al*, 2012), two diseases characterised by anterograde neurodegeneration, as well as with atypical motor syndromes (Filosto *et al*, 2018).

HSP is a clinically and genetically heterogeneous disease presenting with lower limb spasticity and weakness of variable degree (pure HSP) but can be complicated with additional features such as cognitive impairment, dementia and seizures (Fink, 2013). The age of onset varies from early childhood to late 70s and mutations with variable penetrance in more than 80 genetic loci have been identified (SPG). Most of these genes however seem to affect the same pathways including axonal transport and the hallmark of all HSP types is a length-dependent distal axonal degeneration (Lo Giudice *et al*, 2014). HSP mutations in *KIF5A* are the second most common autosomal dominant HSP (AD HSP) with an estimated frequency reaching 10% of AD HSP and *KIF5A* mutations are found in

both pure and complicated types with a phenotypic spectrum from HSP to axonal Charcot-Marie-Tooth type 2 (CMT2). To date more than 30 HSP-CMT2 *KIF5A* misense mutations have been reported with the majority of them localising in the motor domain (26 mutations) and only 5 in the stalk domain (HGMD mutation database). Functional studies of HSP mutations revealed a loss or a significant impairment in microtubule binding and in motility/kinetics of transport and/or a reduced ATP hydrolysis, resulting in decreased cargo velocity (Jennings *et al,* 2017; Ebbing *et al,* 2008). These findings are consistent with the location of the mutations, the motor domain, which is responsible for the microtubule binding of KIF5A and ATP hydrolysis, as already discussed.

In contrast, mutations in the C-terminal are causative of ALS or neonatal intractable myoclonus (NEIMY), a severe congenital syndrome characterised by myoclonic seizures, with evidence of mitochondrial dysfunction (Rydzanicz *et al,* 2017; Duis *et al,* 2016). The three NEIMY mutations described to date c.2854delC, c.2934delG (Duis *et al,* 2016) and c.2921delC (Rydzanicz *et al,* 2017) are frameshift mutations, resulting in the same 14bp longer aberrant protein, predicted not to be degraded by NMD. The authors have hypothesised a defect in mitochondrial transport due to altered binding to the adaptor proteins TRAK1/TRAK2 (Rydzanicz *et al,* 2017) or altered binding of the GABAAR-associated protein (GABARAP) (Duis *et al,* 2016) could be the mechanism of the NEIMY mutations with a dominant-negative effect on the kinesin complex. GABARAP has been previously reported to preferentially bind in the final 73bp region of KIF5A but not in the other KIF5s (Nakajima *et al,* 2012).

The ALS mutations are suggested to be loss of function, disrupting the cargo binding, thus resulting in cargo accummulation in the cell soma and deficiency in axon terminals (Nicolas *et al,* 2018). Brenner *et al* linked the mutations in the N-terminal with HSP/CMT (ie milder phenotype) due to altered kinetics of transport and the mutations in the C-terminal domain with ALS/NEIMY (ie severe phenotype) due to altered binding of cargo, happloinsufficiency or dominant-negative effect of the aberrant protein.

However, two studies have reported two novel mutations in the C-terminal domain, a misense mutation c.2939C>T (p.A980V) and the first truncating mutation in KIF5A, c.2590C>T (p.R864*) (Chrestian et al, 2017; Lynch et al, 2016). Both these mutations are predicted to be deleterious with in silico tools (VEP, Mutation Taster) and they were detected in HSP patients (Fig.1.12).

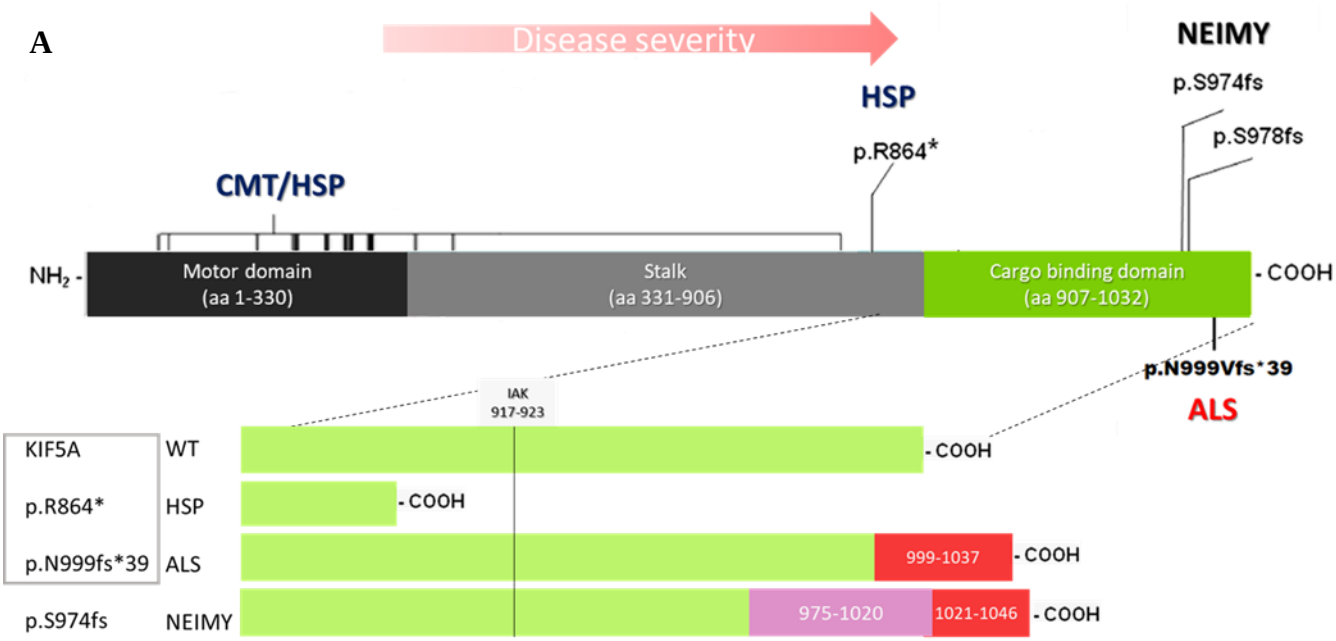

B

```
WT      TKVHKQLVRDNADLRCELPKLEKRLRATAERVKALEGALKEAKEGAMKDKRRYQQEVDRI   900
ALS     TKVHKQLVRDNADLRCELPKLEKRLRATAERVKALEGALKEAKEGAMKDKRRYQQEVDRI   900
NEIMY   TKVHKQLVRDNADLRCELPKLEKRLRATAERVKALEGALKEAKEGAMKDKRRYQQEVDRI   900
HSP     TKVHKQLVRDNADLRCELPKLEK*----------------------------------------863

WT      KEAVRYKSSGKRAHSAQIAKPVRPGHYPASSPTNPYGTRSPECISYTNSLFQNYQNLYLQ   960
ALS     KEAVRYKSSGKRAHSAQIAKPVRPGHYPASSPTNPYGTRSPECISYTNSLFQNYQNLYLQ   960
NEIMY   KEAVRYKSSGKRAHSAQIAKPVRPGHYPASSPTNPYGTRSPECISYTNSLFQNYQNLYLQ   960
HSP     ----------------------------------------------------------------------------------------

WT      ATPSSTSDMYFANSCTSSGATSSGGPLASYQKANMDNGNATDINDNRSDLPCGYEAEDQAKLFPLHQETAAS*  1032
ALS     ATPSSTSDMYFANSCTSSGATSSGGPLASYQKANMDNGVTCRVAMRLRTRPSFSLSTKRQQPANLPHPRLHTCTFSF* 1037
NEIMY   ATPSSTSDMYFANSVPAVEPHLLAAPWLPTRRPTWTMEMPQISMTIGVTCRVAMRLRTRPSFSLSTKRQQPANLPHPRLHTCTFSF*  1046
HSP     ----------------------------------------------------------------------------------------------------------
```

Figure 1.12: A. Schematic representation of KIF5A mutations. *The prevalent hypothesis is that mutations in the motor domain alter the kinetics of cargo transport, leading to a milder phenotype (HSP/CMT) and mutations in the cargo binding domain lead to altered cargo binding and a more severe phenotype (ALS/NEIMY). However, a truncating mutation upstream of the mutational hotspot of ALS has been reported and presented with an SPG10 phenotype. SPG10: spastic paraplegia type 10, NEIMY: neonatal intractable myoclonus* ***B. Protein alignments of representative C-terminal KIF5A mutations in different diseases****. In red is the sequence altered in the ALS mutation and in bold the NEIMY. The black box indicates the common altered protein sequence produced by both the ALS and NEIMY mutations. Note that in the case of the HSP mutation the IAK motif at position 919-921 is truncated.*

1.11 KIF5A & the mitochondrial transport complex

The KIF5A C-terminal domain is responsible for the transport of important cargoes, such as neurofilaments, an accumulation of which is a hallmark in ALS (Xia *et al*, 2003). Other cargoes include RNA granules and RBPs (Fukuda *et al*, 2020; Kanai *et al*, 2004), ALS associated proteins such as FUS, lysosomes (Pu *et al*, 2016), signalling endosomes, amyloid precursor protein (APP) vesicles, AMPA vesicles, GABAA receptors (Nakajima *et al*, 2012) and mitochondria mainly via the adaptor protein complex TRAK/Miro1 (Fig. 1.14) (MacAskill *et al*, 2009; Glater *et al*, 2006).

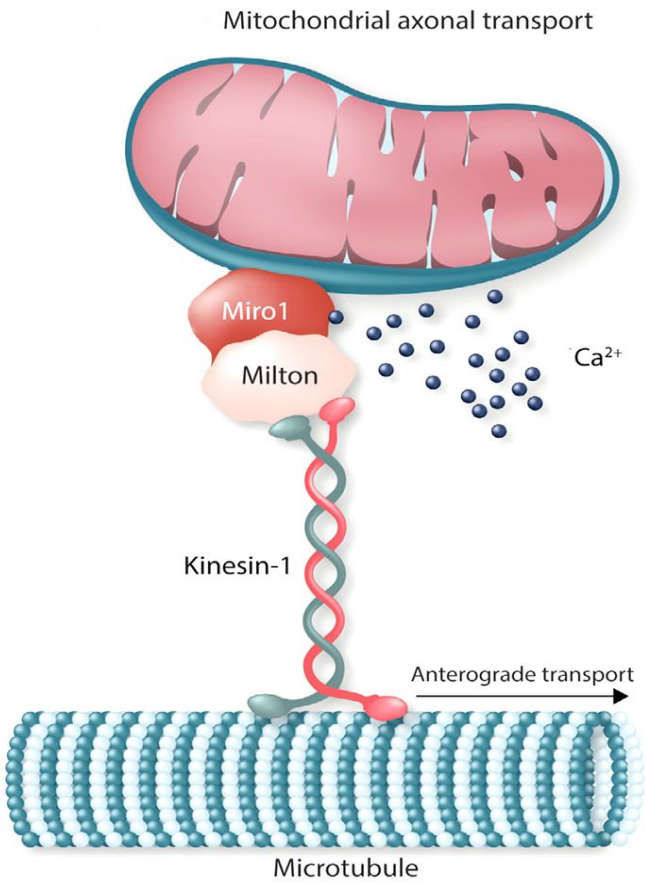

Figure 1.14: Kinesin 1 transports mitochondria through Miro1/Milton (TRAKs) in regions with low Ca^{+2} levels. Mitochondria are transported by all three KIF5s, KIF5A, B and C [Image adapted from Van Den Bosch, 2019].

The Rho GTPase, Miro1 (also named RHOT1), is an outer mitochondrial membrane protein that is the main regulator of mitochondrial transport in response to Ca^{+2} levels and mitochondrial damage. High Ca^{+2} levels inhibit mitochondria motility by binding to the Ca-sensing EF hand domains and it has been shown that mutations in these domains (E208K and E328K) inhibit the kinesin 1-Miro1 interaction (MacAskill *et al*, 2009; Guo *et al*, 2005). Miro1 is further regulated by PINK1/Parkin which are responsible for the dissociation of damaged mitochondria from kinesin and their subsequent clearance (Wang *et al*, 2011). Furthermore, Miro1 is found downregulated in SOD1 ALS by a PINK1/Parkin-dependent degradation mechanism (Moller *et al*, 2017). The Miro1-kinesin1 interaction is mediated by adaptor proteins TRAK/Milton (Fig. 1.14). Mammals have two TRAK orthologs, TRAK1 and 2 and both bind to kinesin 1 and KIF5A via their N-terminal and Miro1 via their C-terminal domain. Studies have shown that although the two TRAKs share a high genetic homology inferring redundant functions, they seem to regulate the mitochondrial distribution in a different manner; while TRAK1 functions as an adaptor in axons, with its depletion reducing axon growth, TRAK2 seems to preferentially regulate dendritic mitochondrial transport, with no effect when depleted (van Spronsen *et al*, 2012). In addition, the TRAKs are recently shown to act as activators, regulating kinesin 1 motility (Fenton *et al*, 2021; Henrichs *et al*, 2020).

A study on the specific binding sites of the two TRAKs to KIF5A with deletion constructs has shown that sequential deletions until the 877bp of the C-terminal didn't reduce the binding efficiency of TRAK1 but the deletion of the extended 826-1032bp region resulted in a significant reduction for TRAK1 and 2 binding. Interestingly, in contrast with TRAK1, TRAK2 showed a 70% increase in binding with KIF5A in the case of the 878-1032bp deletion (Randall *et al,* 2013).

1.12 Concluding remarks

The genetic aitiology and molecular mechanisms of MNDs are vastly heterogeneous, however mRNA splicing defects, transport and local translation seem to be a common theme (Fallini *et al,* 2011). A representative example of this is ALS and SMA, which show a remarkable molecular overlap with an increasing number of studies highlighting this surprising crossover (Cauchi *et al,* 2014). Firstly, there is a significant co-occurrence of ALS and SMA within families (Corsia *et al,* 2018). In addition, SMN levels have been found to be heterogeneous in motor neurons of both ALS and SMA patients, with low levels resulting in increased cell-death (Rodriguez-Muela *et al,* 2017). FUS and TDP-43 are shown to interact with the SMN-Gemins complex with the depletion of gems, directly correlated with reduced SMN, recently reported to be a hallmark not only of SMA but also ALS (Cauchi *et al,* 2014). SMN copy number has been extensively studied as an ALS modifier with conflicting results but a large recent study did not find a direct modifying effect of SMN1 and 2 in disease susceptibility/ severity. However, since the protein levels don't always correlate with SMN copy number, especially in the spinal cord, the authors could not exclude that low SMN levels could contribute to ALS (Moisse *et al,* 2021). Indeed, SMN overexpression seems to be beneficial in both diseases but although it reduced motor neuron loss, an effect on survival is not observed for both the ALS mouse models studied (Perera *et al,* 2016; Turner *et al,* 2014). In contrast, in both SOD1 and TDP-43 mice, there is an endogenous SMN upregulation but also a perinuclear clustering of SMN, pointing to a mislocalisation of SMN as a common pathway in ALS and SMA pathology. This mislocalisation could lead to SMN-deprived axons and it could suggest an axonal transport defect contributing to the limited beneficial effect of SMN upregulation in ALS (Perera *et al,* 2016; Turner *et al,* 2014). Lastly, mitochondrial damage and transport defects have been well established in several ALS types and models (Guo *et al,* 2017; Moller *et al,* 2017), however in SMA, although there are some reports (Xu *et al,* 2016), these defects, especially concerning mitochondrial transport, are poorly understood.

In addition, several studies have reported an association of KIF5A with Alzheimer disease susceptibility (Hares *et al,* 2019; Wang *et al,* 2019), the axonal transport deficits and neurodegenaration in multiple sclerosis (Hares *et al,* 2021) and finally a novel *KIF5A* mutation was recently associated with an adult onset distal spinal muscular atrophy (de Fuenmayor-Fernandez de la Hoz *et al,* 2019), although the clinical characterisation awaits further confirmation (Brenner *et al,* 2019). Nevertheless, this data is suggestive of a key role of *KIF5A* in neurodegeneration and MNDs.
As technical advances in the field of visualisation and tracking of axonal transport allow us to examine more thoroughly the contribution of axonal transport defects in neurological diseases, targeting those systems has arisen as an attractive therapeutic opportunity (Guo *et al,* 2019; De Vos & Hafezparast, 2017). The question whether a common strategy for addressing axonal transport defects could be beneficial for different types of MNDs is yet to be answered (Cacciottolo *et al,* 2020).

2. AIM

As already discussed, normal neuronal function is heavily dependent on the efficient transport of essential proteins and organelles along the axons via the kinesin/dynein system. Disruption of the axonal transport is a common feature of MNDs and can cause neurodegeneration (Guo *et al,* 2019). The most common MNDs, amyotrophic lateral sclerosis (ALS) and spinal muscular atrophy (SMA), although clinically and genetically distinct, they show a remarkable molecular overlap including mitochondrial transport defects (Cacciottolo *et al,* 2020). Familial ALS is caused by mutations in various genes affecting multiple pathways whereas SMA is monogenic, caused by insufficient SMN levels. Mitochondrial transport defects have been well established in several ALS types and models (Guo *et al,* 2017; Moller *et al,* 2017), however in SMA, although there are some reports (Xu *et al,* 2016), these defects are poorly understood. *KIF5A*, recently identified as a novel ALS gene (Nicolas *et al*, 2018), is responsible for the anterograde transport of various cargo including mitochondria, via the KIF5A/TRAK/MIRO1 complex and RNA granules (De Vos & Hafezparast, 2017). This study attempts to explore the potential involvement of KIF5A and the mitochondrial transport complex in a SMA mouse model and functionally characterise two *KIF5A* mutations in MNDs.

1. **Is KIF5A and the Miro1 complex involved in SMA?**
   Investigate Kif5a and Miro1 mRNA and protein levels in a SMA mouse model.
2. **Identify a potential therapeutic intervention to restore Kif5a levels.**
   Screen for potential microRNAs dysregulation in SMA mice.
   Investigate the effect of the identified microRNA on Kif5a expression in vitro.
   Validate microRNA interaction with Kif5a.
3. **Could SMN be a novel cargo of KIF5A?**
   Investigate potential co-localisation/ interaction of KIF5A with the axonal SMN complex in vitro.
4. **Functional study of two C-terminal *KIF5A* mutations reported in ALS & HSP.**
   Examine if the pathological mechanism of the *KIF5A* mutations in ALS and HSP could be caused by defects in the mitochondrial transport via altered binding with TRAK1.

3. MATERIALS/METHODS

3.1 Animals

Moderate Type II SMA (FVB.Cg-*Grm7*$^{Tg(SMN2)89Ahmb}$*Smn1*^{tm1Msd} Tg(SMN2*delta7)4299 Ahmb/J, Δ7 incipient congenic) mice from Jackson Laboratory (strain number 005025, Jackson Laboratories) were used as a SMA mouse model (SMNΔ7 mouse). The strain was maintained by breeding mice homozygous for the *SMN2* and *SMNΔ7* and heterozygous for the *Smn1* locus. Offspring, WT (S*mn*$^{+/+}$), heterozygous (S*mn*$^{+/-}$) or mutant (S*mn*$^{-/-}$) were genotyped at post-natal day 5, according to Jackson protocol (Valsecchi *et al*, 2020). Mice were deeply anaesthetized with 1.5% sevoflurane, and 98.5% of O_2 (Oxygen concentrator, Longfei industry Co, Zhejiang, China, Mod. LFY-I-5) and sacrificed at p5 or p10-12. Brainstem, spinal cord and prefrontal cortex were rapidly removed and immediately frozen on dry ice and stored at −80°C until use for RNA or protein extraction. All procedures were conducted in accordance with the guidelines set by the Ethical Committee of the Federico II University of Naples, Italy and measures were taken to minimise any potential pain or animal discomfort (authorisation number 128/2019-R, issued on 18/2/2019).

3.2 Molecular genetic techniques

DNA extraction of mouse tissue

DNA for genotyping was extracted from mouse tail. The mouse tissue was incubated in 100µl lysis buffer containing 2µg proteinase K (20 mg/ml) (ThermoFisher) at 60°C overnight. After heat-inactivation of proteinase K at 95°C for 10min, the samples were centrifuged at 13,000rpm for 20min at 4°C and the supernatant was collected and stored at 4°C.

Genotyping

Mice were genotyped for the Smn1<tm1Msd> allele with a modified protocol from Jackson Laboratory with the suggested primers (Tables 3.1-3.2).

oIMR3439	5'- TTTTCTCCCTCTTCAGAGTGAT -3'	Common forward
oIMR3440	5'- CTGTTTCAAGGGAGTTGTGGC -3'	Wild-type reverse
oIMR7210	5'- GGTAACGCCAGGGTTTTCC -3'	Mutant reverse

Table 3.1: *Primer sequences for SMAΔ7 mice genotyping for the WT and mutant allele, with PCR products 410 and 110bp respectively (JAX protocol, Jackson Laboratory).*

Two RCR reactions were carried out per sample at a total volume of 20µl, with the common forward and either the WT or mutant reverse at a final concentration of 0.5µM and Wonder Taq Hot Start (0.3 µl) (Euroclone).

STEP	TEMPERATURE (ºC)	TIME	
Denaturation of genomic DNA	95	2min	
	95	15sec	] 35 cycles
Annealing	60	15sec	
Extension	72	30sec	
Completion	72	2min	

Table 3.2: *The PCR program used for genotyping SMAΔ7 mice.*

Agarose gel electrophoresis

Electrophoresis was carried out in 1.5% agarose gel made in 1x Tris-acetate-EDTA buffer (40 mM Tris pH 7.6, 20 mM acetic acid, 1 mM EDTA) with ethidium bromide (250 ng/µl). PCR products were loaded on the gel with 6x loading dye (NEB) and 100bp SHARPMASS DNA ladder (Euroclone). DNA was visualised using a UV transilluminator ChemiDoc™ System with Quantity One™ Software (Bio-Rad) (Fig. 3.1).

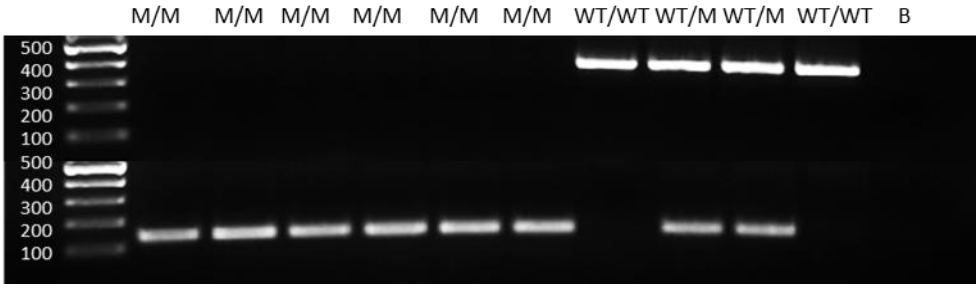

Figure 3.1: Representative image of SMAΔ7 genotyping*. The upper gel shows the amplification of a 410bp band corresponding to a WT allele and the lower gel shows a 110bp band corresponding to the mutant allele. B: no DNA control.*

RNA extraction

Tissues were quickly removed from mice, then immediately frozen on dry ice and stored at −80 °C until use. Total RNA was extracted with Tri Reagent Solution (AM9738, Invitrogen) following the manufacturer's protocol for frozen tissues.

RNA from frozen mouse brain tissue and cultured SH-SY5Y cells for miRNA analysis was isolated with the mirVana miRNA isolation kit, following the protocol for organic extraction of total RNA for frozen tissue and cultured adherent cells, respectively (Ambion, Life Technologies). RNA was then quantified with NanoDrop and stored at -80^{o}C until used.

Reverse transcription and Real-Time quantitative PCR (qPCR)

cDNA for gene expression analysis was synthesized from 2μg of total RNA with the High Capacity cDNA Reverse Transcription Kit using 10x RT random primers at a total volume of 20μl, according to the protocol (Applied Biosystems) (Table 3.3).

Settings	Step 1	Step 2	Step 3	Step 4
Temperature ^{o}C	25	37	85	4
Time	10min	120min	5min	∞

Table 3.3: *Thermocycler conditions for the reverse transcription of total RNA for gene expression assays.*

For miRNA analysis, 33.3ng of total RNA were reverse transcribed using the MultiScribe Reverse transcriptase (Invitrogen) and 5x TaqMan assays for the miRNA targets (Table 3.4) (TaqMan assays, Applied Biosystems) in a total volume of 10μl, according to the protocol (Tables 3.4- 3.5).

miRNA assay name	Assay
hsa-miR-16	000391
hsa-miR-17	002308
hsa-miR-20a	000580
hsa-miR-103	000439
hsa-miR-140-3p	002234
U6 snRNA	001973

Table 3.4: *TaqMan assays from Applied Biosystems for the reverse transcription and qPCR of the 5 miRNAs studied and U6 which was used as endogenous control for data normalisation of qPCR.*

Step	Temperature ^{o}C	Time
Reverse transcription	16	30min
	42	30min
Stop reaction	85	5min
Hold	4	∞

Table 3.5: *Thermocycler conditions for the reverse transcription of total RNA for miRNA analysis.*

For gene expression assays the following 20x TaqMan assays were used: *Kif5a* ID: Mm00515265_m1, *Rhot1* ID: Mm01304158_m1 and the reference gene beta-glucuronidase (*Gusb*) ID: Mm00446953_m1) (ThermoFisher Scientific). For miRNAs, the 20x assays indicated on Table were used.

qPCR was performed with the above TaqMan assays in a 7500 real-time PCR system (Life Technologies). For gene expression and miRNA assays, 6.25ng and 22.3ng of cDNA was used, respectively, in each reaction in 2x master mix, SensiFAST Probe Lo-ROX kit (Bioline) and 20x TaqMan assays at a total volume of 10μl. All samples were run in triplicates. qPCR was carried out in a 7500 Fast Real-Time PCR System (Applied Biosystems) in a standard run mode (Table 3.3). Differences in mRNA levels were calculated as the difference in threshold cycle ($2^{-\Delta\Delta Ct}$) between the target genes and the reference genes (*Gusb* or *U6*).

Settings	**Step 1 (Hold)**		**Step 2 (PCR)**	
Temperature	50 ºC	95 ºC	95 ºC	60 ºC
Time	2 min	10 min	15 sec	1 min

Table 3.6: *The thermocycling conditions for qPCR. The PCR step run for 40 cycles.*

Site-directed mutagenesis for *KIF5A* mutations

The p.Asn999Valfs*39 and p.R864* mutations were introduced with Site Directed Mutagenesis, according to manufacturer's protocol (Q5® Site-Directed Mutagenesis Kit, NEB) on a custom human *KIF5A* cDNA plasmid on a pc.DNA3.1(+) backbone (GenScript). The primers used are shown in Table 3.7.

Mutation	**Forward**	**Reverse**
p.(Asn999Valfs*39)	5'-GAGTGACCTGCCGTGTGG-3'	5'-CATTGTCCATGTTGGCCTTC-3'
p.R864*	5'-ATTGGAAAAATGACTTAGGGC-3'	5'-TTAGGAAGCTCACAACGC-3'

Table 3.7: Primer sequences used for KIF5A mutagenesis*. Primers were designed with NEBaseChanger (New England Biolabs).*

Briefly, the vial with the lyophilised plasmid DNA (~4μg) was centrifuged at 6,000g for 1min and 20μl of sterile H_2O were added, vortexed and heated at 50ºC (~1-2min) until the DNA was dissolved. DNA concentration was determined with Nanodrop.

The PCR reactions were set at a total volume of 25µl and 20ng of *KIF5A* plasmid DNA were used per reaction (Table 3.8). The final concentration for the primers was 0.5µM and 1x Q5 Hot Start High-Fidelity Master Mix.

STEP	TEMPERATURE (C)	TIME	
Denaturation of double stranded DNA	98	30sec	
	98	10sec	] 25 cycles
Annealing of primers*	65 / 59	20sec	
Extension of strand	72	3.5min	
Completion of reaction	72	2min	

Table 3.8: *Thermocycling conditions for the PCR reactions for KIF5A mutagenesis. * Annealing temperatures for the primers of the p.Asn999Valfs*39 and p.R864* mutations were calculated using NEBaseChanger (NEB).*

PCR products were incubated with KLD restriction enzyme for 5 minutes at 37° C. Transformation of KLD reactions was performed with 50µl NEB 5-alpha Competent E.coli bacterial cells (C2987, NEB) according to the protocol. 12 single colonies from each plasmid transformation were selected and grown in LB medium with ampicillin (100µg/ml), DNA was extracted with QIAprep Spin Miniprep kit (Qiagen) according to the protocol and quantified with Nanodrop One (Thermo Scientific).

Validation of *KIF5A* mutations

~1µg of plasmid DNA was digested with 10 units of each enzyme, XhoI (R0146S, NEB) and EcoRV (R0195S, NEB) in Buffer 3 plus BSA in a total volume of 20µl for ~1h at 37°C, according to the protocol (NEBcloner, NEB). Correct-size plasmids were sent for Sanger sequencing using the T7 5'-TAATACGACTCACTATAGGG-3' and the BGH 5'-TAGAAGGCACAGTCGAGG-3' primers to confirm the presence of the mutations.

Molecular cloning of 3'UTR

Initial PCR of 3'UTR

~200ng of cDNA from a WT mouse spinal cord tissue were used to obtain a 253bp region of the 3'UTR of *Kif5a* with PCR. Primers containing the restriction sites of XhoI and NotI were designed using the OligoPerfect tool for primer design for cloning from Thermofisher (Table 3.9).

3'UTR F	5'-CCG**CTCGAG**AGGCCTCTTCTCTCAGCATG -3'	XhoI
3'UTR R	5'- TT**GCGGCCGC**AAAAGAAGAAATATTCCCTCCTCCC-3'	NotI

Table 3.9: *Primers used for the amplification of the 3'UTR region of KIF5A containing the restriction sites for cloning (shown in bold) into the pmirGLO vector. Primers were designed with the OligoPerfect tool (ThermoFisher).*

Two PCR reactions were carried out, each at a total volume of 50μl. The final concentration for the primers was 0.5μM and 0.02U/μl (0.5μl) of Q5 Hot Start High-Fidelity DNA polymerase, according to the protocol (New England BioLabs). The PCR program used is shown in Table 3.10.

STEP	TEMPERATURE (°C)	TIME	
Initial denaturation	98	1min	
	98	10sec	
Annealing	65	10sec	] 35 cycles
Extension	72	20sec	
Completion of reaction	72	2min	

Table 3.10: PCR program for the amplification of the 3'UTR region of KIF5A. *The annealing temperature was calculated with NEBTm Calculator (New England BioLabs).*

Digestion

The PCR product size, 271bp, was verified by electrophoresis on an agarose gel (2%) and quantified with SHARPMASS 100 DNA ladder (Euroclone). ~2μg of the total PCR product and 3μg of pmirGLO vector were then digested overnight at 37°C with NotI and XhoI (20U/μg of DNA) in rCutSmart buffer (New England BioLabs) according to the protocol at a total volume of 150μl. Dephosphorylation of the vector's DNA 5'-ends with Quick CIP (5U/μl) for 10min was followed and then incubation for 2min at 80 °C for heat inactivation of the enzyme. The digested PCR product and vector were the loaded on a 1% agarose gel for ~2h and the DNA was extracted and purified with a QIAquick gel extraction kit (Qiagen) according to manufacturer's protocol. The DNA was eluted with distilled H_2O and quantified with NanoDrop One (Thermo Scientific).

Ligation

Ligation was then followed by calculating the molar insert:vector ratios using the NEBioCalculator (NEB). The vector (pmirGLO) DNA length after digestion was 7233bp and the insert (3'UTR) was 259bp. The vector DNA mass chosen was 120ng and the molar ratios for ligation were 3:1, 5:1 and 7:1. T4 DNA ligase (NEB) was used in a total volume of 20μl for each ratio and one control with only vector DNA, according to the protocol. Ligation reactions were incubated at 16 ^{o}C overnight. Ligase was then inactivated at 65 ^{o}C for 10 min.

Transformation

For the transformation, 5μl of ligation reactions were added to 50μl vials of One Shot TOP10 chemically competent *E.coli* cells and incubated on ice for 30 min according to the protocol (Invitrogen). Then, the vial was incubated for 30sec at 42 ^{o}C and placed on ice for 5min. 250μl of prewarmed S.O.C medium was added and incubated for 1h at 37 ^{o}C in a shaking incubator at 225rpm. Finally, 150μl from each transformation vial were spread on ampicillin LB agar plates and incubated overnight at 37 ^{o}C. The next day colonies were counted for all plates and single colonies were picked and grown overnight at 37 ^{o}C in LB medium with ampicillin (100μg/ml). Plasmid DNA was extracted with QIAprep Spin Miniprep kit (Qiagen) according to the protocol and quantified with Nanodrop One (Thermo Scientific).

Screening and validation of plasmid DNA

1μg of plasmid DNA was digested for 2h at 37 ^{o}C with XhoI and NotI and run on a 1% agarose gel. Correct sized plasmids were then digested again for 2h at 37 ^{o}C with XhoI / BamHI-HF and XhoI / EcoRV (10units) (NEB).

Mutagenesis for *Kif5a* 3'UTR

The 3'UTR-pmirGLO plasmid was used for mutagenesis of 6 bases of the miR-140-3p target sequence on KIF5A 3'UTR. The mutated sequence was designed to correspond to the EcoRV restriction site. The 6-base pair substitution was introduced with Site Directed Mutagenesis, according to manufacturer's protocol (Q5® Site-Directed Mutagenesis Kit) as described above. The primers and PCR program used are shown in Tables 3.11-12.

3'UTR mut F	5'-GCTGCAAAAC**GATATC**TCTCTGACACTAACTCCCTCCC -3'
3'UTR mut R	5'- ATGCTGAGAGAAGAGGCC-3'

Table 3.11: The primers used for mutagenesis of the 3'UTR of KIF5A. *The EcoRV restriction site is highlighted. Primers were designed with NEBaseChanger (New England Biolabs).*

STEP	TEMPERATURE (°C)	TIME
Initial denaturation	98	30 sec
	98	10 sec
Annealing	61	10 sec
Extension	72	3.5 min
Completion of reaction	72	2 min

35 cycles

Table 3.12: The PCR program used for Kif5a 3'UTR mutagenesis. *The annealing temperature was calculated with NEBTm Calculator (New England BioLabs).*

KLD reactions and transformation of One Shot TOP10 chemically competent *E.coli* cells (Invitrogen) were as described above. The plasmid DNA from single colonies was screened for the mutation with restriction digestion with the EcoRV enzyme (NEB). The WT and mutated Kif5a 3'UTR plasmids are shown in Fig. 3.2.

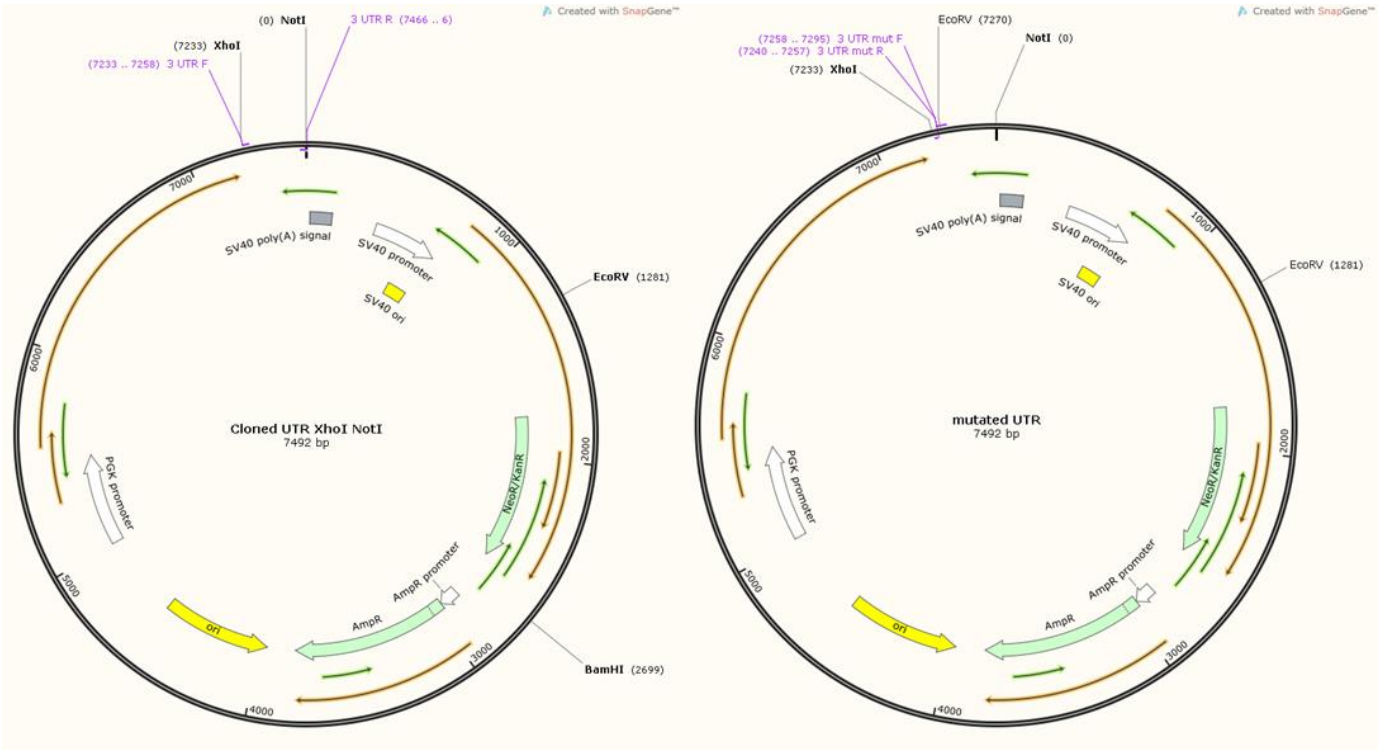

Figure 3.2: Maps of the pmirGLO-UTR plasmids. *pmirGLO vestor containing the cloned fragment of the 3'UTR sequence of Kif5a (left) and the mutated 3'UTR sequence containing the EcoRV restriction site (right). The restriction sites of the enzymes used for cloning and digestions are shown. (Image created with SnapGene).*

Luciferase assay

For the luciferase assays the Dual-Luciferase Reporter assay system was used (E1910, Promega) according to manufacturer's protocol. Briefly, cells were washed with PBS and lysed with 40µl of 1x Passive lysis buffer. Two cycles of freezing (-80 ºC for 30 min) and thawing followed and then the samples were centrifuged for 15 min at 13,000rpm. Finally, 40µl of Luciferase assay Reagent II (LAR II) was added in 20µl of supernatant and the firefly luminesence was measured with a GLOMAX 20/20 Luminometer (Promega). The reaction was then quenched and the Renilla luciferase reaction initiated and measured by adding 40µl of Stop & Glo Reagent in the same sample.

3.3 Cell cultures

Human neuroblastoma SH-SY5Y cells (ATCC) were maintained in culture in Dulbecco's Modified Eagle Medium (DMEM) medium (21969-035, Gibco), complemented with 1% penicillin–streptomycin, 1% L-glutamine and 10% of foetal bovine serum (FBS) and routinely passaged with 0.05% trypsin in phosphate-buffered saline (PBS).

iPSCs were a kind gift from Prof. Van Den Bosch (KU Leuven). Healthy human iPSCs (Sigma) were maintained on GeltrexR LDEV-Free hESC-Qualified Reduced Growth Factor Basement Membrane Matrix (A1413302, Gibco) in Essential 8 medium (A1517001, Gibco) with 1000 U/ml penicillin–streptomycin. Colonies were passaged with 0.5mM EDTA (Invitrogen) in Dulbecco's phosphate-buffered saline (DPBS).

Motor neuron differentiation

Motor neuron differentiation was performed as described in Guo *et al,* 2017. Briefly, iPSCs were treated with collagenase type IV to form small clusters and resuspended in Essential 8 medium. For the first 2 days, medium was changed every day with Neuronal basic medium (DMEM/F12 plus Neurobasal medium with N2 and B27 supplement without vitamin A supplemented with 40 µM SB431542 (Tocris Bioscience), 0.2 µM LDN-193189 (Stemgent), 3 µM CHIR99021 (Tocris Bioscience) and 5 µM Y-27632 (Merck Millipore). From day 3 on, 0.1 µM retinoic acid (Sigma) and 500 nM SAG (Merck Millipore) was added. From day 8 on, BDNF (10 ng/ml, Peprotech) and GDNF (10 ng/ml, Peprotech) were added and on day 9 DAPT (20 µM, Tocris Bioscience) was added. On day 10, clusters were dissociated into single cells with 0.05% trypsin (GibcoTM) and plated on polyornitnine (100µg/ml) and laminin (20

μg/ml)-coated coverslips in 24-well plates (70,000 cells per well). From day 17 on, the cells were switched to motor neuron maturation medium supplemented with BDNF, GDNF, and CNTF (each 10 ng/ml, Peprotech). Every other day half of the medium was replaced.

Transfections

The RNA used for transfections is hsa-miR-140-3p mimic (MC12503), inhibitor (MH12503) from ambion, Life Technologies and AllStars Negative Control siRNA (1027280, Qiagen). The DNA used for all transfections was extracted with HiSpeed Plasmid Maxi kit with an A260/A230 ratio of ~2-2.2. The custom plasmid for HA-KIF5A was from GenScript and GFP-SMN was a gift from Greg Matera (Addgene plasmid # 37057).

SH-SY5Y cells were plated so that cells would be ~70% confluent at the time of transfection. All transient transfections were carried out using Lipofectamine 2000 (Invitrogen, ThermoFisher Scientific) in DMEM medium (without antibiotics). For RNA transfections 5μl of RNA (20μM): 5μl Lipofectamine (1:1 ratio) were used in a final volume of 2ml (60mm plates) and a 1:2 DNA:lipofectamine ratio was used for plasmid DNA transfections (100mm plates), according to the manufacturer's protocol. For HA-KIF5A/GFP-SMN co-transfection 2.5μg of each plasmid was used at a 1:2 total DNA:lipofectamine ratio.

For the luciferase assay, SH-SY5Y cells were transfected in 24-well plates. Cells were co-transfected with 100ng of each DNA plasmids (the pmirGLO-3'UTR, pmirGLO-mutated 3'UTR), 0.45μl of RNA (20μM) (miR-140-3p mimic, inhibitor or AllStars negative control) and 0.6μl of Lipofectamine 2000 in a total volume of 3ml of Optimem medium (Gibco, ThermoFisher) per well. Briefly, the RNA or DNA was incubated with lipofectamine for 20min at room temperature and added to each plate containing fresh medium. Cells were incubated with the complexes at 37^{o}C in a CO_2 incubator for 4h before changing the medium. For RNA transfections, cells were then incubated for an additional 48h and for DNA 24h.

3.4 Protein techniques

Antibodies

ANTIGEN	ANTIBODY	SUPPLIER	HOST	DILUTION
Kinesin 5A	PA1-642	Thermo Scientific	Rabbit	1:1000 WB 1:500 IHC 1:1000 ICC
RHOT1	PA5-96443	Thermo Scientific	Rabbit	1:1000 WB
TRAK1	PA5-44180	Thermo Scientific	Rabbit	1:500 WB
HA Tag	26183	Thermo Scientific	Mouse	1:5000 WB
SMN1/SMN2 (2B1)	MA1-5878	Thermo Scientific	Mouse	1:250 WB 1:200 ICC
GFP	SAB 4301138	Sigma-Aldrich	Rabbit	1:1000 WB
Gem2	ab6048	Abcam	Mouse	1:1000 ICC
Smi32	ab8135	Abcam	Rabbit	1:1000 ICC
Isl1	AB4326	Merck Millipore	Rabbit	1:500 ICC
ChaT	AB144P	Merck Millipore	Goat	1:500 ICC
NeuN	ABN78	Millipore	Mouse	1:1000 IHC

Table 3.13: *List of the primary antibodies used in this study and the dilutions used for each technique. All the secondary antibodies were from Invitrogen and used in 1:5000 for WB and 1:1000 in ICC. WB: western blot, IHC: immunohistochemistry, ICC: immunocytochemistry.*

Protein extraction

Tissue samples were maintained at −80 °C until processed and cells were manually collected on ice. Both tissues and cells were lysed with a lysis buffer containing 50mM HEPES pH 7.5, 150mM NaCl, 1% glycerol, 1% Triton X-100, 1.5mM $MgCl_2$ and 5mM EGTA plus protease inhibitors. For immunoprecipitation experiments, cells were lysed with immunoprecipitation lysis buffer (50mM Tris–HCL, pH 7.5, 1% Triton, 100mM NaF, 150mM NaCl, 1mM EDTA, PMSF 100mM, Na_3VO_4 100 mM,) and protease inhibitors. All samples were lysed with 50-200µl of lysis buffer for 1h on ice and centrifuged for 20min at 13,000rpm at 4°C. Protein concentration was determined with Bradford (Protein Assay Dye Reagent Concentrate, Bio-Rad).

Western Blot

50-100μg of protein was loaded on an 8% polyacrylamide gel and transferred onto nitrocellulose membranes. The membranes were blocked with 5% non-fat dry milk or BSA for 1h and were probed with the appropriate primary antibodies in 5% milk or BSA at 4 °C overnight or HRP conjugated anti-actin (Invitrogen) for 1h. After incubation with anti-mouse or rabbit secondary antibodies for 1h, immunoreactive bands were detected with enhanced chemiluminescence, Pierce ECL Western Blotting Substrate (Thermo Scientific) and visualised on a ChemiDoc imaging system (Bio-Rad). The optical density of the bands was determined by QuantityOne software (Bio-Rad) and normalized to the optical density of β-actin.

Immunoprecipitation

For immunoprecipitation total cell extracts were re-suspended using immunoprecipitation lysis buffer. 300ng-1μg of total protein were used for the experiments in a final volume of 300μl and 50-100μg of sample was used as input for TRAK1 and HA-tag and 50μg for IgG control. Inputs were stored in -20°C. Samples and control were pre-cleared with 10μl Protein A/G PLUS agarose (Santa-Cruz Biotechnology) for 1-2h, centrifuged for 5min at 2,500rpm and the beads were discarded. 5μg of anti-HA antibody was added to each sample and 1μg of anti-mouse for the IgG control and were placed on a rocker at 4 °C overnight. 20-40μl agarose beads were then added and incubated for 3-8h at 4°C. After centrifugation at 2500 rpm for 5 min, the supernatant was discarded, and the pellets were washed four times with 1 ml of cold PBS. The pellet was re-suspended in 20 μl of Laemmli loading buffer 2× boiled for 3-5min and centrifuged, together with the inputs plus Laemmli buffer. After Western blot, the membranes were then visualised on a ChemiDoc imaging system and analysed with Image Lab 6.1 (Bio-Rad).

3.5 Imaging techniques

Immunohistochemistry

Immunostaining and confocal immunofluorescence procedures were performed as previously described (Valsecchi *et al*, 2020). Briefly, animals were anaesthetized and transcardially perfused with a saline solution, followed by 4% paraformaldehyde in 0.1 mol/L PBS saline solution. Brains were rapidly removed on ice and post-fixed overnight at +4°C and

cryoprotected in 30% sucrose in 0.1 M phosphate buffer (PB) with sodium azide 0.02% for 24h at 4°C. Brains were then sectioned frozen on a sliding cryostat at 40μm thickness, in rostrum-caudal direction. Free-floating serial sections were incubated with PB Triton X 0.3% and blocking solution (0.5% milk, 10% FBS, 1% BSA) for 1.5h. The sections were incubated overnight at +4°C with the primary antibodies. The sections were then incubated with the corresponding florescent-labelled secondary antibodies, Alexa 488/Alexa 594 conjugated anti-rabbit and anti-mouse immunoglobulin Gs (1:300) (Jackson Immuno Research, Baltimore, PA). Nuclei were counterstained with Hoechst (Sigma-Aldrich). Images were observed using a Zeiss LSM700 META/laser scanning confocal microscope (Zeiss, Oberkochen, Germany). Single images were taken with a resolution of 1024 ×1024 (20x magnification). In double-labelled sections, the pattern of immune reactivity for both antigens was identical to that seen in single-stained material. The number of KIF5A+ and NeuN+ positive cells was determined in the brainstem of WT and SMA mice, by manual counting at 40x magnification and for SC at 20x magnification. Three mice per group were included in the study of brainstem and five in the spinal cord analysis.

Immunocytochemistry

Cells plated on coverslips were fixed in 4% paraformaldehyde for 20 min at room temperature and were washed with PBS. Permeabilization and blocking was done for 30 min using PBS containing 0.2% Triton X-100 (Acros Organics) and 5% donkey serum (Sigma) for 1 h. Cells were incubated overnight at 4°C in blocking buffer (2% donkey serum) with primary antibodies. After washing with PBS, cells were incubated with secondary antibodies for 1 h at room temperature.

Fluorescent images were captured using with an inverted Leica SP8 DMI8 confocal microscope or a Zeiss LSM700 META/laser scanning confocal microscope at 40x and 60x magnification. All images were analysed using ImageJ. DAPI and neuronal marker positive cells were manually counted. Pearson's correlation coefficients were calculated with the JACoP plug-in and used for expressing the intensity correlation for colocalisation.

3.6 Statistical analysis

Statistical analysis was performed using GraphPad Prism 8.0.1. One-way ANOVA was used for all experiments with post-hoc Bonferroni test to determine statistical differences between groups, unless stated otherwise. All data are represented as mean ± SEM.

4. RESULTS

4.1 Involvement of the Kif5a mitochondrial complex in SMA

Mitochondrial axonal transport defects have been well characterised in MNDs including various types of ALS (Guo *et al*, 2019), however studies on such defects in SMA, to our knowledge, are limited. As the Kif5a-Miro1 complex is largely responsible for the anterograde mitochondrial transport in neurons and there is evidence suggesting mitochondrial transport defects in the spinal motor neurons starting at early stages of SMA (Xu *et al*, 2016), the potential role of the Kif5a-Miro1 complex in SMA pathogenesis was studied.

For the investigation of the potential involvement of Kif5a and the mitochondrial transport complex in SMA pathogenesis a moderate type II SMA mouse model, the SMNΔ7 mouse was used. Brain tissue from SMNΔ7 mice was obtained, from 3 regions that are primarily affected in SMA, brainstem, spinal cord and prefrontal cortex at p5 and p10-14 when mice show a mild to severe phenotype, respectively (Fig. 4.1).

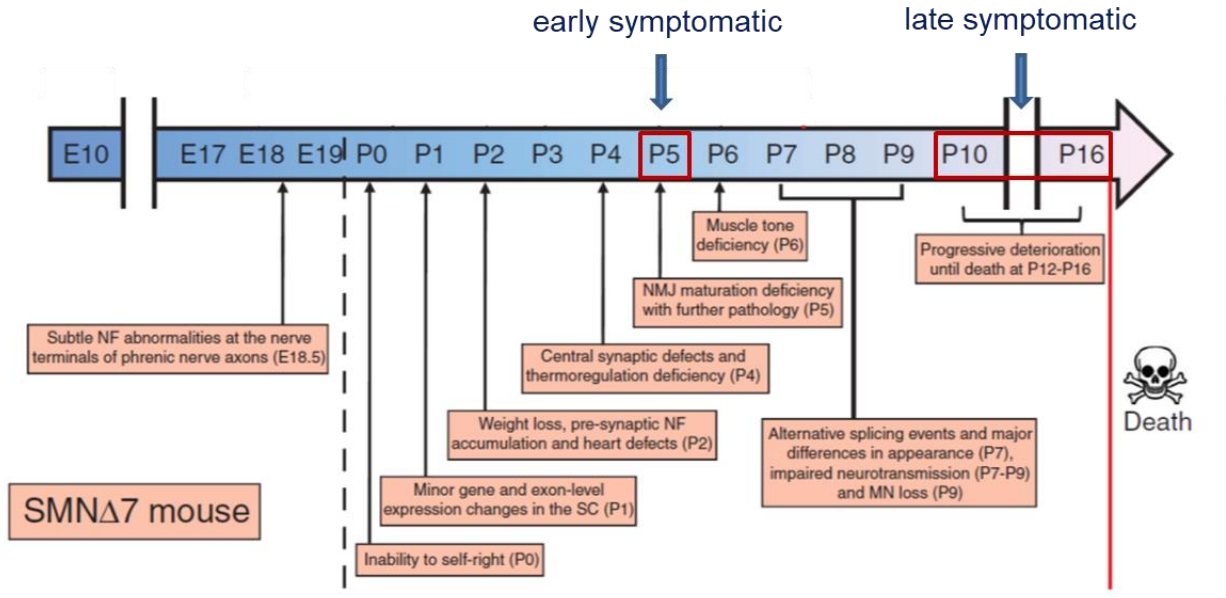

Figure 4.1: *Illustration of the clinical and cellular presentation of the SMNΔ7 mouse model used in this study during embryonic and postnatal development. The two stages, p5 and p10-p14, when brain samples were obtained are shown [Image modified from Sleigh et al, 2011].*

The relative mRNA and protein levels of Kif5a and Miro1 were measured with quantitative real-time PCR (qPCR) and Western blot analysis in WT and SMA mice with the results suggesting the involvement of the complex in SMA. Specifically, in the brainstem there is a downregulation of Kif5a which is significant at a protein level in p5 SMA mice compared with WT. This upregulation of Kif5a was also confirmed with IHC analysis of p5 brainstem tissue compared with WT mice. For Miro1 no significant change was observed to both mRNA and protein levels (Fig. 4.2-3).

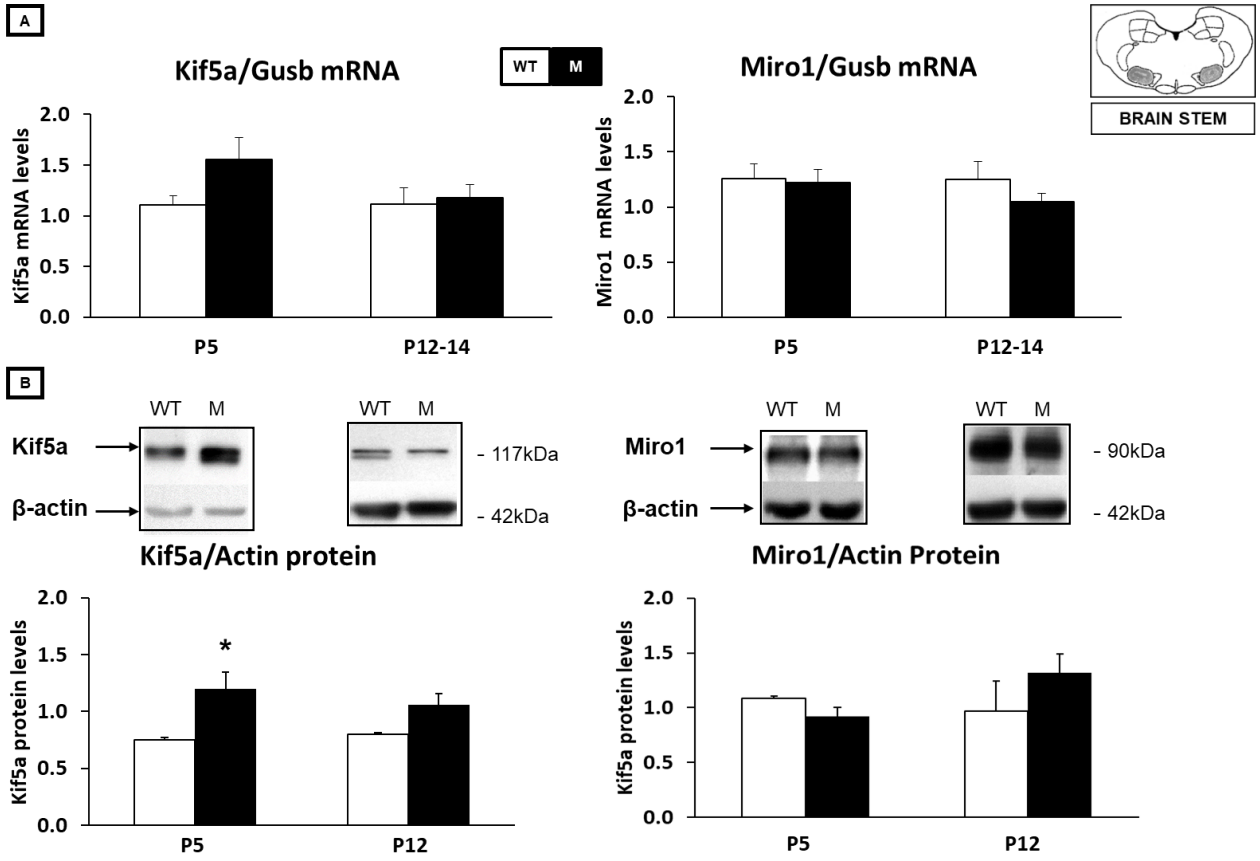

Figure 4.2: *qPCR analysis of Kif5a and Miro1 (A) and representative images and quantification of Western blot analysis (B) of Kif5a and Miro1 in the brainstem of early symptomatic (p5) and late symptomatic (p12-14) SMNΔ7 mice. Kif5a protein levels were found significantly upregulated at p5. Actin, gusb: endogenous controls, N=3-8, p<0.05. One-way ANOVA followed by Bonferroni test [WT: wild-type, M: mutant SMNΔ7 mice].*

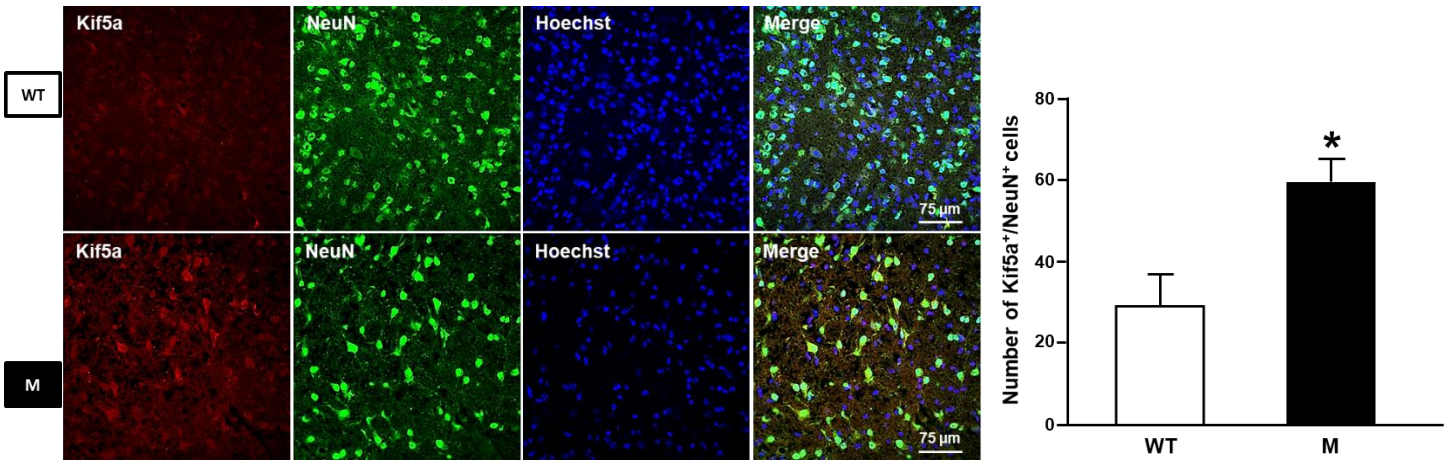

Figure 4.3: *Immunofluorescence staining images of the brainstem of p5 SMNΔ7 mice and healthy controls (WT) at p5. The number of KIF5A+ and NeuN+ positive cells was determined by manual counting at ×40 magnification. The attention has been focused on the analysis of facial nuclei. Neurodegeneration is present at this stage as indicated by the decreased number of the NeuN positive cells in SMA mice (M) compared with controls (WT). Kif5a expression is found to be limited to neurons. Analysis of three mice per group showed that Kif5a expression is significantly upregulated in SMA mice. Green indicates NeuN-stained neuronal nuclei. Blue indicates Hoechst-stained nuclei. Statistical significance was accepted at the 95% confidence level p<0.05, unpaired Student's t test. [WT: wild-type, M: mutant SMNΔ7 mice].*

In the spinal cord (SC), qPCR analysis showed that Kif5a mRNA levels but not Miro1 was downregulated in SMA mice at p5 whereas at a protein level WB revealed a significant downregulation of both Kif5a and Miro1 at p5 and p10 (Figure 4.4). This reduction of Kif5a in the SC at p10 was also confirmed with IHC (Figure 4.5).

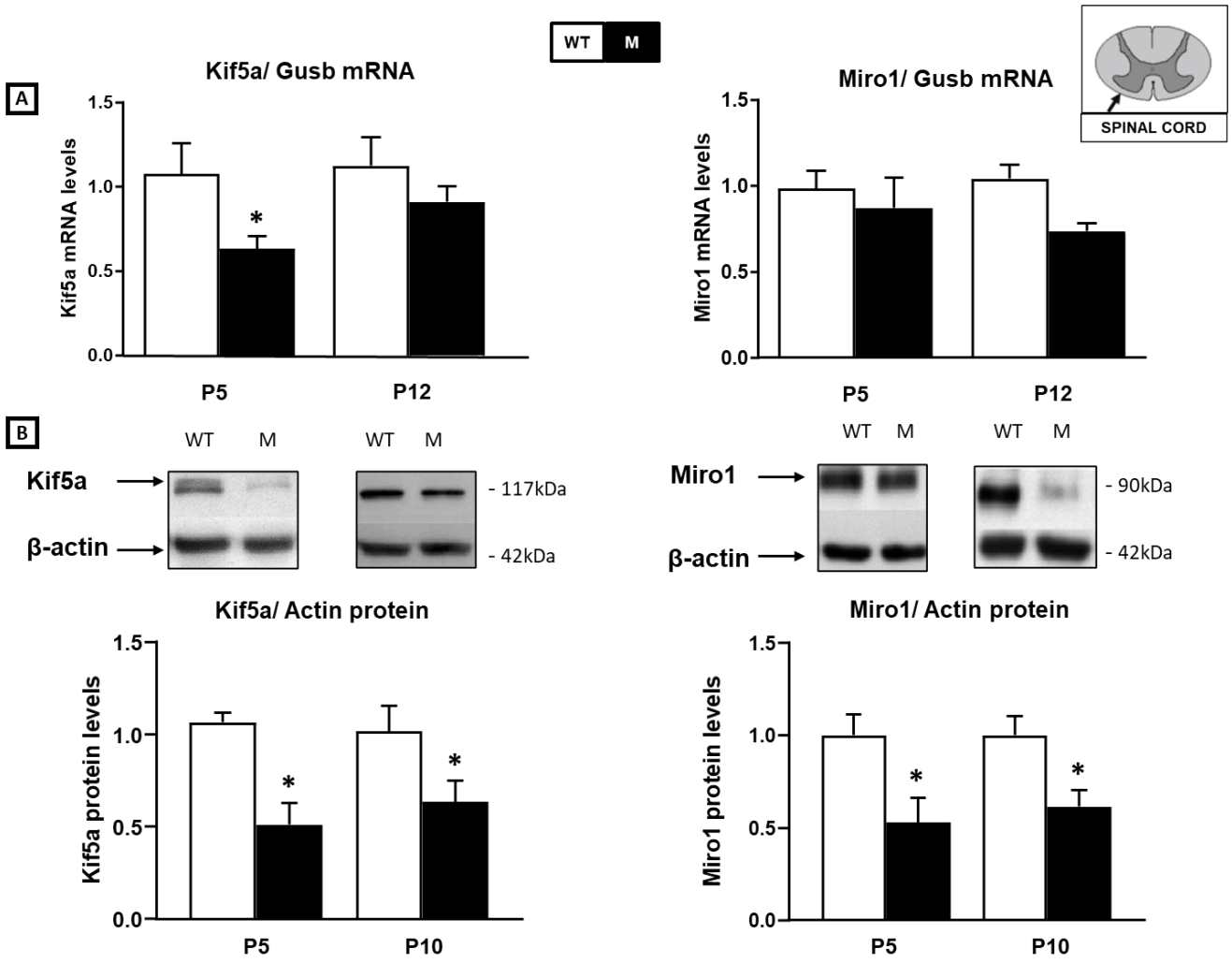

Figure 4.4: qPCR analysis of Kif5a and Miro1 (A) and representative images and quantification of Western blot analysis (B) of Kif5a and Miro1 in the spinal cord of early symptomatic (p5) and late symptomatic (p10-12) SMNΔ7 mice. Kif5a mRNA levels are significantly decreased at p5. Kif5a and Miro1 protein levels were found significantly downregulated at p5 and p10. Actin, gusb: endogenous controls, N=6-11, p<0.05 except Kif5a protein at p5 p<0.005. One-way ANOVA followed by Bonferroni test [WT: wild-type, M: mutant SMNΔ7 mice].

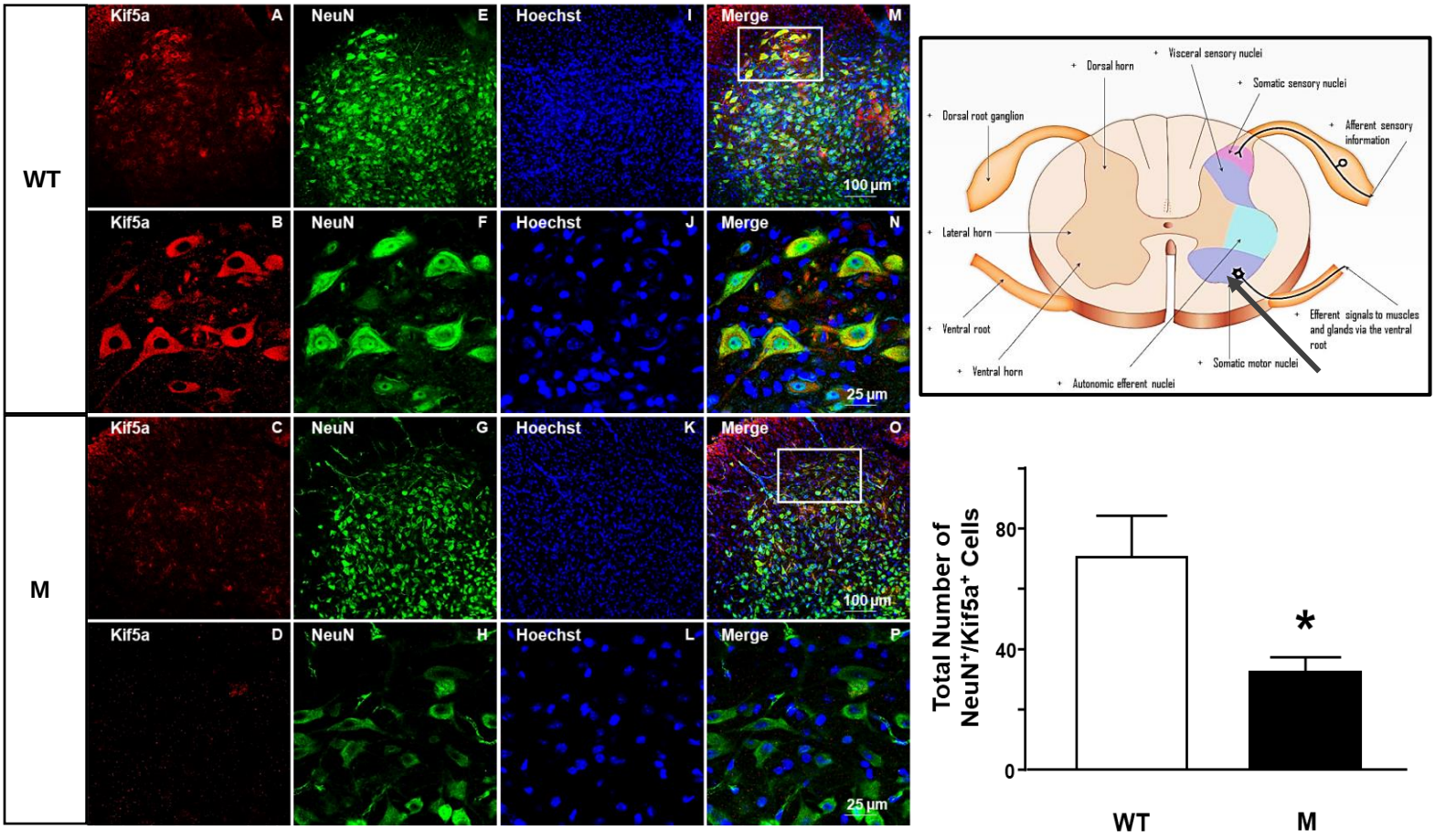

Figure 4.5: Immunofluorescence staining images of the spinal cord of healthy controls and SMNΔ7 mice at p11 (left). The number of KIF5A+ and NeuN+ positive cells was determined by manual counting at ×20 magnification. The spinal cord region analysed is the ventral lumbar area indicated with an arrow (upper right). Kif5a expression is found to be limited to neurons. Analysis of five mice per group showed that Kif5a expression is significantly downregulated in SMA mice (lower right). Green indicates NeuN-stained neuronal nuclei. Blue indicates Hoechst-stained nuclei. Statistical significance was accepted at the 95% confidence level p<0.05, unpaired Student's t test. [WT: wild-type, M: mutant SMNΔ7 mice].

In the cortex qPCR results didn't reveal any significant changes in the mRNA levels of Kif5a and Miro1 in SMA mice compared with WT but showed a significant downregulation of Kif5a at p5 and of Miro1 at p10 at a protein level (Fig. 4.6)

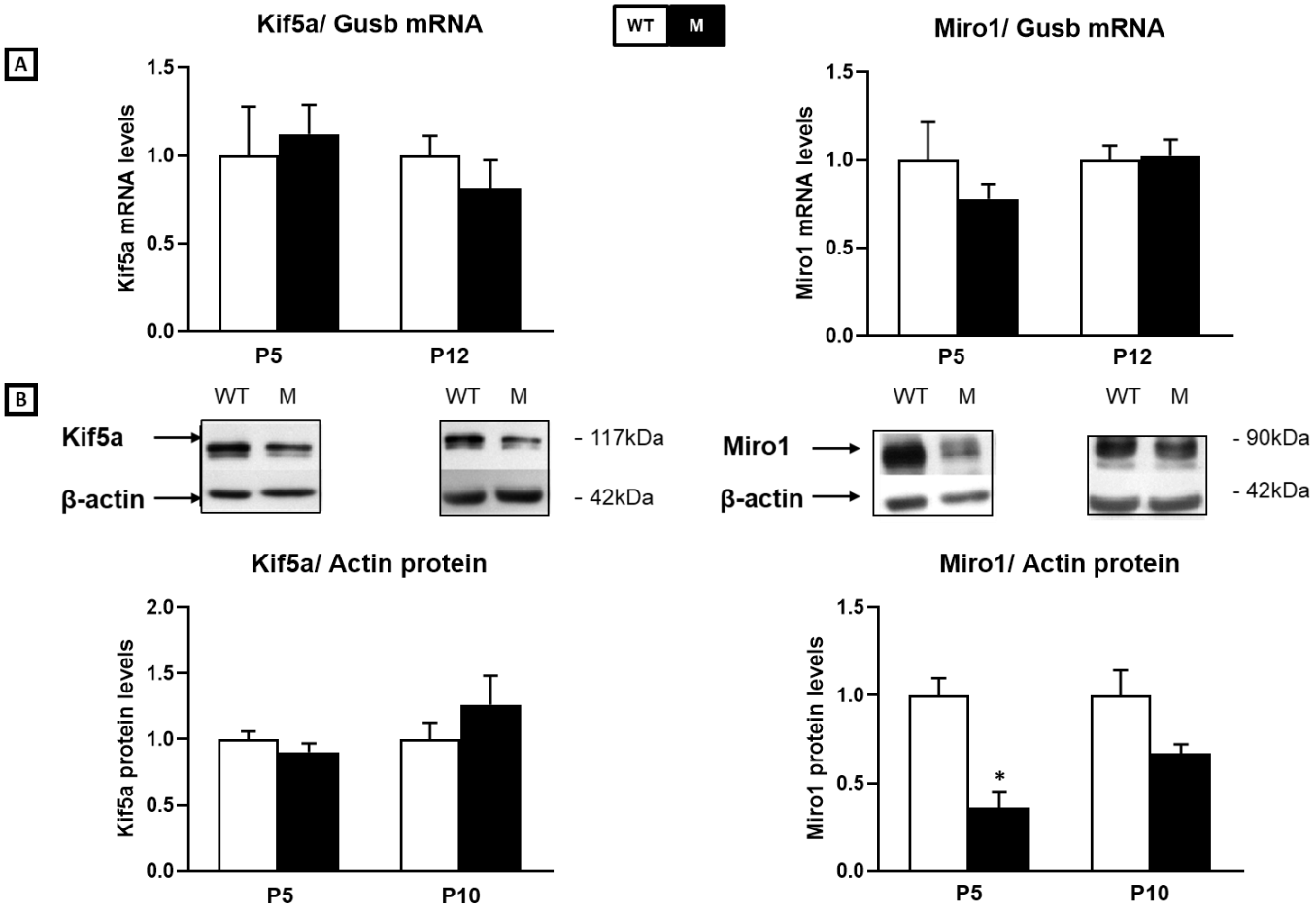

Figure 4.6: qPCR analysis of Kif5a and Miro1 (A) and representative images and quantification of Western blot analysis (B) of Kif5a and Miro1 in the cortex of early symptomatic (p5) and late symptomatic (p10-12) SMNΔ7 mice. Kif5a and Miro1 protein levels were found significantly downregulated at p10 and p5 respectively in SMA mice compared to WT mice. Actin, gusb: endogenous controls, N=3-10, p<0.05. One-way ANOVA followed by Bonferroni test [WT: wild-type, M: mutant SMNΔ7 mice].

4.2. Identification of a therapeutic strategy targeting Kif5a dysregulation in SMA

4.2.a Background information on microRNAs

During the last 15 years an increasing number of small regulatory RNAs have been identified and their potential role in human disease is emerging. A class of these small, non-coding elements are microRNAs (miRNAs). miRNAs are ~18-24 nt long RNA molecules encoded by genes or intronic regions, regulating gene expression by targeting specific sequences (Fig. 4.7). Expression profiling studies have shown that miRNAs expression is tissue and sex-specific but can also vary in different stages of development (Pignataro, 2021). miRNAs silence gene expression via two main mechanisms: mRNA destabilisation/ degradation and translational repression (Fig. 4.8). miRNAs function as part of ribonucleoprotein complexes (miRNPs) and acts as a guide in order to bind to the target 3′-UTR of the mRNA by base pairing via a sequence at position 2-8 called seed. The seed region of each miRNA confers the target specificity, thus miRNAs with identical seed sequences target the same genes and represent a miRNA family (Gurtan & Sharp, 2013).

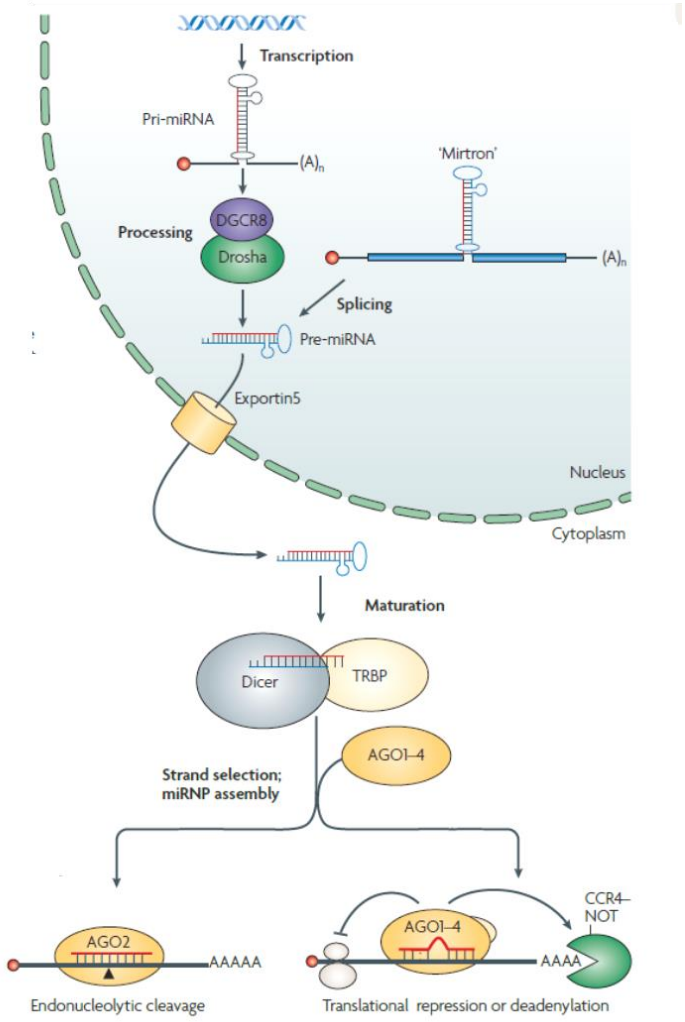

Figure 4.7: Biogenesis and assembly of miRNAs. After the miRNA genes are transcribed in the nucleus, the long pri-miRNAs are processed into shorter pre-miRNAs and exported in the cytoplasm where they are cleaved and form a miRNA:miRNA duplex. In most cases, one strand forms the mature miRNA, usually miRNA-3p, while the other one (miRNA*), usually miRNA-3p, is degraded. However, in some cases both strands can also function as mature miRNAs. The mature miRNAs then assemble into ribonucleoprotein (miRNPs) or miRNA-induced silencing (miRISCs) complexes which bind to the target mRNA and induce silencing either by cleavage of the mRNA or by repressing the translation of the protein [Image from: Filipowicz et al, 2008].*

A single miRNA can have multiple mRNA targets and conversely multiple miRNAs can target a specific mRNA. In this way the transcriptional/translational silencing is enhanced (Gurtan & Sharp, 2013). Most mRNA binding sites are located in the 3'UTR and more than one can be usually present, again enhancing the translational repression (Filipowicz *et al,* 2008).

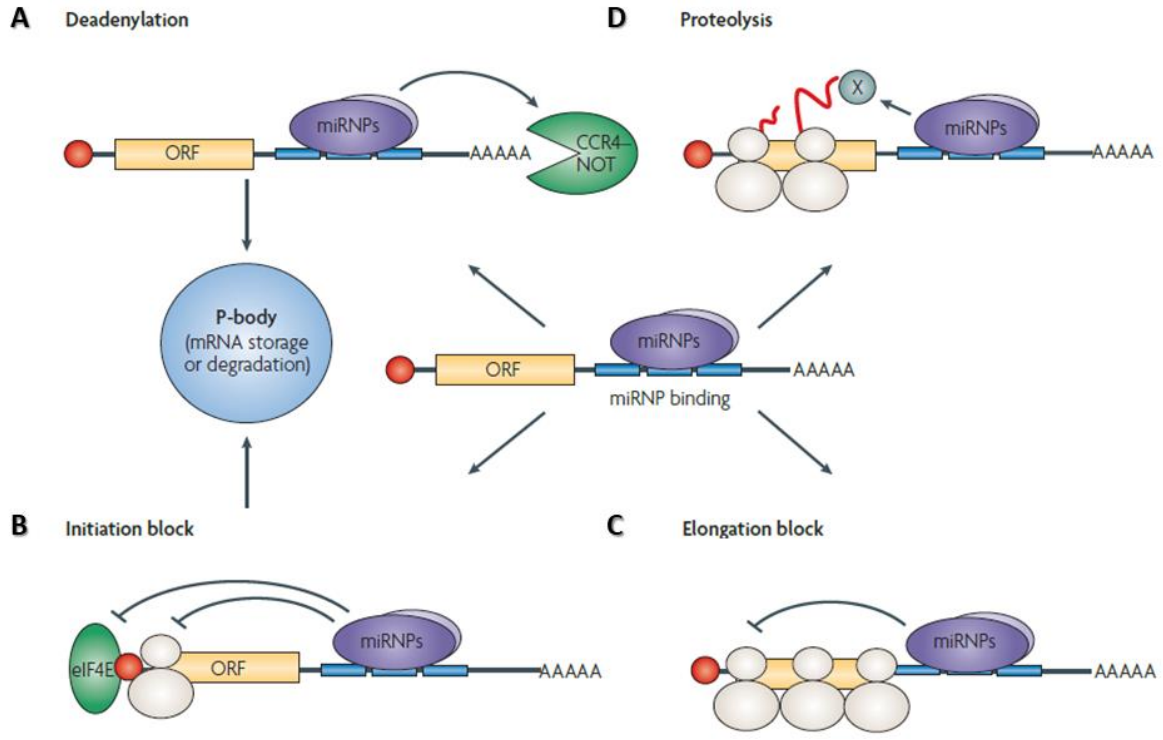

Figure 4.8: Mechanisms of miRNA-induced transcriptional and translational repression. *miRNAs bind to the target mRNA sequence as part of the miRNP complex and can cause* ***A.*** *deadenylation of the target which can lead to mRNA degradation* ***B.*** *blocking of the initiation of translation of the target mRNA and subsequent degradation or storage* ***C.*** *slowing down of the elongation process of translation or blocking of the ribosome.* ***D.*** *miRNAs can also act post-transcriptionally by proteolytic cleavage of the nascent protein [Image from: Filipowicz et al, 2008].*

Many miRNAs are specifically expressed in the CNS and are involved in many biological processes, playing an important role in MN survival and function (De Paola *et al,* 2018). More specifically, miRNAs seem to play a critical role in the spinal cord in pathways such as neuronal progenitor patterning and cell fate specification and survival (Chen & Chen, 2019). As one miRNA can target several mRNA transcripts, an altered expression of a single miRNA can induce effects on multiple pathways. Studies have identified specific miRNA expression profiles associated with neurodegeneration and MNDs including ALS and SMA (Figueroa-Romero *et al,* 2016; Valsecchi *et al,* 2015), which could be suggestive of a role in the selective MN vulnerability observed. These observations suggest that miRNAs could serve as useful clinical biomarkers but more importantly that their targeting could be a promising therapeutical strategy (Rupaimoole & Slack, 2017; De Paola *et al,* 2018).

Despite the recent identification of miRNAs, significant progress has been made in regards to their therapeutical manipulation both in vitro and in vivo, but also in clinical trials (Rupaimoole & Slack, 2017). Several miRNA-based therapeutic approaches have developed, which can be broadly categorised as miRNA mimics and inhibitors or anti-miRs used to replenish the loss or inhibit the overexpression of endogenous miRNA, respectively. miRNA mimics are double stranded RNAs, designed to carry the exact miRNA sequence in order to compensate for the loss of miRNA expression. On the contrary, miRNA inhibitors are single stranded RNAs which target specific miRNA sequences in order to block their expression (Pignataro, 2021; Rupaimoole & Slack, 2017).

4.2.b Screening for potential microRNAs dysregulation in SMA mice

Potential miRNAs targeting the 3' UTR region of mouse Kif5a were identified by TargetScan (Fig. 4.9). The initial screening was performed in SC tissue from SMAΔ7 and WT mice at p10, where we observed a significant downregulation of Kif5a in SMA mice. The following miRNAs were included: miR-17-5p, miR-16-5p, miR-140-3p, miR-103-3p, miR-17-5p and miR-20a, all predicted to target conserved sequences located in the 3' UTR of mouse Kif5a. U6, a small nuclear RNA was used as an endogenous control as it is shown to be highly stable in mouse SC tissues (Kalpachidou *et al*, 2019). The qPCR results showed a significant upregulation of miR140-3p at p10 (Fig. 4.10) which was also observed, to a lesser extent, at p5 (Fig. 4.11). miR-140-3p targets the position 78-84 of Kif5a 3' UTR and the site type is 7mer-m8, an exact match to positions 2-8 of the mature miRNA (the seed and position 8).

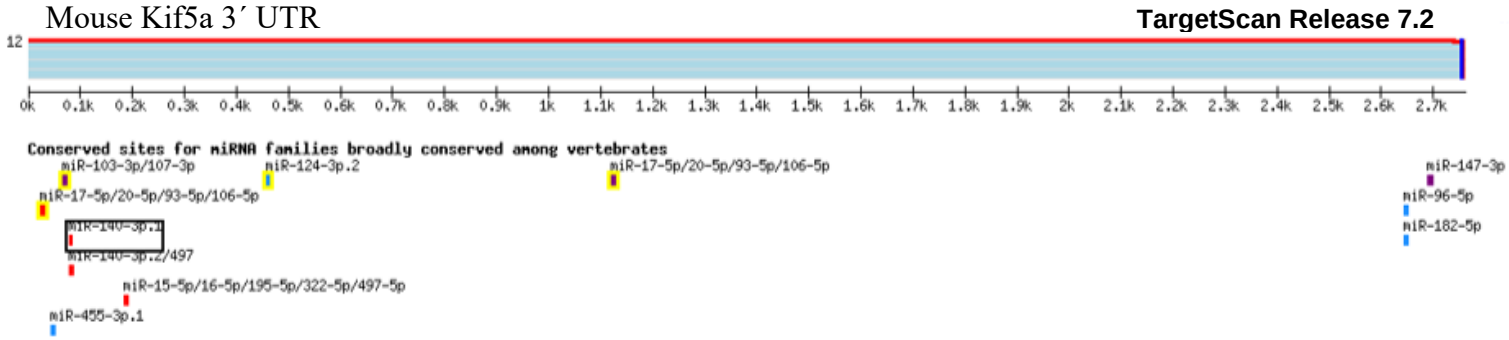

Figure 4.9: TargetScan results on miRNA targets of Kif5a. *These miRNAs are predicted to target the mouse 3′ UTR of Kif5a. This database is basing the predictions on seed matching, evolutionary conservation and complement matching.* ***http://www.targetscan.org/***

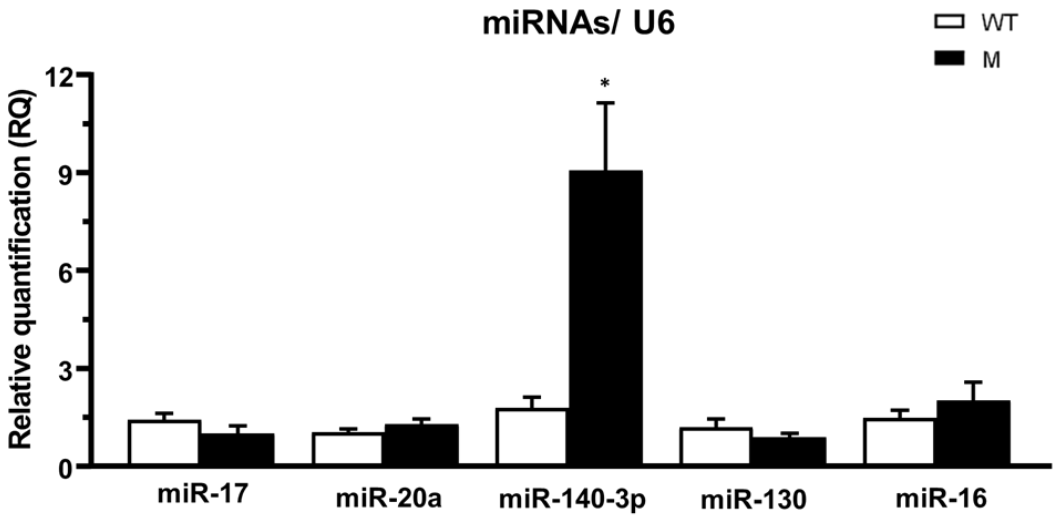

***Figure 4.10**: Quantitative real-time PCR results of selected miRNAs relative levels in the spinal cord of SMNΔ7 mice at p12. miR-140-3p is significantly upregulated in SMNΔ7 mice (M) compared to WT controls. U6: endogenous control, N=5-6, p<0.005. One-way ANOVA* followed by *Bonferroni test.*

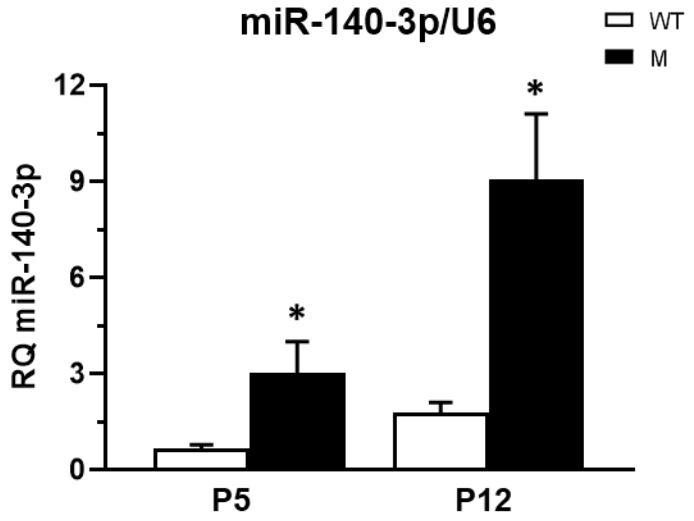

***Figure 4.11:** Quantitative real-time PCR results of miR-140-3p relative levels in the spinal cord of SMNΔ7 mice at p5 and p12. miR-140-3p is significantly upregulated in SMNΔ7 mice (M) compared to WT controls. U6 was used as endogenous control, N=5-6, p<0.05, Student's t test.*

4.2.c Investigation of the effect of mir-140-3p on Kif5a expression in vitro

In order to investigate if the upregulation of miR-140-3p is correlated with KIF5A expression, miR-140-3p mimic, inhibitor and a negative control with no homology to any mammalian gene were transiently transfected in SH-SY5Y cells and the levels of KIF5A were assessed after 48h with western blot analysis. The results showed a significant downregulation of KIF5A protein levels compared to the negative control (Fig. 4.12).

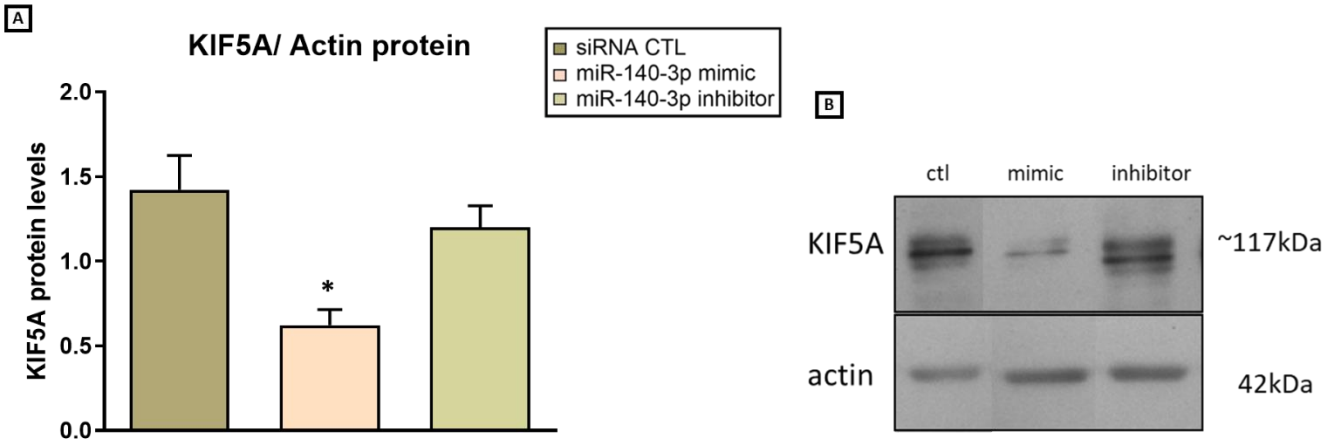

Figure 4.12: A. *KIF5A protein levels in SH-SY5Y cells transiently transfected with miR-140-3p mimic and inhibitor.* ***B:*** *Representative Western Blot images of KIF5A and actin. KIF5A levels are significantly reduced when miR-140-3p mimic is transfected compared to the control ($p<0.005$) and the inhibitor ($p<0.05$). The miRNA inhibitor does not affect KIF5A levels. Actin is used for protein normalisation. siRNA negative control is used as a control, N=3-5. One-way ANOVA* followed by *Bonferroni test.*

4.2.d Validation of microRNA interaction with Kif5a

Finally, the direct targeting of miR-140-3p to the predicted site on the 3' UTR of Kif5a at position 78-84 was investigated with a luciferase assay. First a 252bp region of the mouse 3'UTR containing the predicted miRNA site (position 49-300bp) was amplified from the total cDNA of a WT mouse spinal cord tissue with primers containing the restriction sites of XhoI and NotI used for restriction cloning in the pmirGLO vector. The total size of the PCR product, 271bp, was verified with agarose gel electrophoresis and inserted into the vector by ligation (Fig. 4.13). Six bases of the seed sequence were subsequently mutated and replaced with the EcoRV restriction site.

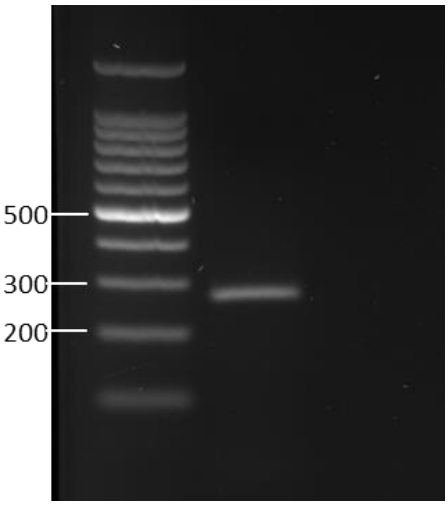

Figure 4.13: *Agarose gel of the PCR product of the mouse Kif5a 3'UTR plus the two restriction sites. The total size of the band is 271bp.*

Correct sized clones (7492bp) were identified by restriction digestion with XhoI and NotI and validated with two additional XhoI double digests with EcoRV or BamHI (Fig. 4.14).

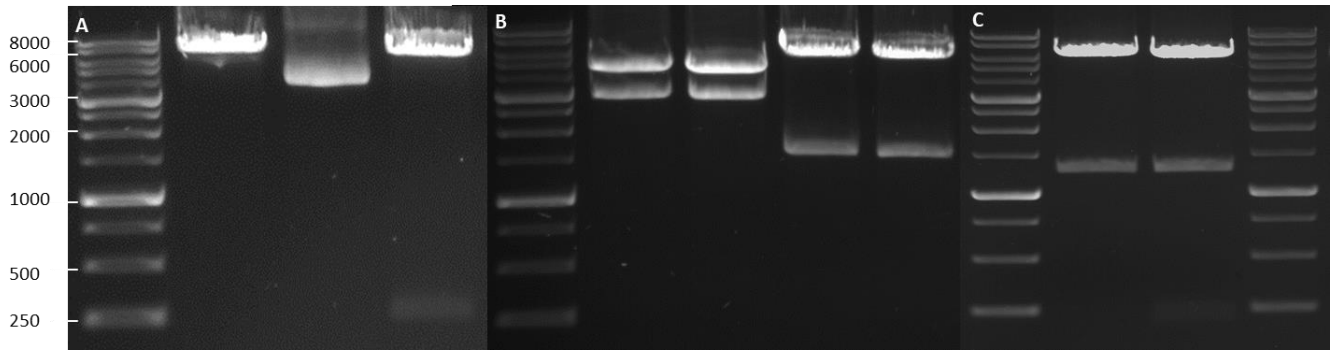

Figure 4.14: *Agarose gel of diagnostic digestions of the WT and mutated Kif5a 3'UTR region cloned into the pmirGLO vector. A. Cloning validation of WT 3'UTR in the pmirGLO vector with A. XhoI and NotI used for restriction cloning (the correct plasmid size is in lane 3, 7233 and 259bp) and B. XhoI and BamHI (4534 and 2958bp lane 1&2) and NotI & BamHI (4793 and 2699bp, lane3&4). C. Digestions of the WT 3'UTR and mutated 3'UTR plasmids with EcoRV and NotI, lane 1: 6211 and 1281bp, lane 2: 5989, 1281 and 222bp, respectively.*

The pmirGLO cloned WT and mutated 3' Kif5a UTR plasmids were then transiently co-transfected in SH-SY5Y cells with mir-140-3p mimic, inhibitor and siRNA negative control and the luciferase activity was measured after 48h as a firefly:renilla (F/R) ratio. The results showed that the luciferase activity was reduced when the WT 3'UTR of Kif5a was co-transfected with mir-140-3p compared with the negative control. The luciferase activity was restored when the 3'UTR was mutated (Fig. 4.15) suggesting that mir-140-3p interacts with the target region of the 3'UTR of Kif5a and moreover represses the expression of luciferase.

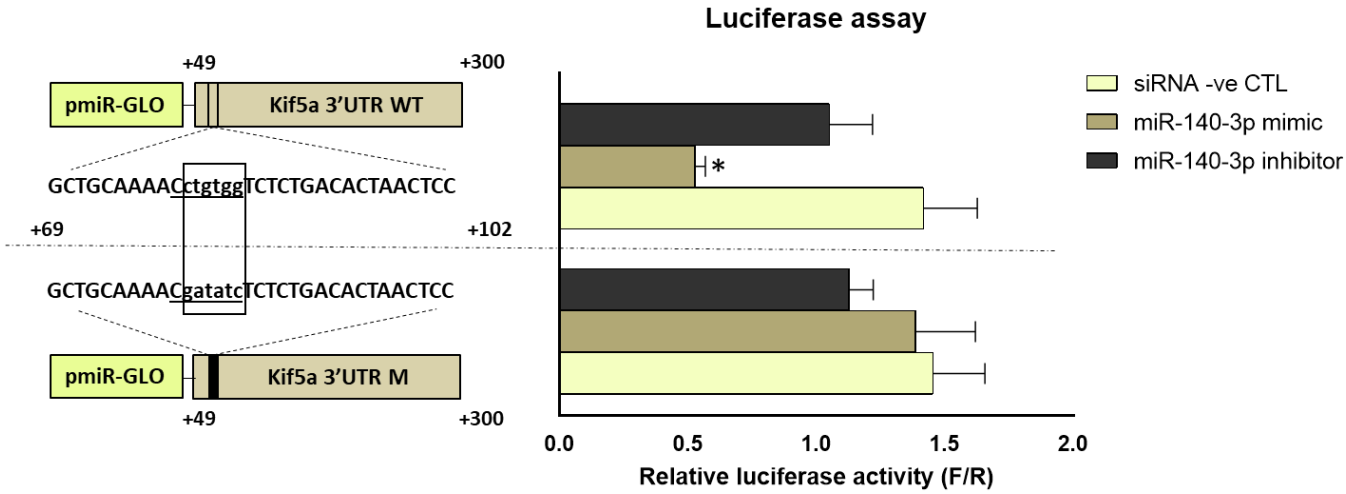

Figure 4.15: *The effect of miR-140-3p mimic and inhibitor on WT and mutated Kif5a 3'UTR in SH-SY5Y cells. The WT and mutated (M) pmiR-GLO-3' UTR plasmids used are shown on the left. 252bp of the mouse Kif5a 3' UTR (from +49- +300) were cloned downstream of the luc2 reporter gene. The seed sequence (+78- +84) is underlined. The box indicates the nucleotides mutated (+79- +84). The luciferase activity of the WT 3'UTR vector was significantly reduced when miR-140-3p mimic was present compared to the negative siRNA controls ($p<0.05$) and the mutated 3'UTR ($p<0.005$). Data are presented as firefly:renilla luminescence ratio (F/R), N=5-9. One-way ANOVA followed by Bonferroni test.*

4.3 Could SMN be a novel cargo of KIF5A?

Preliminary investigation of potential interaction between KIF5A with SMN and Gem2

In order to investigate the potential interaction of KIF5A with SMN, iPSCs from a healthy individual were differentiated into motor neurons. For the differentiation, the protocol described by Guo *et al* (2017) was followed (Fig. 4.16).

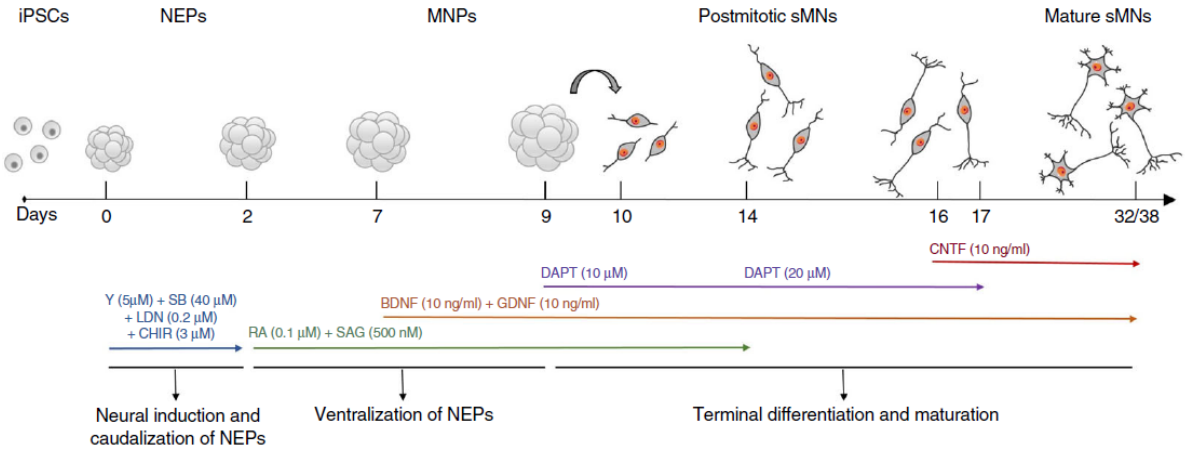

Figure 4.16: Schematic representation of the protocol for motor neuron differentiation*. NEPs neuroepithelial stem cells, MNPs motor neuron progenitors, sMNs spinal motor neurons. Y Y-27632, SB SB 431542, LDN LDN-193189, CHIR CHIR99021, RA retinoic acid, SAG smoothened agonist, DAPT a γ-secretase inhibitor, BDNF brain-derived neurotrophic factor, GDNF glial cell line-derived neurotrophic factor, CNTF, ciliary neurotrophic factor [Image from Guo et al, 2017].*

On day 36 of differentiation the cell line was characterised with staining for different neuronal markers: Isl1 (Islet1) expressed in all MN subtypes, ChAT (choline acetyltransferease) found exclusively in the spinal MNs and Smi32 non-phosphorylated neurofilament marker that stains spinal MNs (Guo *et al*, 2017; Qu *et al*, 2014). The marker immunostaining showed that ~80-90% of cells stained positive for these markers (Fig. 4.17).

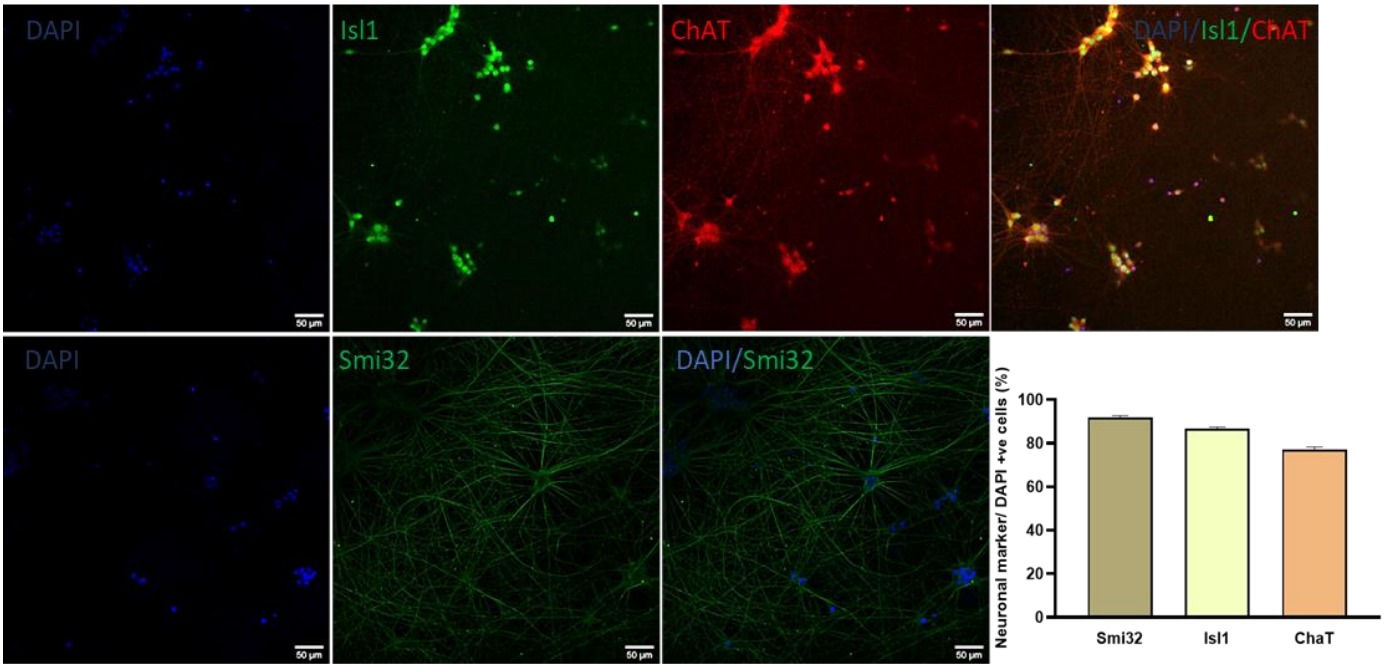

Figure 4.17: Characterisation of the iPSC-derived motor neuron cell line. *Staining for motor neuron markers, Isl1, ChAT, Smi32 and DAPI on day 36 of differentiation. Quantification of neuronal marker positive cells in relation to the total number of DAPI stained cells. N=10 images per staining.*

On day 36 of MN differentiation, the cells were stained for KIF5A and SMN or KIF5A and Gem2 in order to examine if KIF5A co-localises with SMN protein and Gem2, a protein which is a part of the SMN complex in the soma and axons. The results showed that there is a partial co-localisation of KIF5A with both proteins at similar levels in both soma and neurites but at higher levels in the cell soma (Fig. 4.18 &19).

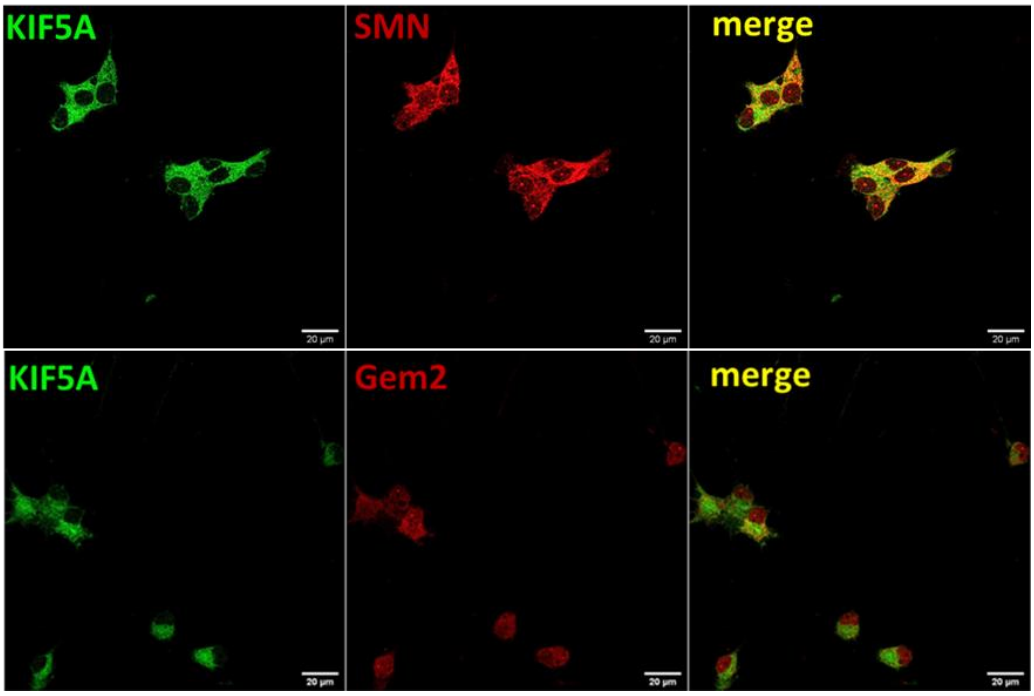

Figure 4.18: Co-localisation of KIF5A with SMN and Gem2 in the cell soma. *iPSC-derived motor neurons on day 36 of differentiation were stained for KIF5A/SMN (upper image) and KIF5A/Gem2 (lower image). Pearson's correlation coefficient for KIF5A and SMN is 0.658±0.02 and for Gem2 0.70±0.01. N=1, 9-10 images per staining were analysed.*

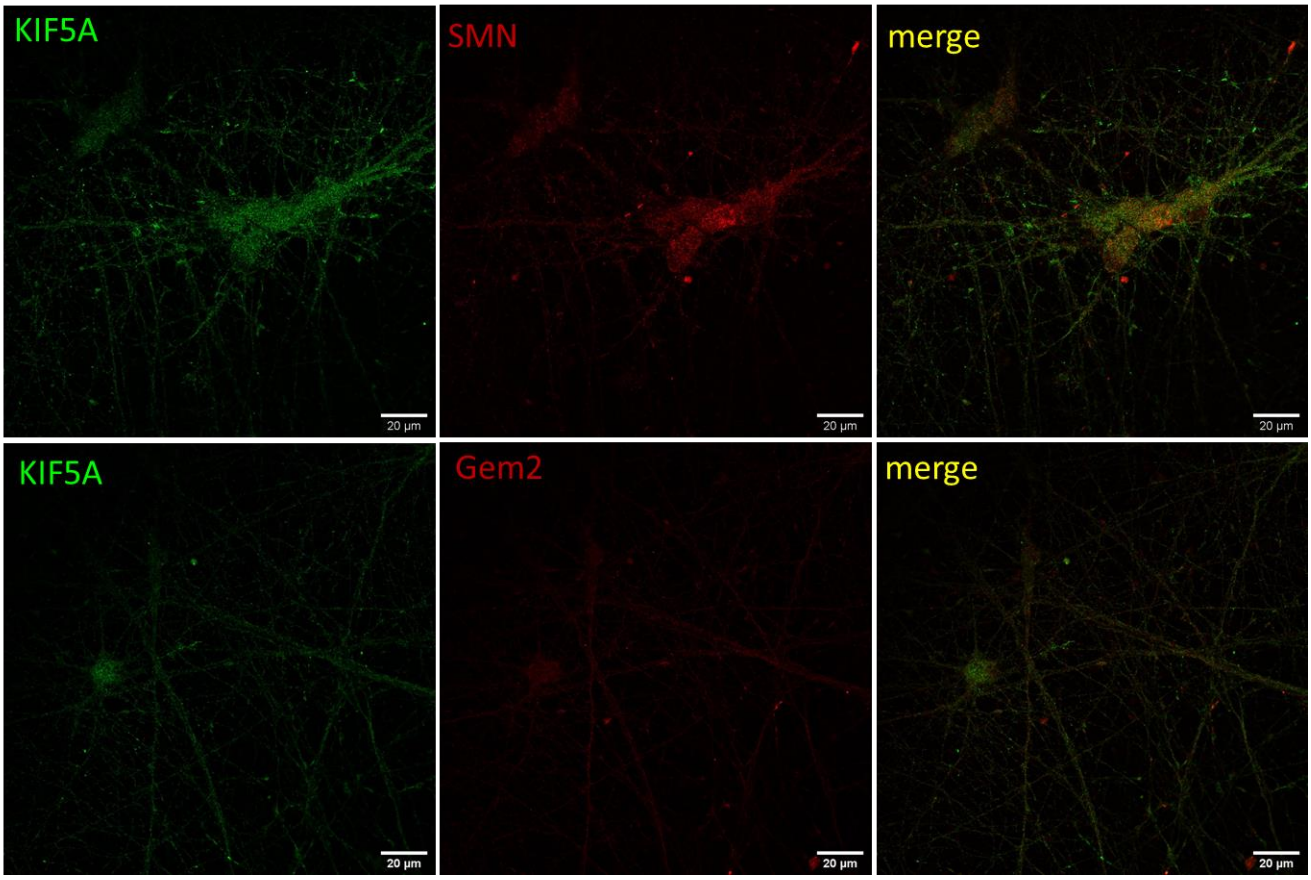

Figure 4.19: Co-localisation of KIF5A with SMN and Gem2, focusing on the neurites. *iPSC-derived motor neurons on day 36 of differentiation were stained for KIF5A/SMN (upper image) and KIF5A/Gem2 (lower image). Pearson's correlation coefficient for KIF5A and SMN is 0.35±0.02 and for Gem2 0.397±0.02. N=1, 9-10 images per staining were analysed.*

We then transfected SH-SY5Y cells with WT HA-KIF5A and GFP-SMN plasmids and after 24h we performed immunoprecipitation of the total KIF5A protein, endogenous and HA-tagged with anti-KIF5A antibody. The preliminary results of the co-IP assay of the total KIF5A with the GFP-SMN protein showed a band at 65kDa, corresponding to the GFP-SMN molecular weight and therefore is suggestive of a KIF5A-SMN interaction (Fig. 4.20).

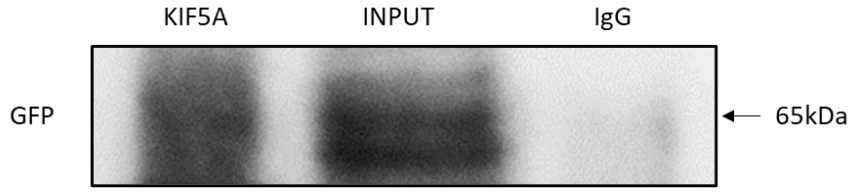

Figure 4.20: Co-immunoprecipitation (Co-IP) results of the interaction of the total KIF5A protein (HA-tagged and endogenous KIF5A) with GFP-SMN in SH-SY5Y cells after transient transfection. The western blot image shows a band at 65kDa in the first lane (co-IP) also present in the input, corresponding to the GFP-SMN protein. IgG: -ve control.

4.4. Functional study of two C-terminal *KIF5A* mutations reported in ALS & HSP

In order to examine if the pathological mechanism of the *KIF5A* mutations in ALS and HSP could be caused by defects in the mitochondrial transport via the TRAKs/Miro1 complex, two reported mutations, p.(Asn999Valfs*39) and p.R864* were introduced in a KIF5A custom plasmid. The presence of the mutations was verified with Sanger sequencing (Fig. 4.21). The plasmids contained an HA-tag in the N-terminal of KIF5A.

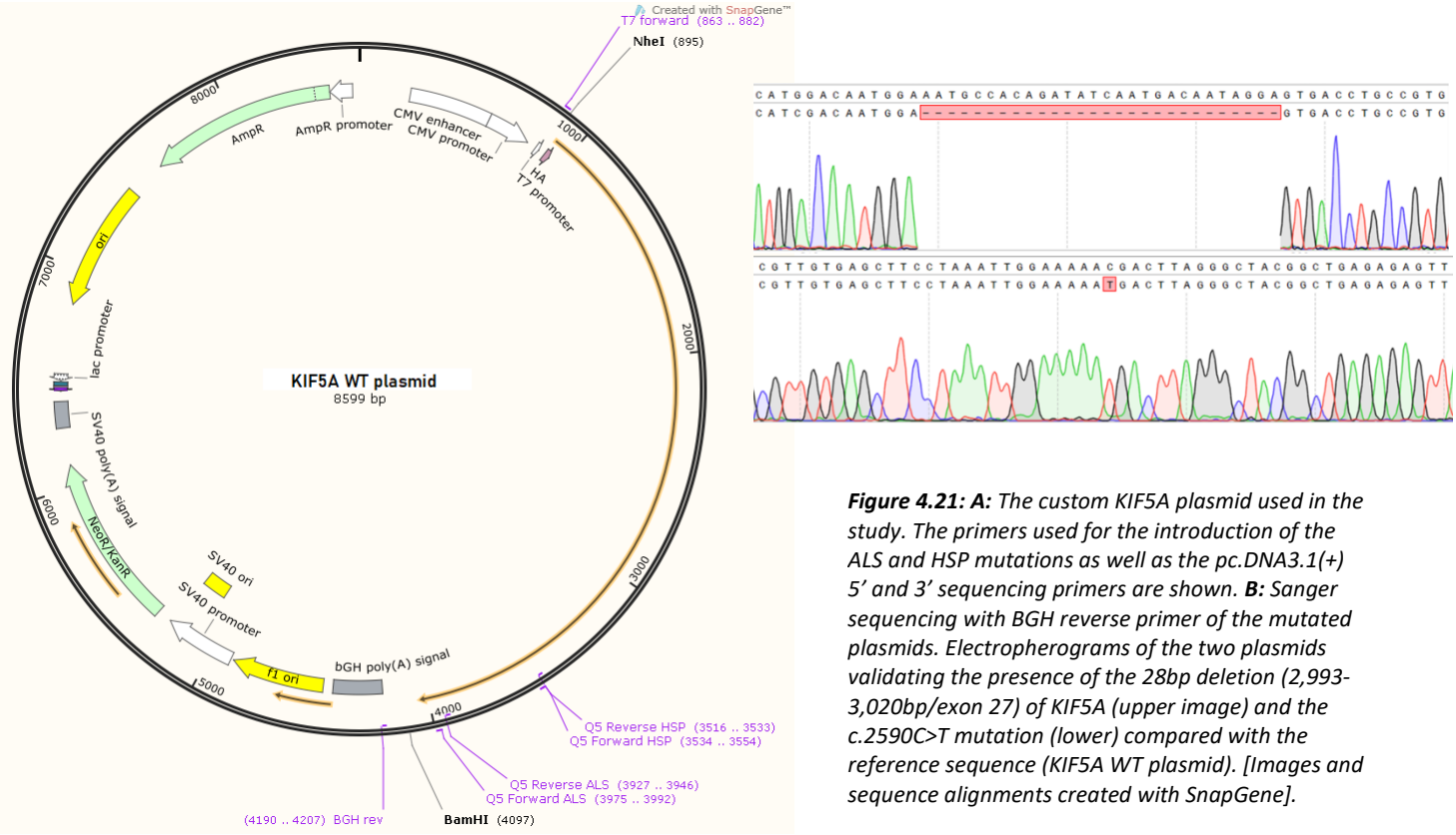

Figure 4.21: A: *The custom KIF5A plasmid used in the study. The primers used for the introduction of the ALS and HSP mutations as well as the pc.DNA3.1(+) 5' and 3' sequencing primers are shown.* ***B:*** *Sanger sequencing with BGH reverse primer of the mutated plasmids. Electropherograms of the two plasmids validating the presence of the 28bp deletion (2,993-3,020bp/exon 27) of KIF5A (upper image) and the c.2590C>T mutation (lower) compared with the reference sequence (KIF5A WT plasmid). [Images and sequence alignments created with SnapGene].*

The three plasmids were transiently transfected in SH-SY5Y cells and after 24h co-immunoprecipitation assays of the HA-tagged KIF5A with the endogenous TRAK1 were followed. Specifically, the same amounts of total protein from the three different transfection lysates were immunoprecipitated with an HA-tag antibody and HA-KIF5A-TRAK1 complexes were detected with Western Blot. The protein concentration of the lysates was also assessed with actin as a housekeeping protein. Two independent experiments were performed.

Since the transfection efficiency of the three plasmids was different, and thus the initial quantity of HA-KIF5A protein available for co-IP with TRAK1, the co-IPs were normalised to the HA-tag/actin ratio, ie the transfection efficiency of each construct. Interestingly, in two independent transfections, the full length KIF5A protein was also expressed in the case of the HSP plasmid with the truncating mutation. The results of the co-IP experiments are shown in Fig. 4.22-23.

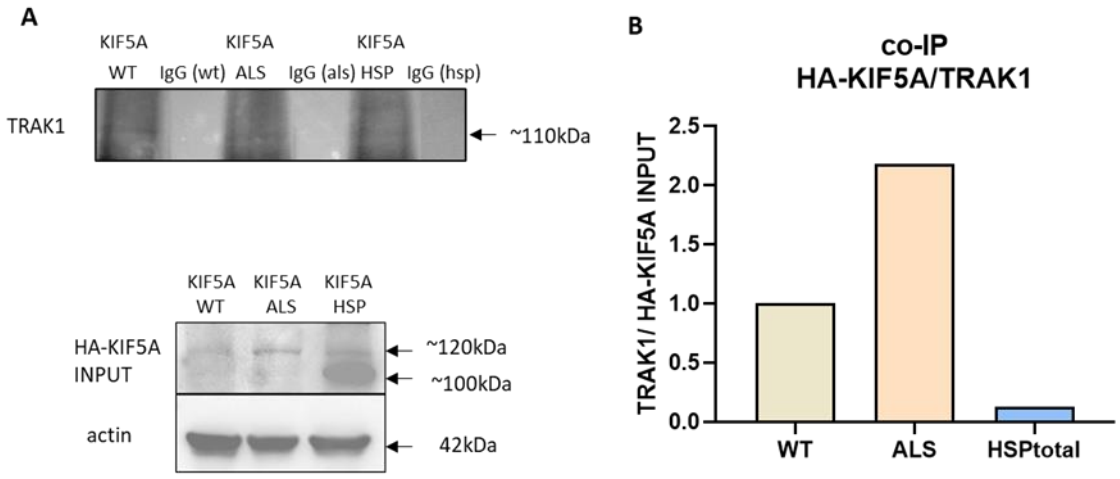

Figure 4.22: *Co-immunoprecipitation (Co-IP) analysis of the interaction of HA-tagged KIF5A constructs and endogenous TRAK1 in SH-SY5Y cells.* ***A.*** *Western blot images of Co-IPs of the three HA-KIF5A plasmids: wild type KIF5A, KIF5A with the ALS and HSP mutations with TRAK1 (upper image) and the transfection efficiency (INPUT) used for normalisation (lower image). HA-KIF5A (WT): 118.9kDa, HA-KIF5A (ALS): 119.7kDa, HA-KIF5A (HSP): 100.4kDa, IgG: negative control.* ***B.*** *Optical density of the co-IP bands of the mutated constructs compared with the WT, after normalisation with the HA-KIF5A INPUT:actin ratio.*

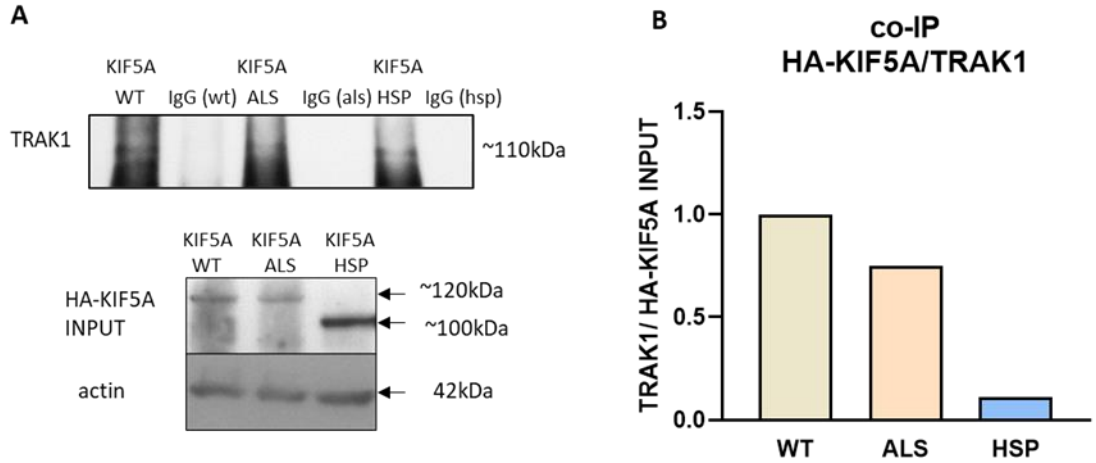

Figure 4.23: *Co-immunoprecipitation (Co-IP) analysis of the interaction of HA-tagged KIF5A constructs and endogenous TRAK1 in SH-SY5Y cells.* ***A****. Western blot images of Co-IPs of the three HA-KIF5A plasmids: wild type KIF5A, KIF5A with the ALS and HSP mutations with TRAK1 (upper image) and the transfection efficiency (INPUT) used for normalisation (lower image). HA-KIF5A (WT): 118.9kDa, HA-KIF5A (ALS): 119.7kDa, HA-KIF5A (HSP): 100.4kDa, IgG: negative control.* ***B.*** *Optical density of the co-IP bands of the mutated constructs compared with the WT, after normalisation with the HA-KIF5A INPUT:actin ratio.*

Although our co-IP analysis cannot quantitatively assess the interaction of KIF5A-TRAK1, the overall results (Fig. 4.24) are suggestive of a loss of interaction of the KIF5A-TRAK1 in the case of the KIF5A p.R864* HSP mutation. For the p.Asn999Valfs*39 ALS mutation although there seems to be an enhanced interaction compared with the WT KIF5A but also the HSP KIF5A, the results were inconclusive.

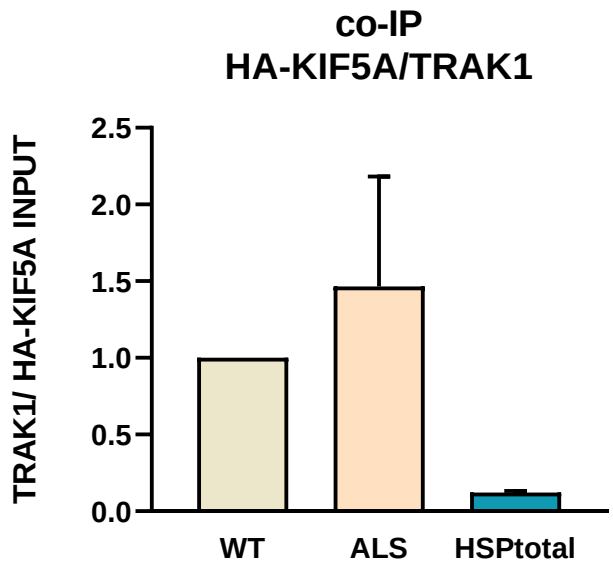

Figure 4.24: *Total co-immunoprecipitation (Co-IP) results of the interaction of HA-tagged KIF5A constructs and endogenous TRAK1 in SH-SY5Y cells. Optical density of the co-IP bands of the mutated constructs compared with the WT, after normalisation with the HA-KIF5A INPUT:actin ratio. N=2.*

Overall, the results could be suggestive of a different mechanism of the ALS and HSP-causing mutations in regards to TRAK1 binding and thus the mitochondrial transport complex.

5. DISCUSSION

In the present study we report for the first time the involvement of the Kif5a-Miro1 mitochondrial transport complex in SMA, the identification of miR-140-3p as a regulator of Kif5a levels and we provide preliminary evidence of a potential interaction of KIF5A with SMN and Gem2 in motor neurons. Finally, our investigation of the first truncating HSP mutation in *KIF5A* is suggestive of a loss of interaction with its mitochondrial adaptor protein, TRAK1 and potentially a different pathogenic mechanism to the ALS mutations.

Axonal transport defects play a critical and, in some cases, a causative role in MNDs. Several studies are currently focusing on axonal transport defects as a common nominator in neurodegeneration (Sleigh *et al,* 2019). KIF5A, a major component of the axonal transport machinery, has been associated with different MNDs and neurodegeneration, including ALS and HSP (Guo *et al,* 2019). Although its role in the axonal transport defects and particularly of mitochondria and neurofilaments in those diseases has been the focus of several studies (Smith *et al,* 2019; De Vos & Hafezparast, 2017), its role in SMA has not been fully characterized yet.

Mitochondria are almost exclusively transported via kinesin 1, with the exception of KIF1Bα (Hirokawa & Noda, 2008). As SMA selectively affects MNs, the role of KIF5A and KIF5C, the neuron specific molecular motors, is of particular interest. The importance of axonal transport is particularly emphasized in the case of neurons and notably spinal MNs, as they constitute the longest known cell type (Stifani, 2014). The axon terminals are the regions with the highest demand of energy, consuming billions of ATP molecules per second even at a resting state (Schwartz, 2013). The transport and distribution of mitochondria is therefore crucial and any damage or impairment to their transport machinery is likely to have a profound impact on the survival and function of neurons as well as on the dying-back pattern described (de Vos *et al,* 2012; Morfini *et al,* 2012).

In our study, the SMNΔ7 mouse, a model corresponding to moderate type II SMA (SMA II) was used. SMNΔ7 is the most widely used SMA mouse model as it has a prolonged lifespan compared with the previously developed severe SMA mice models (Le *et al,* 2005). A previous study on this mouse model had revealed a disruption of the anterograde as well as the retrograde axonal transport and reported reduced cargo transport and dynein levels. Kif5c however was not found reduced at the NMJ (Dale *et al,* 2011). Furthermore, as already discussed, mitochondrial distribution, transport and morphological defects are present in spinal MNs

starting from the early stages of the disease (Xu *et al,* 2016). Our study of different brain regions and the SC of SMNΔ7 mice shows that Kif5a and Miro1 are differentially expressed in WT and SMA mice and could contribute to axonal transport defects in SMNΔ7 mice.

Specifically, in the brainstem we observed a significant upregulation of Kif5a protein only at early stages of the disease which could reflect an early compensatory mechanism to the axonal degeneration, known to begin early in the SMA pathology (Xu *et al,* 2016). In the prefrontal cortex, Kif5a protein levels were reduced at late stages while Miro1 was significantly reduced at early stages and, although not statistically significant, also at late stages of the disease it appeared less expressed. This phenomenon, could be explained as the result of the extensive mitochondrial damage that has been previously reported in SMA (Miller *et al,* 2016; Xu *et al,* 2016). Mitochondrial damage leads to a PINK1/Parkin-dependent degradation of Miro1 with subsequent mitochondrial arrest (Wang *et al,* 2011). This mechanism may also be responsible for Miro1 degradation associated to anterograde mitochondrial transport reduction in SOD1 ALS mice (Moller *et al,* 2017), where low Miro1 levels in the SC and anterograde mitochondrial transport deficits have been repeatedly reported (Zhang *et al*, 2015). It would be interesting to investigate whether the same mechanism could have a role in SMA pathophysiology and if the loss of SMN could be responsible for the induced degradation. However, the disruption of Ca^{+2} homeostasis, previously reported in SMNΔ7 mice (Ruiz *et al,* 2010), possibly due to mitochondrial damage, could also represent a contributing factor in the mitochondrial transport arrest observed in this SMA model. In fact, Miro1 function is Ca^{+2} sensitive (Schwartz, 2013).

In our study in the SC of SMNΔ7 mice, Kif5a mRNA levels were found significantly reduced at early stages of the disease. However, Kif5a and Miro1 protein levels were consistently lower than the WT controls during both early and late stages of the disease. The SC is primarily affected in SMA where there is an extensive loss of lower MNs, a hallmark of SMA pathogenesis. Indeed, IHC analysis of the SC of SMNΔ7 mice revealed an extensive neurodegeneration and also an overall reduction of Kif5a staining in the remaining NeuN+ cells and specifically in the somatic motor nuclei, where we focused our analysis. These results in combination with WB analysis of Kif5a and Miro1 could be suggestive that the previously reported disruption of the anterograde transport of mitochondria and possibly of other cargo could be due to loss of Kif5a complexes with Miro1 or other adaptor proteins and cargos, respectively.

Of course, it would be important to investigate whether the other two isoforms of kinesin 1, KIF5B and C could also be implicated in SMA or if they could compensate for the reduction of KIF5A. It has been suggested that there is a functional redundancy between the three KIF5s not only because of the high homology they share but also as they all mostly bind cargoes through the highly conserved binding regions of KLC (Kanai *et al,* 2000). Although mitochondria are transported with adaptor proteins, TRAK1 and 2, and not KLC, this could apply for other kinesin 1 cargoes. It has been shown that KIF5A and B can rescue the Kif5c null mice from a severe phenotype (Kanai *et al,* 2000). Recent gene expression studies in SOD1 G93A mouse SC have reported only a Kif5a reduction as the disease progresses (Maniatis *et al,* 2019) which could be suggestive that the mitochondrial axonal transport defects that are reported in ALS are not rescued by an upregulation of Kif5b and c.

Future experiments should focus on validating the mitochondrial axonal transport impairment in-vitro in primary SMNΔ7 MN cultures with live imaging but also check the distribution of mitochondria and the Kif5a complex along the axons. Also, it would be important to investigate with IHC the co-localisation of Kif5a with Trak1/2 and Miro1, particularly in the SC of SMA mice at early and late stages of the disease. Our preliminary results show that in the brainstem at p5 the Kif5a upregulation is accompanied with a Trak1 mRNA upregulation and that Trak2 is also found downregulated at p10 in the cortex. Their study could be of significance as these adaptor proteins are recently reported to act as activators of kinesin 1 (Fenton *et al,* 2021; Henrichs *et al,* 2020).

In order to restore Kif5a levels a miRNA strategy was developed. MiRNA tools have emerged as a novel therapeutic approach in order to manipulate gene expression mainly in cancer but also proposed as targets for MND therapeutics. Several miRNAs have been associated with ALS and SMA and their targeting shows some encouraging results in-vivo (Diener *et al,* 2022; De Paola *et al,* 2018). Our initial screening in SMNΔ7 SC tissue, where the most dramatic Kif5a downregulation was observed, revealed a significant increase in miR-140-3p levels as the disease progressed. MiR-140-3p, previously implicated in cancer-related pathways (Liu *et al,* 2021), is a 22nt long molecule, predicted to target the 3'UTR of Kif5a with a stringent 7mer-m8 site type. This miRNA-RNA interaction was confirmed with a luciferase reporter assay in SH-SY5Y cells, resulting in a decrease in luciferase activity when the site was mutated. Although the mouse Kif5a 3' UTR length is over 2,500bp, we cloned only a small region containing the predicted target sequence. In this way, we investigated the mir-140-3p mimic interaction with the specific site as opposed to the whole UTR and non-specific effects were

limited. However, we did not assess any additional interactions with other regions. MiR-140-3p levels in SH-SY5Y cells transfected with mir-140-3p inhibitor and siRNA negative control were also assessed with qPCR and found to be at extremely low levels or undetected compared to the miRNA-mimic transfected cells, therefore an effect of endogenous miRNA on the luciferase expression, if any, would be limited. MiR-140-3p was also shown to downregulate Kif5a expression in-vitro, suggesting that manipulation of miR-140-3p levels could be an effective strategy in elevating Kif5a. We cannot exclude however that a combination of miRNAs could act in order to regulate Kif5a. Future experiments with in-vivo administration of miR-140 inhibitor in SMA mice should also be conducted. These will determine whether the downregulation of miR-140 restores Kif5a levels and can potentially have a beneficial effect on MN survival, motor performance and lifespan of these mice.

Besides the involvement of the Kif5a-Miro1 complex in mitochondrial transport defects in SMA that our study suggests, a reduction of Kif5a levels could also have an effect on the transport of other known Kif5a cargo such as neurofilaments but also novel ones. We hypothesise that SMN could be a novel cargo of KIF5A for two main reasons. First, SMN is actively transported along the axons at rates consistent with fast axonal transport (Donlin-Asp *et al*, 2016). The second reason is that overexpression of SMN in SOD1 and TDP-43 mice resulted in a perinuclear accumulation of SMN limiting its beneficial effects on the phenotype (Perera *et al*, 2016). Both mouse models are known to present with axonal transport impairment and in SOD1 also a Kif5a reduction. Indeed, our preliminary investigation to test this hypothesis showed a partial co-localisation of SMN with Kif5a in human iPSC-derived MNs at similar levels with Gem2, recently shown to be a part of the SMN-complex in the axons (Fallini *et al*, 2011) and an interaction of KIF5A with SMN1 in SH-SY5Y cells. Although this data could be suggestive of KIF5A contributing to the SMN-Gem2 complex transport along the axons, further co-IP experiments of KIF5A with SMN and Gem2 should be conducted to validate these results.

If the hypothesis is confirmed, this will be important not only to understand the axonal role of SMN and the contribution of axonal RNA trafficking and local translation defects in SMA but also in other MNDs. For example, we know that in SMA but also in ALS and healthy MNs, SMN levels are widely heterogeneous with low levels predisposing to cell death (Rodriguez-Muela *et al*, 2017). In FUS ALS the axonal distribution of SMN is disrupted (Groen *et al*, 2013). As already discussed, there are currently many studies suggesting a significant overlap between SMA and ALS and a broader role of SMN in MNDs (Cacciotolo *et al*, 2019;

Rodriguez-Muela *et al,* 2017). With SMN-elevating strategies being currently available (Mercuri *et al,* 2020) it would be particularly interesting to investigate whether restoring not only the levels but also the transport and axonal localisation of SMN via KIF5A or another kinesin in combination could be beneficial in SMA and potentially other MNDs. For all the above-mentioned reasons we believe that KIF5A has a central role in MNDs and that developing a strategy elevating KIF5A levels could be beneficial not only in SMA but in other neurodegenerative diseases.

The role of KIF5A in ALS has been currently the focus of many investigations since the identification of KIF5A as an ALS causative gene in 2018 (Brenner *et al,* 2018; Nicolas *et al,* 2018). Although the KIF5A ALS mutations, all causing a longer-aberrant C-terminal were initially hypothesised to be loss of function (Nicolas *et al,* 2018), three studies now report that they are gain of function (GOF), resulting in increased transport and KIF5A mislocalisation, altered protein and RNA interactions (Baron *et al,* 2022), cytoplasmic aggregate formation (Nakano *et al,* 2022) and increased microtubule binding and activity (Pant *et al,* 2022). Specifically, Baron et al suggest that this GOF is due to the loss of autoinhibition by the IAK motif located upstream of the mutations, resulting in a hyperactive mutant KIF5A and an accumulation of cargo in the growth cones affecting neuron survival. The same group reports altered cargo binding, differences in gene expression and nucleocytoplasmic transport as well as splicing defects and increased anterograde mitochondrial transport and velocity.

KIF5A mutations reported so far cause a range of phenotypes, from mild forms (HSP/CMT) to severe fatal syndromes (ALS/NEIMY). The specific location of the mutation seems to play a crucial role. The mutations chosen for our study are an HSP mutation, truncating the whole C-terminal of KIF5A (864-1032AA), including the IAK motif, and an ALS mutation causing the exon 27-skiping and an aberrant, longer C-terminal. Our aim was to investigate the mitochondria binding differences between these two mutations and the WT protein. The three KIF5A constructs were tagged with HA, a very short sequence, in the N-terminal to minimise an effect on the binding efficiency and the overall function of the proteins. The constructs were overexpressed in human SH-SY5Y cells and the co-IPs of the HA-KIF5A with the endogenous TRAK1 were analysed. The preliminary results suggest a reduced KIF5A-TRAK1 interaction in the case of the HSP mutation compared with the WT-KIF5A.

A previous study reported that although KIF5A retained the ability to bind TRAK1 when the 877-1032AA region was deleted, there is a loss with a larger KIF5A deletion starting from

825AA (Randall *et al,* 2013). Therefore, we suggest that the 864-877 region of KIF5A is critical for TRAK1 binding. The same study had reported an increased TRAK2 binding efficiency when the unique 961-1032AA region was deleted and was reduced only by the larger 825-1032AA deletion. Further studies should examine whether or how the HSP deletion affects the TRAK2 binding. An enhanced TRAK2 interaction could compensate for the loss of TRAK1 mitochondrial binding-transport and thus explain the mild HSP phenotype we observe.

Interestingly, in two transfections the full-length WT protein was also expressed, although at significantly lower levels. The nonsense suppression or else the read-through translation of a nonsense mutation, has been previously described mainly in procaryotes but there are reports of an in-vivo 'correction' of human genes. This read-through is suggested to be caused by natural suppressor tRNAs that mask the stop codon (Beier *et al,* 2001). Although this is a rare phenomenon and the full-length protein produced could be at insufficient amounts, it could in some cases be beneficial. It has been reported that the UGA stop codon, introduced in our KIF5A transcript by the HSP mutation, has been also supressed in a nonsense mutation causing Menkes disease, resulting to an ameliorated clinical presentation (Kaler *et al,* 2009).

In the case of the ALS mutation our initial results suggested an increased interaction with TRAK1, however this was not replicated in the subsequent experiment that showed no significant difference with the WT. Although we attempted a semi-quantification of the co-IPs with normalisation with the input KIF5A, a higher number of experiments is required to reveal small differences and the result is inconclusive. A proximity-ligation-assay (PLA) could also be employed to increase sensitivity. As studies now suggest that ALS mutations are GOF, it is possible that there is indeed an enhanced TRAK1 interaction. TRAK1 is the main kinesin 1 adaptor protein in axons and any differences in binding would most likely reflect an alteration in axonal mitochondrial transport. Nevertheless, the difference that we observed of the two mutations, the HSP and ALS, in binding TRAK1 could be suggestive of a different mechanism of the two mutations in regards to mitochondrial transport. Baron et al reported that the mitochondrial transport is increased in the ALS mutant. Moreover, the motile events and run lengths along the microtubules of the ALS mutant are also increased and comparable to a constitutively active protein. It is interesting that both ALS and HSP mutants are constitutively active, since the autoinhibitory IAK motif is deleted in the HSP mutation. In the case of the HSP mutations, it could be hypothesised that although the protein is constitutively active, the reduction of binding of TRAK1 that we observed, could limit the toxic effects of the loss of autoinhibition that we see in the ALS mutant, at least regarding the mitochondrial transport.

Future live imaging experiments could be performed to compare the mitochondrial transport of the two mutations.

Finally, it's worth noting that the exact aberrant 39aa C-terminal sequence of the ALS mutant, now reported to result in a toxic GOF, is also a part of the longer, 72bp p.S974fs NEIMY KIF5A mutant C-terminal. The phenotype of the NEIMY patients is also severe however notably different from ALS, for example they present with myoclonic seizures and progressive leukoencephalopathy (Rydzanicz *et al,* 2017). It is interesting that GABARAP, a cargo specifically transported by KIF5A, requires the unique C-terminal 73bp in order to bind (Nakajima *et al,* 2012). Thus, we can further assume that the additional residues that are mutated in NEIMY are critical for the GABARAP trafficking, most likely not affected in ALS due to the lack of an epileptic phenotype in the KIF5A patients.

To conclude, there is a growing interest in the role of KIF5A not only in ALS and HSP but also in the context of MNDs and neurodegeneration in general. New studies are now trying to extend our knowledge on KIF5A-specific cargo (Fukuda *et al,* 2021) and are pointing to KIF5A as a major regulator of neurodegeneration (Shah *et al,* 2022). We feel that KIF5A has a critical role in MNDs and KIF5A-targeted strategies to restore defective transport will have an impact not only in ALS and SMA but potentially also in other neurodegenerative diseases.

REFERENCES

Adio S, Reth J, Bathe F, Woehlke G (2006) Review: regulation mechanisms of Kinesin-1. *Journal of Muscle Research and Cell Motility* **27(2):**153-60

Baron DM, Fenton AR, Saez-Atienzar S, Giampetruzzi A, Sreeram A, Shankaracharya, Keagle PJ, Doocy VR, Smith NJ, Danielson EW *et al* (2022) ALS-associated KIF5A mutations abolish autoinhibition resulting in a toxic gain of function. *Cell Reports* **39(1):**110598

Beier H, Grimm M (2001) Misreading of termination codons in eukaryotes by natural nonsense suppressor tRNAs. *Nucleic Acids Research* **29(23):**4767-82

Bilsland LG, Sahai E, Kelly G, Golding M, Greensmith L, Schiavo G (2010) Deficits in axonal transport precede ALS symptoms in vivo. *Proceedings of the National Academy of Sciences of the United States of America* **107(47):**20523-8

Biros I, Forrest S (1999) Spinal muscular atrophy: untangling the knot? *Journal of Medical Genetics* **36(1):**1-8

Boza-Morán MG, Martínez-Hernández R, Bernal S, Wanisch K, Also-Rallo E, Le Heron A, Alías L, Denis C, Girard M, Yee JK, Tizzano EF, Yáñez-Muñoz RJ (2015) Decay in survival motor neuron and plastin 3 levels during differentiation of iPSC-derived human motor neurons. *Scientific Reports* **5:**11696

Brenner D, Yilmaz R, Muller K, Grehl T, Petri S, Meyer T, Grosskreutz J, Weydt P, Ruf W, Neuwirth C *et al* (2018) Hot-spot KIF5A mutations cause familial ALS. *Brain* **141(3):**688-697

Brenner D & Weishaupt GH (2019) Update on amyotrophic lateral sclerosis genetics. *Current Opinion in Neurology* **32:**735–739

Bricceno KV, Fischbeck KH, Burnett BG (2012) Neurogenic and myogenic contributions to hereditary motor neuron disease. *Neurodegenerative Diseases* **9(4):**199-209

Burghes AH & Beattie CE (2009) Spinal muscular atrophy: why do low levels of survival motor neuron protein make motor neurons sick? *Nature Reviews. Neuroscience* **10(8):**597-609

Burk K & Pasterkamp RJ (2019) Disrupted neuronal trafficking in amyotrophic lateral sclerosis. *Acta Neuropathologica* **137(6):**859-877

Cacciottolo R, Ciantar J, Lanfranco M, Borg RM, Vassallo N, Bordonné R, Cauchi RJ (2019) SMN complex member Gemin3 self-interacts and has a functional relationship with ALS-linked proteins TDP-43, FUS and Sod1. *Scientific Reports* **9(1):**18666

Campbell PD, Shen K, Sapio MR, Glenn TD, Talbot WS, Marlow FL (2014) Unique function of Kinesin Kif5A in localization of mitochondria in axons. *The Journal of Neuroscience* **34:**4717–14732

Cauchi RJ (2014) Gem depletion: amyotrophic lateral sclerosis and spinal muscular atrophy crossover. *CNS Neuroscience and Therapeutics* **20(7):**574-81

Chaytow H, Huang YT, Gillingwater TH, Faller KME (2018) The role of survival motor neuron protein (SMN) in protein homeostasis. *Cellular and Molecular Life Sciences* **75(21):**3877-3894

Chen TH, Chen JA (2019) Multifaceted roles of microRNAs: From motor neuron generation in embryos to degeneration in spinal muscular atrophy. *Elife* **8:**e50848

Chrestian N, Dupré N, Gan-Or Z, Szuto A, Chen S, Venkitachalam A, Brisson JD, Warman-Chardon J, Ahmed S, Ashtiani S *et al* (2016) Clinical and genetic study of hereditary spastic paraplegia in Canada. *Neurology, Genetics* **3(1):**e122

Coy DL, Hancock WO, Wagenbach M, Howard J (1999) Kinesin's tail domain is an inhibitory regulator of the motor domain. *Nature cell biology* **1(5):**288-92

Crimella C, Baschirotto C, Arnoldi A, Tonelli A, Tenderini E, Airoldi G, Martinuzzi A, Trabacca A, Losito L, Scarlato M, Benedetti S, Scarpini E, Spinicci G, Bresolin N, Bassi MT (2012) Mutations in the motor and stalk domains of KIF5A in spastic paraplegia type 10 and in axonal Charcot-Marie-Tooth type 2. *Clinical Genetics* **82(2):**157-64

Dale JM, Shen H, Barry DM, Garcia VB, Rose FF Jr, Lorson CL, Garcia ML (2011) The spinal muscular atrophy mouse model, SMAΔ7, displays altered axonal transport without global neurofilament alterations. *Acta Neuropathologica* **122(3):**331-41

de Fuenmayor-Fernández de la Hoz CP, Hernández-Laín A, Olivé M, Sánchez-Calvín MT, Gonzalo-Martínez JF, Domínguez-González C (2019) Adult-onset distal spinal muscular atrophy: a new phenotype associated with KIF5A mutations. *Brain* **142(12):**e66

De Paola E, Verdile V, Paronetto MP. Dysregulation of microRNA metabolism in motor neuron diseases: Novel biomarkers and potential therapeutics (2018) *Noncoding RNA Research* **4(1):15-**22

De Vos & Hafezparast (2017) Neurobiology of axonal transport defects in motor neuron diseases: Opportunities for translational research? *Neurobiology of disease **105:**283-299*

De Vos KJ, Grierson AJ, Ackerley S, Miller CC (2008) Role of axonal transport in neurodegenerative diseases. *Annual Review of Neuroscience* **31:**151-73

Dietrich KA, Sindelar CV, Brewer PD, Downing KH, Cremo CR, Rice SE (2008) The kinesin-1 motor protein is regulated by a direct interaction of its head and tail. *Proceedings of the National Academy of Sciences of the United States of America* **105(26):**8938-43

Dombert B, Sivadasan R, Simon CM, Jablonka S, Sendtner M (2014) Presynaptic localization of Smn and hnRNP R in axon terminals of embryonic and postnatal mouse motoneurons. *PLoS One* **9(10):**e110846

Donlin-Asp PG, Fallini C, Campos J, Chou CC, Merritt ME, Phan HC, Bassell GJ, Rossoll W (2017) The Survival of Motor Neuron Protein Acts as a Molecular Chaperone for mRNP Assembly. *Cell Reports* **18(7):**1660-1673

Duis J, Dean S, Applegate C, Harper A, Xiao R, He W, Dollar JD, Sun LR, Waberski MB, Crawford TO, Ada Hamosh A, Stafstrom CE (2016) *KIF5A* mutations cause an infantile

onset phenotype including severe myoclonus with evidence of mitochondrial dysfunction. *Annals of Neurology* **80(4):**633–637

Ebbing B, Mann K, Starosta A, Jaud J, Schöls L, Schüle R, Woehlke G (2008) Effect of spastic paraplegia mutations in KIF5A kinesin on transport activity. *Human Molecular Genetics* **17(9):**1245-52

Fallini C, Zhang H, Su Y, Silani V, Singer RH, Rossoll W, Bassell GJ (2011) The survival of motor neuron (SMN) protein interacts with the mRNA-binding protein HuD and regulates localization of poly(A) mRNA in primary motor neuron axons. *The Journal of Neuroscience* **31(10):**3914-25

Fenton AR, Jongens TA, Holzbaur EL (2021) Mitochondrial adaptor TRAK2 activates and functionally links opposing kinesin and dynein motors. *Nature Communications* **12(1):**1-5

Figueroa-Romero C, Hur J, Lunn JS, Paez-Colasante X, Bender DE, Yung R, Sakowski SA, Feldman EL (2016) Expression of microRNAs in human post-mortem amyotrophic lateral sclerosis spinal cords provides insight into disease mechanisms. Molecular and Cellular Neurosciences 71:34-45

Filipowicz W, Bhattacharyya SN, Sonenberg N (2008) Mechanisms of post-transcriptional regulation by microRNAs: are the answers in sight? *Nature Reviews. Genetics* **9(2):**102-14

Filosto M, Piccinelli SC, Palmieri I, Necchini N, Valente M, Zanella I, Biasiotto G, Lorenzo DD, Cereda C, Padovani A (2018) A Novel Mutation in the Stalk Domain of *KIF5A* Causes a Slowly Progressive Atypical Motor Syndrome. *Journal of Clinical Medicine* **8(1):**17

Fink JK (2013) Hereditary spastic paraplegia: clinico-pathologic features and emerging molecular mechanisms. *Acta Neuropathologica* **126(3):**307-28

Fukuda Y, Pazyra-Murphy MF, Silagi ES, Tasdemir-Yilmaz OE, Li Y, Rose L, Yeoh ZC, Vangos NE, Geffken EA, Seo HS *et al* (2021) Binding and transport of SFPQ-RNA granules by KIF5A/KLC1 motors promotes axon survival. *Journal of Cell Biology* **220(1):**e202005051

Giavazzi A, Setola V, Simonati A, Battaglia G (2006) Neuronal-specific roles of the survival motor neuron protein: evidence from survival motor neuron expression patterns in the developing human central nervous system. *Journal of Neuropathology and Experimental Neurology* **65(3):**267-77

Glater EE, Megeath LJ, Stowers RS, Schwarz TL (2006) Axonal transport of mitochondria requires milton to recruit kinesin heavy chain and is light chain independent. *The Journal of Cell Biology* **173(4):**545-57

Groen EJ, Fumoto K, Blokhuis AM, Engelen-Lee J, Zhou Y, van den Heuvel DM, Koppers M, van Diggelen F, van Heest J, Demmers JA *et al* (2013) ALS-associated mutations in FUS disrupt the axonal distribution and function of SMN. *Human Molecular Genetics* **22(18):**3690-704

Granatiero V & Manfredi G (2019) Mitochondrial transport and turnover in the pathogenesis of Amyotrophic Lateral Sclerosis. *Biology* **8:**36

Guedes-Dias P & Holzbaur ELF (2019) Axonal transport: Driving synaptic function. *Science* **366:**6462

Guillaud L, El-Agamy SE, Otsuki M, Terenzio M (2020) Anterograde Axonal Transport in Neuronal Homeostasis and Disease. *Frontiers in Molecular Neuroscience* **13:**556175

Guo W, Dittlau KS, Van Den Bosch L (2019) Axonal transport defects and neurodegeneration: Molecular mechanisms and therapeutic implications. *Seminars in Cell and Developmental Biology* https://doi.org/10.1016/j.semcdb.2019.07.010

Guo W, Naujock M, Fumagalli L, Vandoorne T, Baatsen P, Boon R, Ordovás L, Patel A, Welters M, Vanwelden T *et al* (2917) HDAC6 inhibition reverses axonal transport defects in motor neurons derived from FUS-ALS patients. *Nature Communications* **8(1):**861

Guo X, Macleod GT, Wellington A, Hu F, Panchumarthi S, Schoenfield M, Marin L, Charlton MP, Atwood HL, Zinsmaier KE (2005) The GTPase dMiro is required for axonal transport of mitochondria to Drosophila synapses. *Neuron* **47(3):**379-93

Gurtan AM, Sharp PA (2013) The role of miRNAs in regulating gene expression networks. *Journal of Molecular Biology* **425(19):**3582-600

Hackney DD, Stock MF (2020) Kinesin's IAK tail domain inhibits initial microtubule-stimulated ADP release. *Nature cell biology* **2(5):**257-60

Hackney DD, Stock MF (2008) Kinesin tail domains and Mg2+ directly inhibit release of ADP from head domains in the absence of microtubules. *Biochemistry* **47(29):**7770-8

Hancock WO (2016) The Kinesin-1 Chemomechanical Cycle: Stepping Toward a Consensus. *Biophysical Journal* **110(6):**1216-25

Hares K, Kemp K, Loveless S, Rice CM, Scolding N, Tallantyre E, Robertson N, Wilkins A (2021) KIF5A and the contribution of susceptibility genotypes as a predictive biomarker for multiple sclerosis. *Journal of Neurology* **268(6):**2175-2184

Hares KM, Miners S, Scolding N, Love S, & Wilkins A (2019) KIF5A and KLC1 expression in Alzheimer's disease: relationship and genetic influences. *AMRC Open Research* **1:[1]** https://doi.org/10.12688/amrcopenres.12861.1

Henrichs V, Grycova L, Barinka C, Nahacka Z, Neuzil J, Diez S, Rohlena J, Braun M, Lansky Z (2020) Mitochondria-adaptor TRAK1 promotes kinesin-1 driven transport in crowded environments. *Nature communications* **11(1):**1-3

Hirokawa N, Niwa S, Tanaka Y (2010) Molecular motors in neurons: transport mechanisms and roles in brain function, development, and disease. *Neuron* **68(4):**610-38

Hirokawa N, Noda Y, Tanaka Y, Niwa S (2009) Kinesin superfamily motor proteins and intracellular transport. *Nature Reviews. Molecular Cell Biology* **10(10):**682-96

Hirokawa N & Noda Y (2008) Intracellular transport and kinesin superfamily proteins, KIFs: structure, function, and dynamics. *Physiological Reviews* **88(3):**1089-118

Hirokawa N & Takemura R (2005) Molecular motors and mechanisms of directional transport in neurons. *Nature Reviews. Neuroscience* **6(3):**201-14

Isojima H, Iino R, Niitani Y, Noji H, Tomishige M (2016) Direct observation of intermediate states during the stepping motion of kinesin-1. *Nature chemical biology* **12(4):** 290-297

Jablonka S, Sendtner M (2017) Developmental regulation of SMN expression: pathophysiological implications and perspectives for therapy development in spinal muscular atrophy. *Gene Therapy* **24(9):**506-513

James PA, Talbot K (2006) The molecular genetics of non-ALS motor neuron diseases. *Biochimica and Biophysica Acta* **1762(11-12):**986-1000

Jennings S, Chenevert M, Liu L, Mottamal M, Wojcik EJ, Huckaba TM (2017) Characterization of kinesin switch I mutations that cause hereditary spastic paraplegia. *PLoS One* **12(7):**e0180353

Jeppesen GM, Hoerber JH (2012) The mechanical properties of kinesin-1: a holistic approach. *Biochemical Society Transactions* **40(2):**438-43

Kaan HY, Hackney DD, Kozielski F (2011) The structure of the kinesin-1 motor-tail complex reveals the mechanism of autoinhibition. *Science* **333(6044):**883-5.

Kalantari S, Filges I (2020) 'Kinesinopathies': emerging role of the kinesin family member genes in birth defects. *Journal of Medical Genetics* **57(12):**797-807

Kaler SG, Tang J, Donsante A, Kaneski CR (2009) Translational read-through of a nonsense mutation in ATP7A impacts treatment outcome in Menkes disease. *Annals of Neurology* **65(1):**108-13

Kallinski AL, Kar AN, Craver J, Tosolini AP, Sleigh JN, Lee SJ, Hawthorne A, Brito-Vargas P, Miller-Randolph S, Passino R *et al* (2019) Deacetylation of Miro1 by HDAC6 blocks mitochondrial transport and mediates axon growth inhibition. *The Journal of cell biology* **218(6):**1871-1890

Kalpachidou T, Kummer KK, Mitrić M, Kress M (2019) Tissue Specific Reference Genes for MicroRNA Expression Analysis in a Mouse Model of Peripheral Nerve Injury. *Frontiers in Molecular Neuroscience* **12:**283

Kanai Y, Dohmae N, Hirokawa N (2004) Kinesin transports RNA: isolation and characterization of an RNA-transporting granule. *Neuron* **43(4):**513-25

Kanai Y, Okada Y, Tanaka Y, Harada A, Terada S, Hirokawa N (2000) KIF5C, a novel neuronal kinesin enriched in motor neurons. *The Journal of Neuroscience* **20(17):**6374-84

Karle KN, Möckel D, Reid E, Schöls L (2012) Axonal transport deficit in a *KIF5A*$^{-/-}$ mouse model. *Neurogenetics* **13:**169–179

Khalil B, Morderer D, Price PL, Liu F, Rossoll W (2018) mRNP assembly, axonal transport, and local translation in neurodegenerative diseases. *Brain Research* **1693(Pt A):**75-91

Kim G, Gautier O, Tassoni-Tsuchida E, Ma XR, Gitler AD (2020) ALS Genetics: Gains, Losses, and Implications for Future Therapies. *Neuron* **108(5):**822-842

Kim SH, Shanware NP, Bowler MJ, Tibbetts RS (2010) Amyotrophic Lateral Sclerosis-associated Proteins TDP-43 and FUS/TLS Function in a Common Biochemical Complex to Co-regulate HDAC6 mRNA. *The Journal of Biological Chemistry* **285(44):**34097–34105

Kuźma-Kozakiewicz M, Chudy A, Gajewska B, Dziewulska D, Usarek E, Barańczyk-Kuźma A (2013) Kinesin expression in the central nervous system of humans and transgenic hSOD1G93A mice with amyotrophic lateral sclerosis. *Neurodegenerative Diseases* **12(2):**71-80

Lefebvre S, Bürglen L, Reboullet S, Clermont O, Burlet P, Viollet L, Benichou B, Cruaud C, Millasseau P, Zeviani M *et al* (1995) Identification and characterization of a spinal muscular atrophy-determining gene. *Cell* **80(1):**155-65

Lo Giudice T, Lombardi F, Santorelli FM, Kawarai T, Orlacchio A (20014) Hereditary spastic paraplegia: clinical-genetic characteristics and evolving molecular mechanisms. *Experimental Neurology* **261:**518-39

Longinetti E, Fang F (2019) Epidemiology of amyotrophic lateral sclerosis: an update of recent literature. *Current Opinion in Neurology* **32(5):**771-776

Lynch DS, Koutsis G, Tucci A, Panas M, Baklou M, Breza M, Karadima G, Houlden H (2016) Hereditary spastic paraplegia in Greece: characterisation of a previously unexplored population using next-generation sequencing. *European Journal of Human Genetics* **24(6):**857-63

MacAskill AF, Rinholm JE, Twelvetrees AE, Arancibia-Carcamo IL, Muir J, Fransson A, Aspenstrom P, Attwell D, Kittler JT (2009) Miro1 is a calcium sensor for glutamate receptor-dependent localization of mitochondria at synapses. *Neuron* **61:**541–555

Magrane´ J, Cortez C, Gan WB, Manfredi G (2013) Abnormal mitochondrial transport and morphology are common pathological denominators in SOD1 and TDP43 ALS mouse models. *Human Molecular Genetics* **23(6):**1413–1424

Maniatis S, Äijö T, Vickovic S, Braine C, Kang K, Mollbrink A, Fagegaltier D, Andrusivová Ž, Saarenpää S, Saiz-Castro G, Cuevas M, Watters A, Lundeberg J, Bonneau R, Phatnani H (2019) Spatiotemporal dynamics of molecular pathology in amyotrophic lateral sclerosis. *Science* **364(6435):**89-93

Mann BJ & Wadsworth P (2019) Kinesin-5 Regulation and Function in Mitosis. *Trends in Cell Biology* **29(1):**66-79

Mercuri E, Finkel RS, Muntoni F, Wirth B, Montes J, Main M, Mazzone ES, Vitale M, Snyder B, Quijano-Roy S *et al*, SMA Care Group. (2018) Diagnosis and management of spinal muscular atrophy: Part 1: Recommendations for diagnosis, rehabilitation, orthopedic and nutritional care. *Neuromuscular Disorders NMD* **28(2):**103-115

Miller S & Julien JP (2013) Axonal transport deficits and neurodegenerative diseases. *Nature reviews. Neuroscience* **14(3):**161-76

Moisse M, Zwamborn RAJ, van Vugt J, van der Spek R, van Rheenen W, Kenna B, Van Eijk K, Kenna K, Corcia P, Couratier P *et al* (2021) Project MinE Sequencing Consortium. The

Effect of SMN Gene Dosage on ALS Risk and Disease Severity. *Annals of Neurology* **89(4):**686-697

Moller A, Bauer CS, Cohen RN, Webster CP, De Vos K J (2017) Amyotrophic lateral sclerosis- associated mutant SOD1 inhibits anterograde axonal transport of mitochondria by reducing Miro1 levels. *Human Molecular Genetics* **26:**4668–4679

Morfini GA, Burns MR, Stenoien DL, Brady ST (2012) Axonal transport. In *Basic Neurochemistry: Principles of Molecular, Cellular and Medical Neurobiology,* 8th Ed, S Brady, G Siegel, W Albers, D Price [Eds] Elsevier, Boston, pp 146–164

Nakamura R, Tohnai G, Atsuta N, Nakatochi M, Hayashi N, Watanabe H, Yokoi D, Watanabe H, Katsuno M, Izumi Y *et al* (2021) Japanese Consortium for Amyotrophic Lateral Sclerosis Research (JaCALS). Genetic and functional analysis of KIF5A variants in Japanese patients with sporadic amyotrophic lateral sclerosis. *Neurobiology of Aging* **97:**147.e11-147.e17

Nakano J, Chiba K, Niwa S (2022) An ALS-associated KIF5A mutant forms oligomers and aggregates and induces neuronal toxicity. *Genes Cells* doi: 10.1111/gtc.12936 *Epub ahead of print*

Nicolas A, Kenna KP, Renton AE, Ticozzi N, Faghri F, Chia R, Dominov JA, Kenna BJ, Nalls MA, Keagle P *et al* (2018). Genome-wide analyses identify *KIF5A* as a novel ALS gene. *Neuron* **97(6):**1268-1283

Olenick MA, Holzbaur ELF (2019) Dynein activators and adaptors at a glance. *Journal of Cell Science* **132(6):**jcs227132

Pagliardini S, Giavazzi A, Setola V, Lizier C, Di Luca M, DeBiasi S, Battaglia G (2000) Subcellular localization and axonal transport of the survival motor neuron (SMN) protein in the developing rat spinal cord. *Human Molecular Genetics* **9(1):**47-56

Pant DC, Parameswaran J, Rao L, Shi L, Chilukuri G, McEachin ZT, Glass J, Bassell GJ, Gennerich A, Jiang J (2022) ALS-linked KIF5A ΔExon27 mutant causes neuronal toxicity through gain of function. bioRxiv doi: https://doi.org/10.1101/2022.03.05.483071

Perera ND, Sheean RK, Crouch PJ, White AR, Horne MK, Turner BJ (2014) Enhancing survival motor neuron expression extends lifespan and attenuates neurodegeneration in mutant TDP-43 mice. *Human Molecular Genetics* **25(18):**4080-4093

Pignataro G (2021) Emerging Role of microRNAs in Stroke Protection Elicited by Remote Postconditioning. *Frontiers in Neurology* **12:**748709

Poirier K, Lebrun N, Broix L, Tian G, Saillour Y, Boscheron C, Parrini E, Valence S, Pierre BS, Oger M (2013) Mutations in TUBG1, DYNC1H1, KIF5C and KIF2A cause malformations of cortical development and microcephaly. *Nature Genetics* **45(6):**639-47

Prior TW, Leach ME, Finanger E (2000) [Updated 2020] Spinal Muscular Atrophy. In: Adam MP, Ardinger HH, Pagon RA, *et al*, editors. GeneReviews®. Seattle (WA): University of Washington, Seattle; 1993-2022 Available from: https://www.ncbi.nlm.nih.gov/books/NBK1352/

Pu J, Guardia CM, Keren-Kaplan T, Bonifacino JS (2016) Mechanisms and functions of lysosome positioning. *Journal of Cell Science* **129(23):**4329-4339

Qin J, Zhang H, Geng Y, Ji Q (2020) How Kinesin-1 Utilize the Energy of Nucleotide: The Conformational Changes and Mechanochemical Coupling in the Unidirectional Motion of Kinesin-1. *International Journal of Molecular Sciences* **21(18):**6977

Qu Q, Li D, Louis KR, Li X, Yang H, Sun Q, Crandall SR, Tsang S, Zhou J, Cox CL, Cheng J, Wang F (2014) High-efficiency motor neuron differentiation from human pluripotent stem cells and the function of Islet-1. *Nature Communications* **5:3**449

Ramos DM, d'Ydewalle C, Gabbeta V, Dakka A, Klein SK, Norris DA, Matson J, Taylor SJ, Zaworski PG, Prior TW (2019) Age-dependent SMN expression in disease-relevant tissue and implications for SMA treatment. *The Journal of Clinical Investigations* **129(11):**4817-4831

Randall TS, Moores C, Stephenson FA (2013) Delineation of the TRAK binding regions of the kinesin-1 motor proteins. *FEBS Letters* **587(23):**3763-9

Reid E, Kloos M, Ashley-Koch A, Hughes L, Bevan S, Svenson IK, Graham FL, Gaskell PC, Dearlove A, Pericak-Vance MA, Rubinsztein DC, Marchuk DA (2002) A kinesin heavy chain (KIF5A) mutation in hereditary spastic paraplegia (SPG10). *American Journal of Human Genetics* **71(5):**1189-94

Rodriguez-Muela N, Litterman NK, Norabuena EM, Mull JL, Galazo MJ, Sun C, Ng SY, Makhortova NR, White A, Lynes MM *et al* (2017) Single-Cell Analysis of SMN Reveals Its Broader Role in Neuromuscular Disease. *Cell Reports* **18(6):**1484-1498

Rossaert E & Van Den Bosch L (2020) HDAC6 inhibitors: translating genetic and molecular insights into a therapy for axonal CMT. *Brain research* **1733:**146692

Rossoll W, Kröning AK, Ohndorf UM, Steegborn C, Jablonka S, Sendtner M (2002) Specific interaction of Smn, the spinal muscular atrophy determining gene product, with hnRNP-R and gry-rbp/hnRNP-Q: a role for Smn in RNA processing in motor axons? *Human Molecular Genetics* **11(1):**93-105

Ruiz R, Casañas JJ, Torres-Benito L, Cano R, Tabares L (2010) Altered intracellular Ca^{2+} homeostasis in nerve terminals of severe spinal muscular atrophy mice. *The Journal of Neuroscience* **30(3):**849-57

Rupaimoole R, Slack FJ (2017) MicroRNA therapeutics: towards a new era for the management of cancer and other diseases. *Nature Reviews. Drug Discovery* **16(3):**203-222

Rydzanicz M, Jagła M, Kosinska J, Tomasik T, Sobczak A, Pollak A, Herman-Sucharska I, Walczak A, Kwinta P, Płoski R (2017) *KIF5A de novo* mutation associated with myoclonic seizures and neonatal onset progressive leukoencephalopathy. *Clinical Genetic*s **91:** 769–773

Schwarz TL (2013) Mitochondrial trafficking in neurons. *Cold Spring Harbor Perspectives in Biology* **5(6):**a011304

Shah SH, Schiapparelli LM, Ma Y, Yokota S, Atkins M, Xia X, Cameron EG, Huang T, Saturday S, Sun CB *et al* (2022) Quantitative transportomics identifies Kif5a as a major regulator of neurodegeneration. *Elife* **11:**e68148

Shpargel KB, Matera AG (2005) Gemin proteins are required for efficient assembly of Sm-class ribonucleoproteins. *Proceedings of the National Academy of Sciences of the United States of America* **102(48):**17372-7

Siddique N, Siddique T. (2001) [Updated 2021] Amyotrophic Lateral Sclerosis Overview. In: Adam MP, Ardinger HH, Pagon RA, et al., editors. *GeneReviews*®. Seattle (WA): University of Washington, Seattle; 1993-2022. Available from: https://www.ncbi.nlm.nih.gov/sites/books/NBK1450/

Simone C, Ramirez A, Bucchia M, Rinchetti P, Rideout H, Papadimitriou D, Re DB, Corti S (2016) Is spinal muscular atrophy a disease of the motor neurons only: pathogenesis and therapeutic implications? *Cellular and Molecular Life Sciences* **73(5):**1003-20

Singh RN, Howell MD, Ottesen EW, Singh NN (2017) Diverse role of survival motor neuron protein. *Biochimica Biophysica Acta. Gene Regulatory Mechanisms* **1860(3):**299-315

Sleigh JN, Rossor AM, Fellows AD, Tosolini AP, Schiavo G (2019) Axonal transport and neurological disease. *Nature Reviews. Neurology 15(12):*691-703

Smith EF, Shaw PJ, De Vos KJ (2019) The role of mitochondria in amyotrophic lateral sclerosis. *Neuroscience Letters* **710:**132933

Stifani N (2014) Motor neurons and the generation of spinal motor neuron diversity. *Frontiers in Cellular Neuroscience* **8:**293

Thelen MP, Kye MJ (2020) The Role of RNA Binding Proteins for Local mRNA Translation: Implications in Neurological Disorders. *Frontiers in Molecular Biosciences* **6:**161

Turner BJ, Alfazema N, Sheean RK, Sleigh JN, Davies KE, Horne MK, Talbot K (2014) Overexpression of survival motor neuron improves neuromuscular function and motor neuron survival in mutant SOD1 mice. *Neurobiology of Aging* **35(4):**906-15

Valsecchi V, Anzilotti S, Serani A, Laudati G, Brancaccio P, Guida N, Cuomo O, Pignataro G, Annunziato L (2020) miR-206 Reduces the Severity of Motor Neuron Degeneration in the Facial Nuclei of the Brainstem in a Mouse Model of SMA. *Molecular Therapy* **28(4):**1154-1166

Valsecchi V, Boido M, De Amicis E, Piras A, Vercelli A (2015) Expression of Muscle-Specific MiRNA 206 in the Progression of Disease in a Murine SMA Model. *PLoS One* **10(6):**e0128560

van Blitterswijk M, van Es MA, Hennekam EA, Dooijes D, van Rheenen W, Medic J, Bourque PR, Schelhaas HJ, van der Kooi AJ, de Visser M, de Bakker PI, Veldink JH, van den Berg LH (2012) Evidence for an oligogenic basis of amyotrophic lateral sclerosis. *Human Molecular Genetics* **21(17):**3776-84

Van Den Bosch L (2019) HDAC6 and Miro1: Another interaction causing trouble in neurons. *Journal of Cell Biology* **218(6):**1769–1770

van Spronsen M, Mikhaylova M, Lipka J, Schlager MA, van den Heuvel DJ, Kuijpers M, Wulf PS, Keijzer N, Demmers J, Kapitein LC *et al* (2013) TRAK/Milton motor-adaptor proteins steer mitochondrial trafficking to axons and dendrites. *Neuron* **77:**485–502

Verhey KJ & Hammond JW (2009) Traffic control: regulation of kinesin motors. *Nature reviews Molecular cell biology* **10(11):**765-77

Volk AE, Weishaupt JH, Andersen PM, Ludolph AC, Kubisch C (2018) Current knowledge and recent insights into the genetic basis of amyotrophic lateral sclerosis. *Medizinische Genetik* **30(2):**252-258

Wang Q, Tian J, Chen H, Du H, Guo L (2019) Amyloid beta-mediated KIF5A deficiency disrupts anterograde axonal mitochondrial movement. *Neurobiology of Disease* **127:**410-418

Wang X & Schwarz TL (2009) The Mechanism of Kinesin Regulation by Ca^{++} for Control of Mitochondrial Motility. *Cell* **136(1):**163–174

Wirth B, Karakaya M, Kye MJ, Mendoza-Ferreira N (2020) Twenty-Five Years of Spinal Muscular Atrophy Research: From Phenotype to Genotype to Therapy, and What Comes Next. *Annual Review of Genomics and Human Genetics* **21:**231-261

Woehlke G, Schliwa M (2000) Walking on two heads: the many talents of kinesin. *Nature Reviews. Molecular Cell Biology* **1(1):**50-8

Wong YL & Rice SE (2010) Kinesin's light chains inhibit the head-and microtubule-binding activity of its tail. *Proceedings of the National Academy of Sciences of the United States of America* **107(26):**11781-6

Xia CH, Roberts EA, Lu-Shiun Her LS, Liu X, Williams DS, Don W, Cleveland DW, Goldstein LSB (2003) Abnormal neurofilament transport caused by targeted disruption of neuronal kinesin heavy chain KIF5A. *The Journal of Cell Biology* **61(1):**55–66

Yasuda K, Clatterbuck-Soper SF, Jackrel ME, Shorter J, Mili S (2017) FUS inclusions disrupt RNA localization by sequestering kinesin-1 and inhibiting microtubule detyrosination. *The Journal of Cell Biology* **216(4):**1015-1034

Zhang HL, Pan F, Hong D, Shenoy SM, Singer RH, Bassell GJ (2003) Active transport of the survival motor neuron protein and the role of exon-7 in cytoplasmic localization. *The Journal of Neuroscience* **23(16):**6627-37

Zhang K, Liu Q, Shen D, Tai H, Liu S, Wang Z, Shi J, Fu H, Wu S, Ding Q, Hu Y, Wu Y, Li X, Guan Y, Liu M, Cui L, Zhang X (2019) Mutation analysis of KIF5A in Chinese amyotrophic lateral sclerosis patients. *Neurobiology of Aging* **73:229**.e1-229.e4